



Metal–organic framework membranes: Production, modification, and applications



Wanbin Li

School of Environment, and Guangdong Key Laboratory of Environmental Pollution and Health, Jinan University, Guangzhou 511443, PR China

ARTICLE INFO

Keywords:

Metal–organic frameworks
Membrane separation
Formation mechanisms
Modification strategies
Applications

ABSTRACT

Great developments in the field of metal–organic framework (MOF) membranes have been achieved recently, especially in production with a large membrane area, modification for better performance, and application with additional functions. However, their significance has not been fully recognized and understood. This review summarizes production methodologies, including direct crystallization, interfacial/contra-diffusion synthesis, layer-by-layer assembly, confinement conversion, microfluidic processing, and vapor deposition. The mechanisms and merits of these synthesis methods are analyzed. Modification strategies for the combination of MOFs and introduced components are discussed, and classified into coating, heteroepitaxial growth, embedding, occupation, grafting, and substitution. Modification improves the performance distinctly by changing the construction, microstructure, affinity, and pore size of MOF membranes. The application of MOF membranes in gas separation, nanofiltration, ionic sieving, stimuli responsiveness, and catalysis are reviewed, and the separation mechanisms are analyzed. Moreover, some possible opportunities and challenges for further development of MOF membranes are pointed out.

1. Introduction

Separation processes performed by distillation, extraction, condensation, evaporation, crystallization, and filtration consume about half the total energy used in the chemical industry. Membrane processes, including, but not limited to, micro/ultra/nanofiltration, reverse osmosis, electro-osmosis, pervaporation, distillation, and gas separation, have been attracting much attention because of their energy-saving and environment-friendly features [1–4]. Membrane properties impact the separation efficiency immensely. The development of membrane materials draws much attention [5]. Polymers such as cellulose acetate, polyamide, polyimide, polysulfone (PSF), polyvinylidene fluoride (PVDF), and polydimethylsiloxane (PDMS) are the dominant materials in practical membrane fabrication. These membranes show some irreplaceable merits, especially a low production cost and high processability [6]. However, polymeric membranes generally suffer from a trade-off limitation between selectivity and permeability [7]. To improve the separation performance, micro/nanoparticles are introduced and blended into polymeric matrices to change the formation mechanism, phase composition, and transport channels, thereby yielding high-performance mixed-matrix membranes (MMMs) [8–10]. The aggregation of particles and the formation of invalid particle–polymer interfaces are the opportunities and challenges in the progress of MMMs [11–13]. Recently, carbon membranes [14–16], especially graphene-based membranes, fabricated from graphene or its derivatives [17–21], have been demonstrated, with excellent performance in gas separation, nanofiltration, and organic solvent nanofiltration. Inorganic materials are employed to fabricate separation membranes as well. Owing to their commendable thermal and chemical properties and uniform microporous structures, zeolite membranes show great developments in

E-mail address: gandeylin@126.com.

<https://doi.org/10.1016/j.pmatsci.2018.09.003>

Received 13 January 2018; Received in revised form 11 September 2018; Accepted 24 September 2018

Available online 26 September 2018

0079-6425/ © 2018 Elsevier Ltd. All rights reserved.

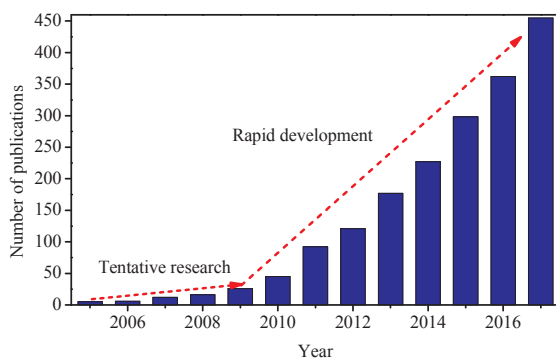


Fig. 1. Number of publications per year on “metal–organic framework membranes,” from Web of Science.

separation application [22–25]. Benefiting from plentiful catalytic sites, zeolites are very promising for the fabrication of catalytic membranes [26].

As a type of microporous material such as zeolites, metal–organic frameworks (MOFs), composed of organic linkers and metal centers, have large surface areas and well-defined pore structures. These materials show great potential in energy storage, molecular capture, catalysis, separation, and information encryption [27–30]. MOFs have been deposited on dense substrates to produce films for better application [31–33]. Unlike MOF films with dense substrates, MOF membranes are formed by growing continuous polycrystalline MOF layers on porous substrates. MOF layers offer selectivity for different feed components, and substrates provide mechanical strength for the membrane package and practical application [34–37]. Moreover, MOF membranes require more continuity than that for MOF films. Continuous MOF membranes for separation were successfully fabricated until 2009 [38–42]. Thereafter, research on MOF membranes showed rapid developments (Fig. 1). Various fabrication methods, including hydro/solvothermal synthesis, interfacial growth, and layer-by-layer assembly, have been reported for producing continuous membranes [34–36]. As shown in Table 1, substrates for supporting MOF layers are similarly multitudinous. Inorganic (e.g. Al_2O_3 , TiO_2 , and SiO_2) discs and metal (Cu and Ni) meshes are the most reported substrates for supporting MOF membranes, due to their commendable chemical and thermal stabilities [38–44]. To enhance processability, improve membrane area per volume, and reduce fabrication cost, polymeric substrates, especially hollow fiber substrates, are advocated to prepare MOF membranes for better industrial application. However, polymeric substrates have relatively poor thermal stability, solvent resistance, and mechanical strength [36]. These disadvantages may impede the application of related MOF membranes in harsh conditions, such as high temperature, strongly aggressive solvents, and extreme pressure. Free-standing MOF membranes at the centimeter scale have been fabricated, but their poor mechanical properties are a vital problem, especially under pressure-based separation [45]. With respect to application, Table 2 shows the most commonly prepared MOF membranes and the expected permeance and selectivity in gas separation, which are based on the data of reported studies. Owing to ultrahigh porosities, coherent transport channels, uniform apertures, and unique adsorptions, MOF membranes are widely applied for H_2 purification, CO_2 capture, and hydrocarbon separation, and show superior permeance and selectivity than those of state-of-the-art conventional polymeric membranes [46–49]. Relative to the types of reported MOFs, the types of MOFs for membrane fabrication are very few. Owing to strict requirements, such as, but not limited to, suitable aperture size, high sorption dissimilarity of feed components in frameworks, high chemical stability, and good membrane-forming property, the reported MOF membranes mainly comprise ZIF-7, ZIF-8, ZIF-90, MOF-5, CuBTC, NH_2 -MIL-53, and UiO-66 [28,34,36,37].

Although the great potential of MOF membranes has been proposed and demonstrated, several bottlenecks that impact separation applications should be overcome urgently. Firstly, the commonly applied synthesis strategies usually fabricate MOF membranes with a small area of several square centimeters, which is much smaller than the requirement for industrial separation applications. The methodology for large-scale production of MOF membranes should be developed imminently. Secondly, the fabrication of defect-free polycrystalline MOF membranes through heterogeneous crystal growth is seriously hobbled by the formation of grain boundaries, which may induce void transport channels and thus reduce the selectivity. On the other hand, channel refining and sorption tuning are very attractive for improving the separation performance. Thirdly, separation membranes with additional functions are interesting and needed, to satisfy the demands of the chemical industry. It is very important to extend the application scope of MOF membranes. As shown in Fig. 2, great developments in the production, modification, and application of MOF membranes have been achieved recently, but their significance has not been fully recognized and understood. This review mainly focuses on the progress in

Table 1

Comparison of MOF membranes with different substrates in stability, economy, and processability.

Substrate	Substance	Stability	Economy	Processability
Inorganic	Al_2O_3 , TiO_2 , SiO_2 , Cu, Ni	High	Low	Moderate
Polymer	Polyimide, Polyvinylidene fluoride, Polysulfone, Nylon, Torlon	Moderate	Moderate	High
Free-standing	Non	Low	High	Low

Table 2The commonly prepared MOF membranes and the expected permeance and selectivity. X_n presents CO_2 , N_2 or CH_4 .

MOF	Gas pair	Expected permeance	Expected selectivity
ZIF-7	H_2/X_n	10^{-7} – $10^{-6} \text{ mol s}^{-1} \text{ m}^{-2} \text{ Pa}^{-1}$	10–20
ZIF-8	H_2/X_n	10^{-7} – $10^{-6} \text{ mol s}^{-1} \text{ m}^{-2} \text{ Pa}^{-1}$	5–25
	$\text{H}_2/\text{C}_3\text{H}_8$	10^{-7} – $10^{-6} \text{ mol s}^{-1} \text{ m}^{-2} \text{ Pa}^{-1}$	~2500
	$\text{C}_3\text{H}_6/\text{C}_3\text{H}_8$	$\sim 10^{-8} \text{ mol s}^{-1} \text{ m}^{-2} \text{ Pa}^{-1}$	50
CuBTC	H_2/X_n	$\sim 10^{-6} \text{ mol s}^{-1} \text{ m}^{-2} \text{ Pa}^{-1}$	5–15
NH_2 -MIL-53	H_2/X_n	$\sim 10^{-6} \text{ mol s}^{-1} \text{ m}^{-2} \text{ Pa}^{-1}$	20–30

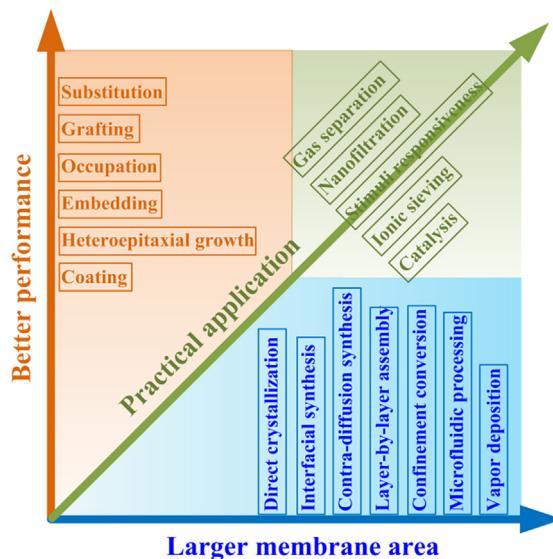


Fig. 2. Development tendency of MOF membranes, and main points of this review.

continuous MOF membranes, and is organized into introduction, production of MOF membranes, modification of MOF membranes, applications of MOF membranes, and conclusions and outlook.

2. Production of MOF membranes

Hydro/solvothermal growth was the first proposed method for synthesizing MOF membranes, and is widely used. This method is carried out by immersing substrates in precursor solutions with both metal sources and linkers. To accelerate the synthesis process, hydro/solvothermal growth is performed with microwave treatment [42]. Both heterogeneous crystallization on substrates and homogeneous crystallization in bulk solutions occur under thermal treatment. Heterogeneous crystallization may lead to the formation of continuous MOF membranes, whereas homogeneous crystallization may increase the risk of cracked membrane formation. Hence, the modification of substrates to increase heterogeneous nucleation is exploited to promote the formation of defect-free membranes. Seeding the substrates with nano/micrometer-sized MOF crystals can enhance heterogeneous crystallization [50–57]. Various techniques, such as dip coating and rubbing, are utilized for seeding. The adhesion between MOF layers and substrates relates to the stability and long-term application of MOF membranes. Chemical modification by grafting the molecules with the $-\text{NH}_2$ and $-\text{COOH}$ groups on the substrates, which can combine linkers or metal ions, has been proposed to simultaneously strengthen the compatibility and provide nucleation sites [58–64]. Because the connection between the substrates and MOF layers is chemical bonding, the membranes usually show good mechanical stability against the abscission of the MOF layers. Considering the hybrid property and coordination process of MOFs, substrates with congeneric metals have also been developed for synthesizing MOF membranes [65–69].

For industrial separation applications, the large-scale production of membranes is important. However, because of the complicated procedures of inorganic substrate fabrication, modification/seeding, and high-temperature crystallization, scaling up the production of MOF membranes by the hydro/solvothermal method is difficult and expensive. Moreover, as mentioned above, the crystallization in bulk solutions causes a great wastage of raw materials. To improve the potential of MOF membrane production, polymeric substrates with high processability, low cost, and large membrane area per volume, are employed to support the MOF membranes. Furthermore, many strategies, including direct crystallization, interfacial synthesis, contra-diffusion growth, layer-by-layer assembly, microfluidic processing, confinement conversion, and vapor deposition, have been developed to produce MOF membranes. In this section, we discuss the strategies that are feasible to efficiently produce MOF membranes on a large scale. Table 3

Table 3
 Synthesis conditions, membrane properties, and separation performance of reported membranes that are feasible for production on a large scale.

MOF	Substrate	Method	Solvent	Syn Tem (°C)	Th (µm)	Per Tem (°C)	Gas pair	Per ($\times 10^{-8}$ mol s ⁻¹ m ⁻² Pa ⁻¹)	Sel	Ref.
ZIF-7	PVDF fiber	Direct crystallization	DMF	130	10	RT	H ₂ /CO ₂	235.4 ^a	18.4 ^b	[76]
ZIF-7	PVDF fiber	Direct crystallization	DMF	130	30	RT	H ₂ /CO ₂	235.4 ^a	20.3 ^b	[78]
ZIF-8	Al ₂ O ₃ disc	Direct crystallization	Water	30	2.2	22	H ₂ /N ₂ C ₃ H ₆ / C ₃ H ₈	102.2 132.9 ^a 2.1–3.8	15.86 18.3 ^b 28.0–45.0	[70]
ZIF-8	YSZ fiber	Direct crystallization	Water	30	2.0	22	H ₂ /CH ₄ H ₂ /C ₃ H ₆ H ₂ /C ₃ H ₈	139 121 71	10 10 47.4	[71]
ZIF-8	AAO	Direct crystallization	Water	30	0.5	25	CH ₄ /C ₃ H ₈ C ₂ H ₆ / C ₃ H ₈	10 7.0	69 44	[72]
ZIF-8	PVDF fiber	Direct crystallization	Water	RT	1	–	H ₂ /CO ₂ H ₂ /O ₂ H ₂ /N ₂ H ₂ /CH ₄ H ₂ /CO ₂ H ₂ /N ₂ H ₂ /O ₂	830 ^b 830 ^b 830 ^b 830 ^b 201.0 ^b 2010 ^a 2010 ^a 2010 ^a 201.4 ^b 201.4 ^b 9.1 9.2 9.3	7.3 15.5 16.2 2655 31.6 7.1 ^a 8.2 ^a 8.2 ^b 9.1 ^a 16.3 ^b 18.1 ^a 5.0 6.9 20.4	[74]
ZIF-8	PVDF fiber	Direct crystallization	MeOH	110	50	RT	H ₂ /CO ₂	201.4 ^b	16.3 ^b	[76]
ZIF-8	PES fiber	Direct crystallization	MeOH	80	20	20	H ₂ /CO ₂ H ₂ /O ₂ H ₂ /N ₂	9.1 9.2 9.3	5.0 6.9 20.4	[77]
ZIF-8	PVDF fiber	Direct crystallization	MeOH	110	40	RT	H ₂ /CO ₂ H ₂ /N ₂ H ₂ /CO ₂	190.3 244.3 ^b 19.4 ^a	12.42 14.3 ^b 1.8 ^b	[78]
ZIF-90	Torlon fiber	Direct crystallization	MeOH	65	5	35	H ₂ /CO ₂ H ₂ /N ₂ CO ₂ /CH ₄	19.4 ^a 19.4 ^a 10.8 ^b	6.3 ^a 6.3 ^a 1.5 ^b	[73]
CuBTC	PAN fiber	Direct crystallization	Water/EtOH	110	13	20	CO ₂ /N ₂	10.8 ^a	3.5 ^a	[75]
CuBTC	PVDF fiber	Direct crystallization	Water/EtOH	110	43	RT	H ₂ /CO ₂	7050.0	7.1	[78]
NH ₂ -MIL-53	PVDF fiber	Direct crystallization	DMF	150	8	RT	H ₂ /CO ₂ H ₂ /O ₂ H ₂ /N ₂	601.2 846.0 ^b 421 542 ^b 542 ^b	7.91 5.87 ^b 32.4 24.1 ^a 27.9 ^a	[79]
ZIF-8	Nylon flat	Contra-diffusion	MeOH-MeOH	RT	16	20	H ₂ /CH ₄	542 ^a	27.3 ^b	[82]
ZIF-8	Nylon flat	Contra-diffusion	Water-Water	RT	2.5	20	H ₂ /N ₂	197.0 ^b 113 ^a	4.3 ^b 4.6 ^a	[83]

(continued on next page)

Table 3 (continued)

MOF	Substrate	Method	Solvent	Syn. Temp (°C)	Th (µm)	Per. Tem (°C)	Gas pair	Per ($\times 10^{-8}$ mol s $^{-1}$ m $^{-2}$ Pa $^{-1}$)	Sel	Ref.
ZIF-8	BPPO flat	Contra-diffusion	Water-Water	22	2	RT	H ₂ /CO ₂ H ₂ /N ₂ H ₂ /CH ₄ H ₂ /C ₃ H ₈ C ₃ H ₆ /C ₃ H ₈	61 ^a 61 ^a 61 ^a 61 ^a 0.75 ^a	5.5 ^a 9.2 ^a 10.2 ^a 2259 ^a 27.8 ^a	[85]
ZIF-8	PTSC flat	Contra-diffusion	MeOH-MeOH	RT	0.6	RT	H ₂ /C ₃ H ₆ C ₃ H ₆ /C ₃ H ₈ C ₃ H ₆ /C ₃ H ₈	32 ^a 0.6 ^b	8358 ^a 150 ^a	[86]
ZIF-8	Al ₂ O ₃ tube	Contra-diffusion	MeOH-MeOH	150	2.0	RT	H ₂ /CO ₂	5730 ^b	15.5 ^b	[87]
ZIF-8	Al ₂ O ₃ disc	In situ contra-diffusion	MeOH-MeOH	120	1.5	RT	H ₂ /N ₂ C ₃ H ₆ /C ₃ H ₈	5730 ^b 2.0	17.1 ^a 55	[89]
ZIF-8	Al ₂ O ₃ disc	In situ contra-diffusion	MeOH-MeOH	120	1	RT	C ₃ H ₆ /C ₃ H ₈	2.7	70	[91]
ZIF-8	Al ₂ O ₃ disc	Layer by layer	MeOH-MeOH	RT	1.6	35	C ₃ H ₆ /C ₃ H ₈ H ₂ /CO ₂	1.9 ^a 1.9 ^a	5 ^a 11 ^a	[97]
CuBTC	PSF flat	Layer by layer	DMF/EtOH/H ₂ O-DMF/EtOH/ H ₂ O	60	25	RT	H ₂ /CO ₂ H ₂ /C ₃ H ₆	7.9 ^a 7.9 ^a	7.2 ^a 5.7 ^a	[98]
ZIF-8	Al ₂ O ₃ disc	Spin Coating/Layer by layer	MeOH-MeOH	RT	3.0	35	H ₂ /CO ₂	–	4.6	[99]
CuBTC	Al ₂ O ₃ disc	Spray/Layer by layer	EtOH-EtOH	–	0.5	RT	H ₂ /CO ₂	3	8.5	[100]
ZIF-7	PSF fiber	Microfluidic/Direct crystallization	EtOH	RT	2.4	35	H ₂ /N ₂ H ₂ /CH ₄ CO ₂ /N ₂ CO ₂ /CH ₄	0.2 0.2 0.09 0.09	35.1 34.6 13.6 13.5	[102]
ZIF-8	Al ₂ O ₃ fiber	Microfluidic/Direct crystallization	Water	30	2.0	RT	H ₂ /CO ₂ H ₂ /N ₂ H ₂ /CH ₄	43.2 ^a 43.2 ^a 43.2 ^a	3.3 11.1 12.1	[101]
ZIF-8	PSF fiber	Microfluidic/Direct crystallization	MeOH	RT	3.6	35	H ₂ /N ₂ H ₂ /CH ₄	0.5	18.3	[102]
ZIF-8	Matrimid fiber	Microfluidic/Direct crystallization	Water	20	0.8	20	H ₂ /CH ₄ C ₃ H ₆ /C ₃ H ₈	0.5 1.8	17.2 46	[104]
ZIF-8	Torlon fiber	Microfluidic/Interfacial synthesis	Octanol-Water	30	9	25	C ₃ H ₆ /C ₃ H ₈ C ₃ H ₆ /C ₃ H ₈	1.2	12	[105]
ZIF-8	Torlon fiber	Microfluidic/Interfacial synthesis	Octanol-Water	22–42	5	25	C ₃ H ₆ /C ₃ H ₈	2.2	65	[106]
ZIF-8	Torlon fiber	Microfluidic/Interfacial synthesis	Octanol-Water	22–42	8	25	C ₃ H ₆ /C ₃ H ₈	1.5	180	[107]
ZIF-8	Torlon fiber	Microfluidic/Contra-diffusion	Water-Water	RT	8.5	25	CO ₂ /N ₂	0.7	52	[110]
CuBTC	PBI fiber	Microfluidic/Contra-diffusion	Water-Isobutanol	65	15	35	He/N ₂ He/C ₃ H ₈	0.04 ^a 0.04 ^a	12 ^a 17 ^a	[109]
ZIF-8	Al ₂ O ₃ disc	Confinement conversion	DMF/Water	80	0.33		H ₂ /CO ₂ H ₂ /N ₂ H ₂ /CH ₄	1.4 ^b 1.4 ^b 1.4 ^b	7.5 ^b 23.2 ^b 83.1	[118]

(continued on next page)

Table 3 (continued)

MOF	Substrate	Method	Solvent	Syn Tem (°C)	Th (µm)	Per Tem (°C)	Gas pair	Per ($\times 10^{-8}$ mol s ⁻¹ m ⁻² Pa ⁻¹)	Sel	Ref.
ZIF-8	Al ₂ O ₃ tube	Confinement conversion	MeOH	100	15–20		H ₂ /CO ₂	5–10 ^a	7.8 ^a	[119]
ZIF-8/LDH	Al ₂ O ₃ disc	Confinement conversion	MeOH	80	1.1/1.3	90	H ₂ /CH ₄	5–10 ^a	12.5 ^a	[117]
CuBTC	Non	Confinement conversion	EtOH/Water	RT	5.0	RT	H ₂ /N ₂	4.1 ^a	16.8	[111]
							H ₂ /CO ₂	158 ^a	6.1	
							H ₂ /N ₂	158 ^a	5.0	
							H ₂ /CH ₄	158 ^a	4.0	
CuBTC	PVDF fiber	Confinement conversion	EtOH/Water	RT	3.0	RT	H ₂ /CO ₂	201	8.1	[114]
							H ₂ /N ₂	201	6.5	
							H ₂ /CH ₄	201	5.4	
CuBTC	Non	Confinement conversion	EtOH	RT	5.5	RT	CO ₂ /SF ₆	34	13.1	[115]
ZIF-8	AAO	Confinement conversion-Direct crystallization	EtOH/Water-Water	RT-30	2.5	RT	H ₂ /CO ₂	471 ^a	3.6 ^a	[112]
							H ₂ /N ₂	471 ^a	12.5 ^a	
							H ₂ /CH ₄	471 ^a	9.8 ^a	
ZIF-8	AAO	Confinement conversion-Direct crystallization	EtOH/Water-EtOH/Water	RT-30	2.0	RT	H ₂ /N ₂	768 ^a	9.5	[113]
							H ₂ /CH ₄	768 ^a	14.3	
ZIF-8	Al ₂ O ₃ tube	Confinement conversion-Direct crystallization	MeOH-MeOH	50–100	8.0	25	H ₂ /N ₂	20.8 ^a	10.3 ^a	[120]
							H ₂ /CH ₄	20.8 ^a	10.4 ^a	
							H ₂ /C ₃ H ₈	20.8 ^a	149.6 ^a	
							H ₂ /SF ₆	20.8 ^a	281.5 ^a	
ZIF-8	Al ₂ O ₃ tube	Confinement conversion-Direct crystallization	MeOH-MeOH	50–100	6.0	30	H ₂ /CO ₂	15.8	4.6	[121]
							H ₂ /N ₂	16.9	8.2	
							H ₂ /CH ₄	16.7	9.8	
ZIF-8	Al ₂ O ₃ -ZnO fiber	Confinement conversion-Direct crystallization	MeOH-MeOH	60–100	5–6	RT	H ₂ /N ₂	18.1 ^a	10.4 ^a	[123]
							H ₂ /CH ₄	18.1 ^a	11.7 ^a	
ZIF-8	Al ₂ O ₃ disc	Confinement conversion/Direct crystallization	MeOH	100	20	RT	H ₂ /CO ₂	14	4.2	[116]
							H ₂ /N ₂	14	10.0	
							H ₂ /CH ₄	14	12.5	
ZIF-8	PAN flat	Confinement conversion/Direct crystallization	Water	RT	0.9	RT	H ₂ /C ₃ H ₈	12.3 ^a	26 ^a	[122]
ZIF-8	PVDF fiber	Vapor deposition	Non	150	0.087	RT	H ₂ /O ₂	1190 ^a	14.1 ^a	[126]
							H ₂ /N ₂	1190 ^a	22.4 ^a	
							H ₂ /CH ₄	1190 ^a	27.3 ^a	
							H ₂ /C ₃ H ₈	1178	3126	
							C ₃ H ₆ /C ₃ H ₈	28	73.4	
CuBTC	Al ₂ O ₃ disc	Rapid thermal deposition	DMF	180	20–25		H ₂ /N ₂	30 ^a	13.7 ^a	[127]
							H ₂ /CH ₄	30 ^a	8.8 ^a	
							H ₂ /SF ₆	30 ^a	600 ^a	
ZIF-8	Al ₂ O ₃ disc	Rapid thermal deposition	DMF/Water	200	5–20		C ₃ H ₆ /C ₃ H ₈	0.7	30	[127]
ZIF-7	Al ₂ O ₃ disc	Electrospray deposition	DMF	160–200	4.5	25	C ₃ H ₈	46.1	9.6	[128]
							H ₂ /CO ₂	30.5	18.3	

^a The data was obtained from the single-component permeation. RT-room temperature.

shows the synthesis conditions, membrane properties, and separation performance of these reported membranes.

2.1. Direct crystallization

Direct crystallization is the synthesis of membranes by the crystallization of MOF layers on substrates in mixed precursor solutions. The substrates are immersed in metal ion/linker solutions directly, and heterogeneous crystallization of MOFs on the substrates leads to the formation of continuous MOF membranes. To enhance the density of heterogeneous nucleation sites and adhesion between the MOF layers and substrates, seeds and functional groups are introduced onto the substrates to form defect-free MOF membranes with high compatibility. This synthesis method is similar to that used for zeolite membranes. As the synthesis conditions for some MOFs are mild, the related membranes can be fabricated at low temperatures and show good feasibility of production. Pan et al. fabricated a ZIF-8 membrane on an alumina substrate with coated seeds, by direct crystallization in zinc nitrate hexahydrate and 2-methylimidazole (MeIm) aqueous solution at a low temperature of 30 °C. A membrane with a thickness of 2.2 μm was prepared after crystallization for 6 h. As the actual window size of ZIF-8 is 4.0–4.2 Å, the prepared membrane displayed a high C₃H₆ (kinetic diameter, KD: 4.0 Å)/C₃H₈ (KD: 4.3 Å) selectivity of 50 and a C₃H₆ permeance of $3.0 \times 10^{-8} \text{ mol s}^{-1} \text{ m}^{-2} \text{ Pa}^{-1}$ at -15 °C [70]. Due to a large membrane area per unit volume, yttria-stabilized zirconia (YSZ) hollow fibers were employed as the substrate to support the ZIF-8 membrane. At room temperature, the H₂ permeance and H₂/C₃H₈ selectivity of the prepared ZIF-8 membrane was $1.54 \times 10^{-6} \text{ mol s}^{-1} \text{ m}^{-2} \text{ Pa}^{-1}$ and 1100, respectively [71]. To deposit thin MOF membranes on unmodified substrates, He et al. grew MOF nanocrystals on substrates, by the electrophoretic method, and then crystallized continuous membranes by direct crystallization in precursor solutions at a temperature of 30 °C. The prepared ZIF-8 membrane had a thickness of 500 nm, and showed a high H₂ permeance of $8.3 \times 10^{-8} \text{ mol s}^{-1} \text{ m}^{-2} \text{ Pa}^{-1}$ and good ideal selectivities of 7.3 (H₂/CO₂), 15.5 (H₂/N₂), 16.2 (H₂/CH₄), and 2655 (H₂/C₃H₈) [72]. However, the types of MOFs that can be fabricated into membranes at low temperatures are limited. Moreover, the crystallization of the MOFs in bulk solution, and the high linker/metal salt molar ratio of 75 in these studies, led to a high consumption of the expensive linkers. To accelerate the membrane formation, microwave synthesis was proposed. This method was performed by thermal treatment of the precursor solutions with immersed substrates using microwave processing. Owing to the rapid and volumetric heating, the synthesis time can be shortened greatly [42].

Compared with that of inorganic substrates, polymeric hollow fiber substrates display better feasibility for MOF membrane production, due to their excellent processability and large area per unit volume. Brown et al. fabricated ZIF-90 membranes on poly (amide-imide) hollow fibers with a nanocrystal seed layer, under relatively mild conditions with a temperature of 65 °C. The prepared membranes had a thickness of 5 μm, and showed moderate ideal selectivities of 1.5 for CO₂/CH₄ and 3.5 for CO₂/N₂ [73]. Hou et al. deposited a ZIF-8 membrane on PVDF hollow fibers using (3-aminopropyl)triethoxysilane (APTES)-functionalized titania

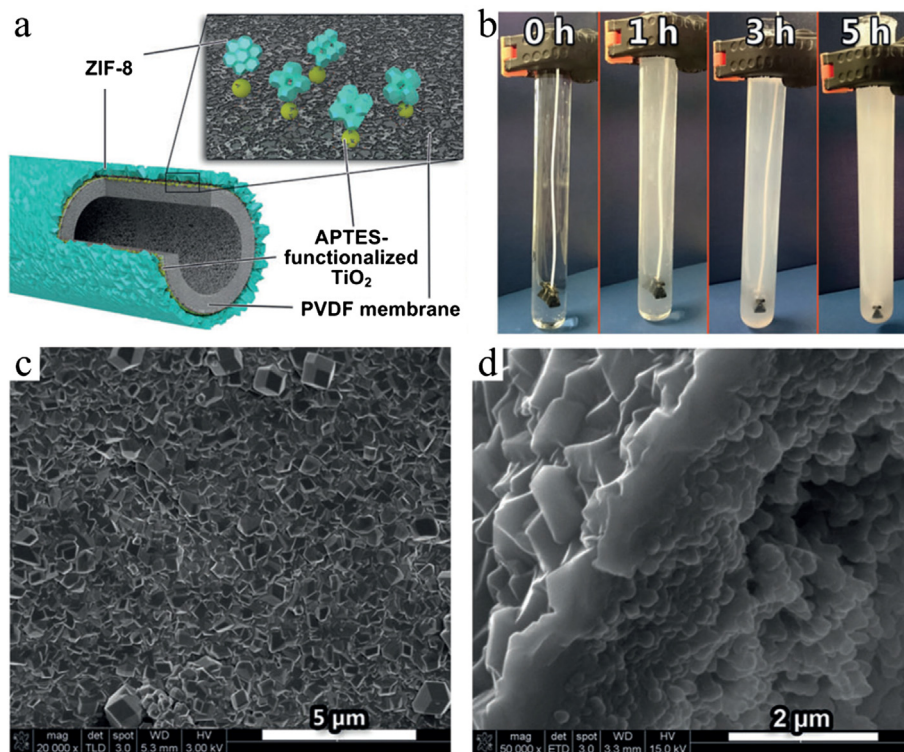


Fig. 3. (a) Scheme of ZIF-8 membrane on PVDF hollow fibers with APTES-functionalized TiO₂ nanoparticles. (b) Photograph of the deposition process. (c and d) SEM images of the prepared ZIF-8 membrane. Adapted from Ref. [74] with permission from Wiley-VCH.

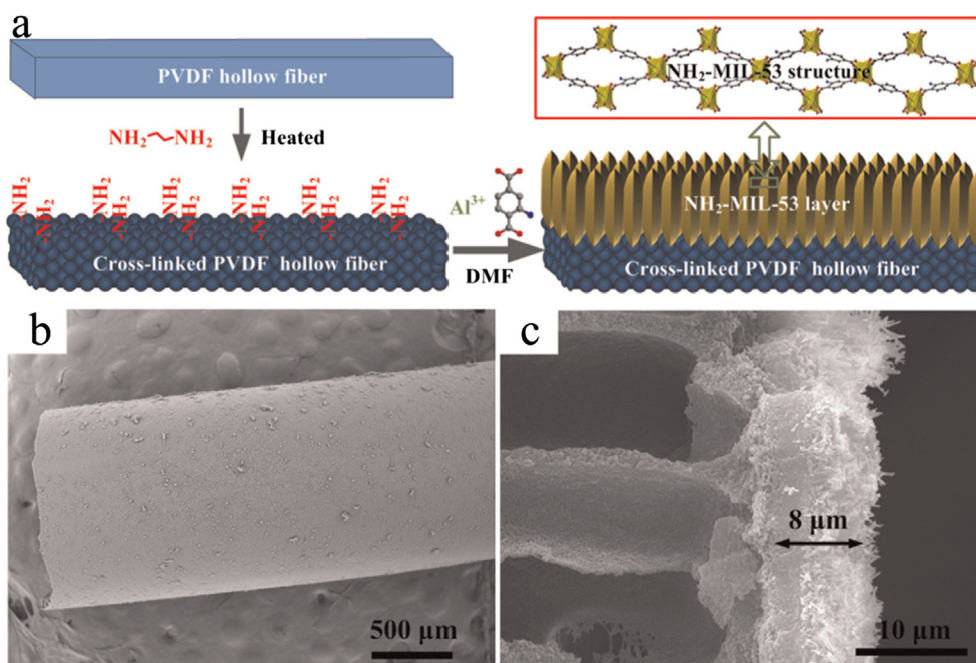


Fig. 4. (a) Schematic diagram of preparation of MOF membrane. (b and c) SEM images of $\text{NH}_2\text{-MIL-53}$ hollow fiber membranes. Adapted from Ref. [79] with permission from Elsevier.

nanoparticles as seeds (Fig. 3a and b). The ZIF-8 membrane, with a thickness of about $1.0\ \mu\text{m}$, was synthesized by the immersion technique, at room temperature (Fig. 3c and d). The synthesized ZIF-8 membrane showed excellent separation performance, with a high H_2 permeance of $201 \times 10^{-7}\ \text{mol s}^{-1}\ \text{m}^{-2}\ \text{Pa}^{-1}$ and a H_2/CO_2 ideal selectivity of 7.1 [74].

Under high pressures, the contraction of flexible polymeric substrates may lead to crack formation in MOF membranes. To enhance the stiffness of the MOF hollow fiber membranes, Li et al. fabricated ZIF-8 and CuBTC membranes on polyacrylonitrile (PAN) hollow fibers. The hollow fibers were firstly hydrolyzed using an alkaline solution to transform the $-\text{CN}$ groups into $-\text{COO}-$ groups, thereby improving heterogeneous nucleation by coordinating the metal ions. During crystallization by hydrothermal treatment, the cross-linking, cyclization, and dehydrogenation reactions of PAN molecules increased the stiffness of the membranes. The prepared CuBTC membrane showed a high H_2 permeance of $7.05 \times 10^{-5}\ \text{mol s}^{-1}\ \text{m}^{-2}\ \text{Pa}^{-1}$ and a H_2/CO_2 selectivity of 7.1 [75]. To enhance the adhesion of the MOF layers onto the substrates, the MOF membranes were deposited on the substrates with ZnO buffer array layers. As the ZnO layer was synthesized using MeIM as the pH regulator, MOF membranes could be fabricated without the procedure of ZnO activation. The prepared ZIF membranes were crack-free and exhibited excellent compatibility. After ultrasonic treatment for 60 min, the membranes maintained an intact continuity. The prepared ZIF-8 membrane displayed high H_2/CO_2 and H_2/N_2 ideal selectivities of 16.3 and 18.4, respectively, with a H_2 permeance of $20.1 \times 10^{-7}\ \text{mol s}^{-1}\ \text{m}^{-2}\ \text{Pa}^{-1}$ [76]. Metal-based gels were similarly developed as buffer layers for MOF membrane production. As a result of gel impregnation in the substrate, MOF crystals were formed in polyethersulfone (PES) hollow fibers, and the compatibility and stiffness of the prepared MOF membranes improved drastically. The prepared ZIF-8 membrane showed a high H_2/N_2 selectivity of 20.4 [77].

MOFs, which can be synthesized on polymeric substrates, usually require relatively mild synthesis conditions. To increase the topological types of MOFs in membrane fabrication, PVDF hollow fibers were ammoniated using molecules with two amino groups, such as ethanediamine (EDA), to improve the chemical stability (Fig. 4). After ammoniation, the hollow fibers displayed excellent solvent resistance and thermal stability due to their cross-linked chemical structure. Moreover, the ammoniated hollow fibers contained nanoparticle structures and amino groups, which represented vast nucleation sites on the surface, for better formation of continuous MOF layers. In addition to ZIF-8 and CuBTC membranes, ZIF-7 and $\text{NH}_2\text{-MIL-53}$ membranes were fabricated in N,N-dimethylformamide (DMF) solutions at high temperatures of 130 and $150\ ^\circ\text{C}$, respectively. All the prepared MOF hollow fiber membranes displayed outstanding H_2 separation performance, e.g., the H_2 permeance of the prepared $\text{NH}_2\text{-MIL-53}$ membrane was $42.1 \times 10^{-7}\ \text{mol s}^{-1}\ \text{m}^{-2}\ \text{Pa}^{-1}$, whereas the corresponding H_2/CO_2 selectivity was 32.4 [78,79].

2.2. Interfacial and contra-diffusion synthesis

Different from the mixed precursor solutions in direct crystallization, interfacial and contra-diffusion synthesis have two separated linker and metal source solutions, through isolation by the substrates (contra-diffusion synthesis) or the interfaces of two immiscible solvents (interfacial synthesis) [80,81]. Crystallization on the substrates or at the interfaces results in the formation of continuous MOF membranes. In these methods, MOFs are preferentially crystallized at the defects of the membranes, because the

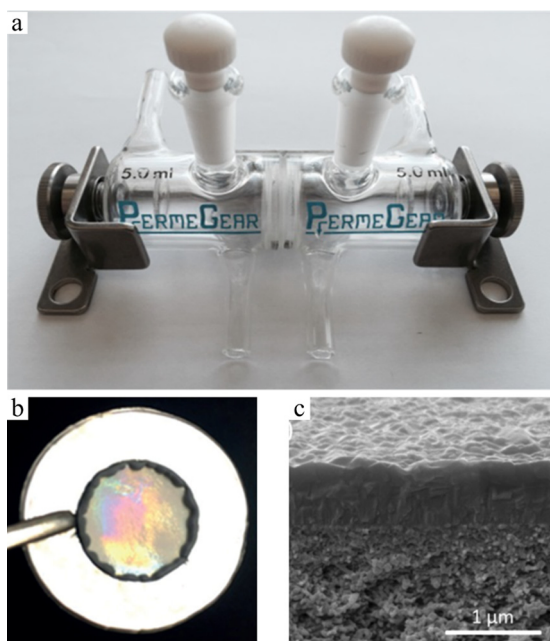


Fig. 5. (a) Synthesis cell used for preparing ZIF-8 membrane. (b and c) Digital photograph and SEM image of ZIF-8 membrane. Adapted from Ref. [86] with permission from Wiley-VCH.

defects provide a pathway for the diffusion of MOF precursors. These methods are very suitable for fabricating defect-free MOF membranes. Moreover, owing to the two non-interfering solutions, there is no bulk MOF formation, thereby reducing the wastage of MOF precursors. Yao et al. exploited the contra-diffusion method to synthesize ZIF-8 membranes on flat nylon substrates [82]. To grow the ZIF-8 membranes, MeIM and zinc nitrate methanol solutions were placed on different sides of the substrate. After synthesis for 72 h, with a MeIM/ Zn^{2+} molar ratio of 8, the membrane was formed, and showed a high H_2 permeance of $1.97 \times 10^{-6} \text{ mol s}^{-1} \text{ m}^{-2} \text{ Pa}^{-1}$, but a moderate H_2/N_2 ideal selectivity of 4.3, possibly due to the inferior microstructures. An NH_4^+ additive was added into the precursor aqueous solution to improve the continuity of the ZIF-8 membrane [83]. Interfacial synthesis provides a more confined region for crystallization than that by contra-diffusion. Li et al. prepared ZIF-8 membranes on a polymeric flat membrane by interfacial synthesis. Zinc nitrate aqueous solution was firstly impregnated into the PES substrate, and MeIM/1-octanol solution was subsequently poured on the PES substrate for interfacial synthesis. After growth, an ultrathin ZIF-8 membrane was formed, and showed commendable performance in nanofiltration and organic solvent nanofiltration for dye removal [84].

Similar to direct crystallization, the nucleation density of substrates plays a critical role in the formation of MOF membranes. Shamsaei et al. combined contra-diffusion synthesis and vapor modification of substrates to prepare ZIF-8 membranes at room temperature. The vapor modification of bromomethylated poly(2,6-dimethyl-1,4-phenylene oxide) (BPPO) substrates using EDA was employed to enhance the nucleation density. Compared with that of the membrane fabricated with the original substrate, the ZIF-8 membrane on the modified BPPO substrate showed better continuity. The prepared membrane displayed a C_3H_6 permeance of $0.75 \times 10^{-8} \text{ mol s}^{-1} \text{ m}^{-2} \text{ Pa}^{-1}$ and a $\text{C}_3\text{H}_6/\text{C}_3\text{H}_8$ ideal selectivity of 28.8 after annealing at 150°C [85]. Using a metal-chelating poly-thiosemicarbazide (PTSC) substrate, Barankova et al. fabricated a compact and ultrathin ZIF-8 membrane with a thickness of 620 nm. The contra-diffusion synthesis cell and SEM image of the prepared ZIF-8 membrane are shown in Fig. 5. The membrane displayed distinct $\text{H}_2/\text{C}_3\text{H}_8$ and $\text{C}_3\text{H}_6/\text{C}_3\text{H}_8$ ideal selectivities of 8350 and 150, respectively [86].

The tube- and hollow fiber-type constructions of separation membranes are beneficial for industrial applications. Xie et al. combined contra-diffusion synthesis and substrate modification to prepare ZIF-8 membranes on macroporous Al_2O_3 tubes. To decrease the pore size and improve heterogeneous crystallization, the macroporous substrate was coated with Al_2O_3 particles having grafted APTES, before growth. After crystallization by contra-diffusion synthesis, a ZIF-8 membrane with a thickness of 2 μm was formed. The H_2 permeance and H_2/N_2 ideal selectivity of the membrane were $5.73 \times 10^{-5} \text{ mol s}^{-1} \text{ m}^{-2} \text{ Pa}^{-1}$ and 17.1, respectively [87]. Huang et al. used the contra-diffusion method to synthesize a ZIF-71 membrane on an inorganic hollow fiber substrate (Fig. 6). Owing to the fast reaction, it is difficult to synthesize ZIF-71 membranes in mixed precursor solutions. However, using contra-diffusion synthesis, the crystallization between the Zn-based solution and imidazole linker solution was easily controlled. The prepared ZIF-71 membrane presented good performance in pervaporation for alcohol–water separation [88].

Using the concept of contra-diffusion synthesis, Kwon and Jeong developed a novel in situ contra-diffusion growth method to prepare a ZIF-8 membrane. A porous substrate was impregnated with a zinc source solution, and subsequently immersed into MeIM solution, for crystallization under thermal treatment. The formed ZIF-8 membrane, with a thickness of 1.5 μm , was well-intergrown. Owing to MOF formation in the porous substrate, the membrane showed excellent compatibility. The membrane displayed good separation performance, with a C_3H_6 permeance of $2.0 \times 10^{-8} \text{ mol s}^{-1} \text{ m}^{-2} \text{ Pa}^{-1}$ and a $\text{C}_3\text{H}_6/\text{C}_3\text{H}_8$ selectivity of 55 [89]. The

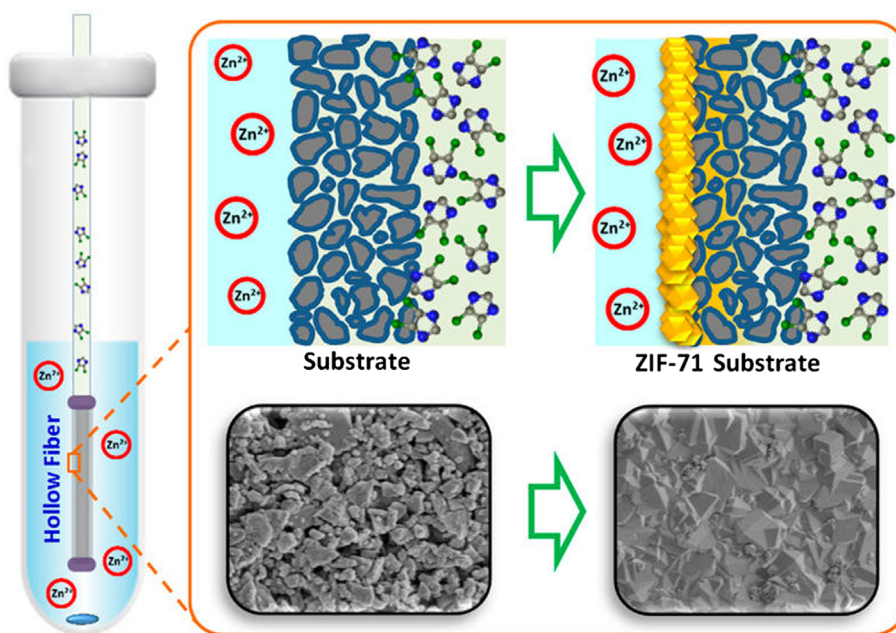


Fig. 6. Schematic illustration for preparation of ZIF-71 membrane by contra-diffusion. Adapted from Ref. [88] with permission from the American Chemical Society.

method was also employed to repair MOF membranes with cracks, and offer seeds for obtaining MOF membranes by the solvothermal method [90]. To further enhance the selectivity, they controlled the microstructures of the ZIF-8 membrane by varying the sodium formate/MeIM ratio and zinc salt type. When the membrane was synthesized with a sodium formate/MeIM ratio of 0.12 and mixed zinc nitrate–zinc chloride source, an improved C_3H_6/C_3H_8 selectivity of 70 and a C_3H_6 permeance of $2.7 \times 10^{-8} \text{ mol s}^{-1} \text{ m}^{-2} \text{ Pa}^{-1}$ were achieved [91]. Furthermore, the same group employed microwave synthesis instead of thermal treatment to enhance the crystallization. The synthesis time could even be shortened to about 90 s [92].

2.3. Layer-by-layer assembly

For layer-by-layer (LBL) assembly, metal salt solutions and linker solutions are applied successively to coat the substrates [93–96]. During the interval of precursor coating, the substrate is rinsed using a pure solvent to remove the excess precursors. Using the inconsecutive MOF crystallization process, the membrane thickness can be precisely controlled. Moreover, this method is performed at mild conditions and is feasible for the production of MOF membranes on a large scale. Shekhah et al. employed this approach to fabricate continuous ZIF-8 membranes on Al_2O_3 substrates. Zinc nitrate and MeIM solutions were deposited on the substrate consecutively. The prepared ZIF-8 membrane showed a controllable thickness from 0.5 to 1.6 μm , with an increase in the number of growth cycles from 150 to 300. However, in C_3H_6/C_3H_8 separation, the membrane with a thickness of 1.6 μm displayed a relatively poorer selectivity of 2.2 and a lower gas permeance than those of the membranes in earlier studies. This phenomenon was attributed to the relatively poor internal microstructure of the prepared ZIF layer [97]. Owing to the mild synthesis conditions, this method is suitable for assembling MOF membranes on polymeric substrates. A PSF ultrafiltration membrane was employed to support the CuBTC and ZIF-8 layers. After LBL assembly for 7 cycles at ambient conditions, the prepared CuBTC membrane with a thickness of 25 μm , and a ZIF-8 membrane with a thickness of 10 μm , were formed. The CuBTC membrane exhibited H_2/CO_2 and H_2/C_3H_6 selectivities of 7.2 and 5.7, but the ZIF-8 membrane displayed a poor separation performance [98].

For a better control of the LBL assembly, spin coating was introduced to fabricate MOF membranes via a high-throughput route. Compared with that of traditional LBL assembly, this approach made a more significant progress in shortening the preparation time and reducing precursor consumption [99]. Using this method, CuBTC and ZIF-8 membranes were deposited on various substrates, including glass, silicon, stainless steel, and aluminum oxide. Heinke et al. combined the spraying technique and LBL assembly to prepare MOF films and membranes (Fig. 7). By spray-coating different precursor solutions through movable nozzles, MOF films and membranes were prepared on dense and porous substrates and could be produced on a large scale. The thickness of the CuBTC membrane on the porous Al_2O_3 substrate was controllable and low. For example, the membranes prepared with 100 and 150 cycles had thicknesses of 460 and 500 nm, respectively. The CuBTC membrane exhibited a good H_2/CO_2 separation performance, with a selectivity of up to 8.5 and a H_2 permeance of $3.0 \times 10^{-8} \text{ mol s}^{-1} \text{ m}^{-2} \text{ Pa}^{-1}$ [100].

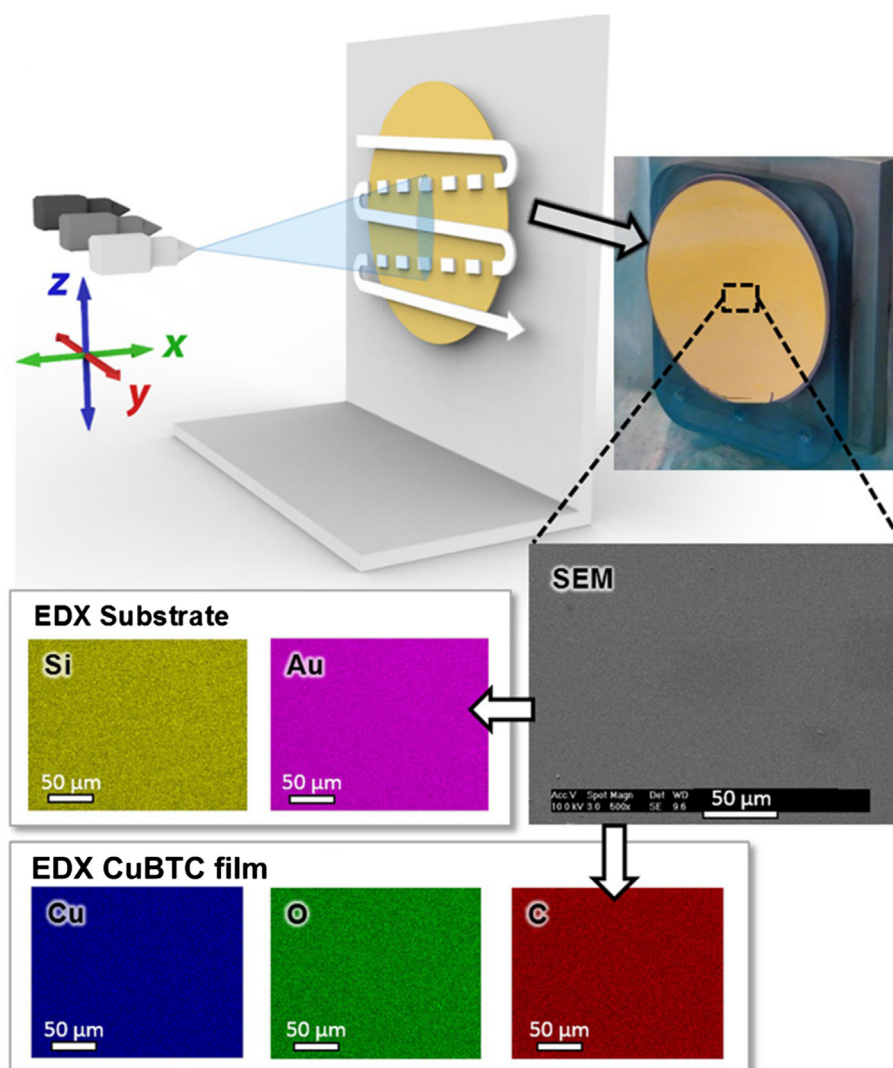


Fig. 7. Synthesis setup of LBL assembly assisted by the spraying technique, and EDX mapping of the prepared CuBTC membrane. Adapted from Ref. [100] with permission from Wiley-VCH.

2.4. Microfluidic processing

Microfluidic processing is based on the combination of membrane module construction and the crystallization mechanisms of direct crystallization, interfacial synthesis, or contra-diffusion synthesis. Profiting from the use of hollow fiber substrates, mixed precursors or two non-hybrid precursors can flow in the tube side or separately in the tube and shell sides. MOF membranes are deposited on the substrates by the flowing precursors. Huang et al. successfully grew a ZIF-8 membrane on the inner surface of a ceramic hollow fiber using a flowing precursor mixture. APTES with amine groups was grafted onto the surface of the substrate to improve the density of heterogeneous nucleation sites. After crystallization, a continuous ZIF-8 membrane with a thickness of 2.0 μm was deposited on the inner surface of the ceramic hollow fiber. The outer hollow fiber could protect the inner MOF membranes from mechanical scratches. The membrane showed a high H_2 permeance of $4.3 \times 10^{-7} \text{ mol s}^{-1} \text{ m}^{-2} \text{ Pa}^{-1}$, with a selectivity of 11.1 for H_2/N_2 and 12.1 for H_2/CH_4 . The membrane also exhibited excellent long-term stability, with almost no change in H_2/CH_4 separation over 200 h [101]. As mentioned above, polymeric hollow fibers exhibit good processability. Cacho-Bailo et al. synthesized ZIF-7 and ZIF-8 membranes on the inner surface of PSF hollow fibers using the microfluidic processing method (Fig. 8a and b). The continuous ZIF-7 and ZIF-8 membranes with good compatibility had thicknesses of 2.4 and 3.6 μm , respectively (Fig. 8c and d). The H_2 permeance through the prepared ZIF-7 and ZIF-8 membranes was 2.2 and $4.7 \times 10^{-9} \text{ mol s}^{-1} \text{ m}^{-2} \text{ Pa}^{-1}$, respectively. These values were much smaller than $8.2 \times 10^{-8} \text{ mol s}^{-1} \text{ m}^{-2} \text{ Pa}^{-1}$ for the original PSF hollow fiber. Compared with the PSF hollow fiber membrane H_2/N_2 - H_2/CH_4 selectivities of 3.1–3.6, the ZIF membranes exhibited much higher H_2/N_2 - H_2/CH_4 selectivities of 35.1–34.6 (ZIF-7 membrane) and 18.3–17.2 (ZIF-8 membrane). These results demonstrated that the MOF layers played critical roles in gas separation. The prepared ZIF-7 membrane also showed an excellent performance in CO_2/N_2 and CO_2/CH_4 separation, with

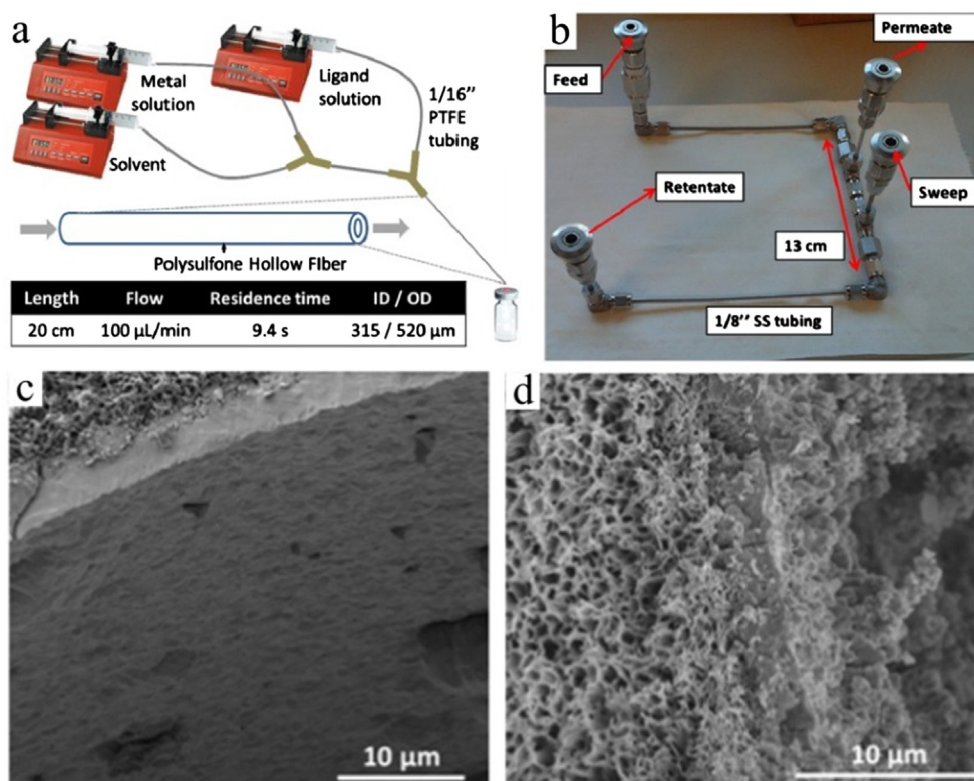


Fig. 8. (a) Microfluidic setup for membrane synthesis. (b) Stainless-steel module for permeation tests. (c and d) SEM images of ZIF-8 and ZIF-7 hollow fiber membranes. Adapted from Ref. [102] with permission from Elsevier.

selectivities of 13.6 and 13.5, respectively [102]. Using a similar method, the ZIF-93 membrane was synthesized on the inner surface of a co-polyimide P84 hollow fiber. After annealing, the membrane exhibited much higher selectivities of 97 (H_2/CH_4) at 100 °C and 17 (CO_2/CH_4) at 35 °C [103]. However, compared with those of other reported membranes, these membranes exhibited a relatively lower permeance, due to the high mass transfer resistance from the applied hollow fiber substrates (Table 3). To enhance heterogeneous crystallization, Lee et al. firstly prepared seed layers on the inner surface of Matrimid hollow fibers and then fabricated a defect-free ZIF-8 membrane by microfluidic processing, using a flowing precursor mixture. The prepared ZIF-8 membrane with a thickness of 800 nm displayed a good permeance of $1.8 \times 10^{-8} \text{ mol s}^{-1} \text{ m}^{-2} \text{ Pa}^{-1}$ and a selectivity of 46 in $\text{C}_3\text{H}_6/\text{C}_3\text{H}_8$ separation [104].

Although microfluidic synthesis from direct crystallization has a good potential for the production of MOF membranes, bulk crystallization still occurs. Using a combination of microfluidic processing and interfacial synthesis, as shown in Fig. 9a, Brown et al. developed interfacial microfluidic membrane processing (IMMP) to produce ZIF-8 membranes on Torlon hollow fibers. Different from the microfluidic synthesis with mixed precursor solutions, two non-interfering Zn/octanol and MeIM/water solutions were separately passed into the tube side and shell side. The ZIF-8 membrane was synthesized on/in polymeric hollow fibers that had been packaged into membrane modules beforehand (Fig. 9b and c). By changing the solvents for dissolving the reactants, and the positions of the precursor solutions, the ZIF-8 layers were controllably deposited on the inner surface, on the outer surface, and in the fiber. Benefiting from the two non-hybrid precursor solutions, the reactants could be recycled. The prepared ZIF-8 hollow fiber membrane, with a thickness of 9 µm, exhibited moderate $\text{H}_2/\text{C}_3\text{H}_8$ (370) and $\text{C}_3\text{H}_6/\text{C}_3\text{H}_8$ (12) selectivities (Fig. 9d and e) [105]. Employing non-isothermal processing with linearly increasing temperature from 22 to 42 °C, and using modified polyamide-imide (PAI) hollow fibers as the substrate, the defects and the thickness of the ZIF-8 membrane were controlled, owing to the enhanced nucleation of the initial ZIF-8 crystals. The prepared ZIF-8, with a thickness of 5 µm, showed higher $\text{H}_2/\text{C}_3\text{H}_8$ (2018) and $\text{C}_3\text{H}_6/\text{C}_3\text{H}_8$ (65) selectivities [106]. By further controlling the synthesis conditions of the ZIF-8 membrane, extraordinary selectivities of 3200 for $\text{H}_2/\text{C}_3\text{H}_8$ and 180 for $\text{C}_3\text{H}_6/\text{C}_3\text{H}_8$ were achieved, and maintained at 90 for $\text{C}_3\text{H}_6/\text{C}_3\text{H}_8$ under a high feed pressure of 9.5 bar. This is very important for the practical application of ZIF-8 membranes in $\text{C}_3\text{H}_6/\text{C}_3\text{H}_8$ separation [107]. This method was also applied to synthesize ZIF-90 membranes on carbon hollow fibers for separating water/organic mixtures [108]. The volatile CHCl_3 and isobutanol were employed as solvents to fabricate MOF membranes by IMMP. The application of volatile solvents was beneficial to the activation of the MOF membranes. Through this method, CuBTC and ZIF-8 membranes were deposited on polybenzimidazole (PBI) hollow fiber modules directly. The prepared CuBTC membrane exhibited He/N_2 and $\text{He}/\text{C}_3\text{H}_8$ selectivities of 12 and 17, respectively [109]. In consideration of environmentally friendly production, Marti et al. employed water as the solvent to perform microfluidic processing based on contra-diffusion synthesis. By passing zinc nitrate and MeIM aqueous solutions through the shell and tube sides,

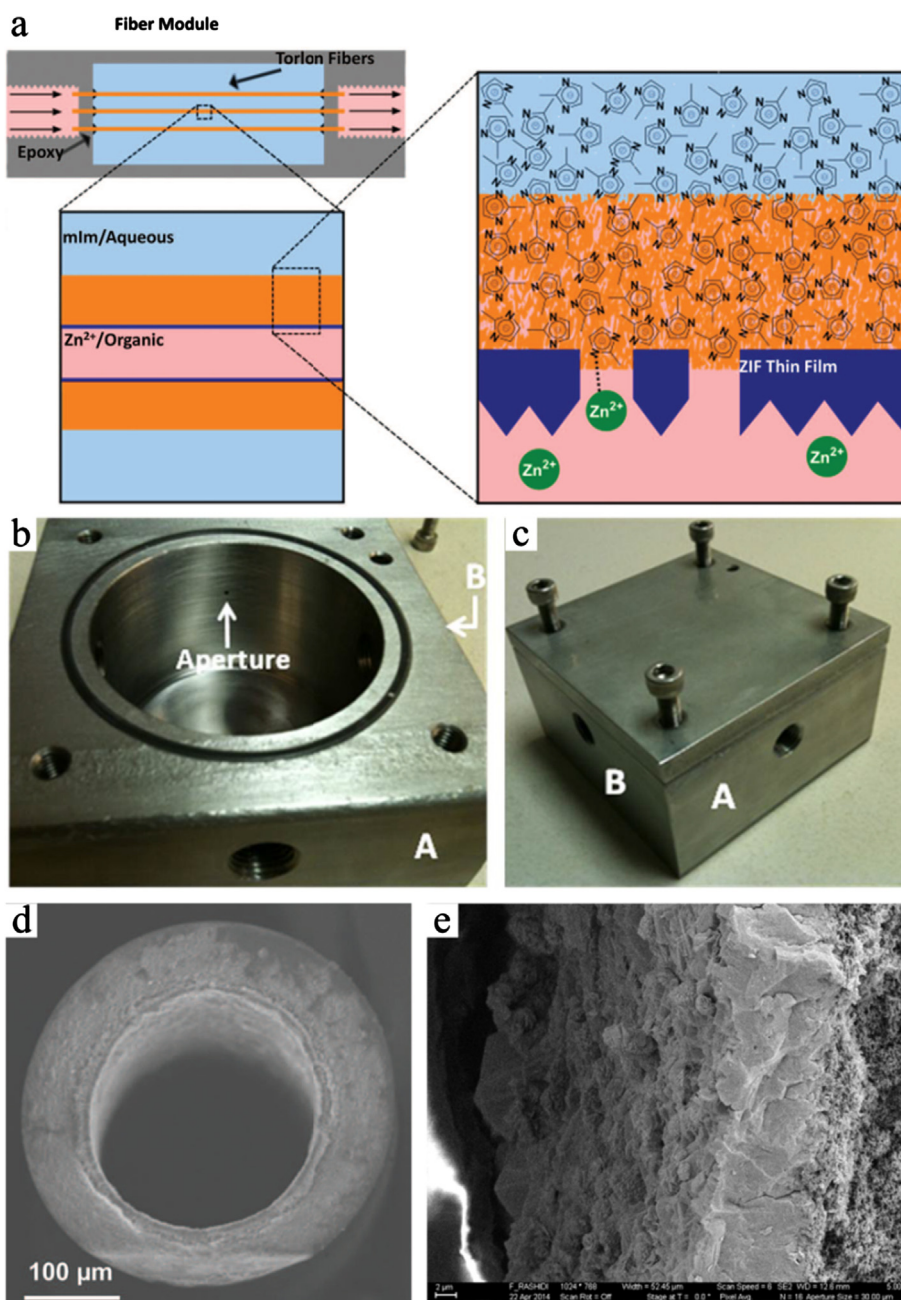


Fig. 9. (a) Scheme of IMMMP. (b) IMMMP reactor and permeation module. (c and d) SEM images of the prepared ZIF-8 membrane. Adapted from Ref. [105] with permission from the American Academy of Sciences.

respectively, a continuous ZIF-8 membrane was formed on the outer surface of a Torlon hollow fiber, and exhibited a high CO_2/N_2 selectivity of 52 and a CO_2 permeance of $7.3 \times 10^{-9} \text{ mol s}^{-1} \text{ m}^{-2} \text{ Pa}^{-1}$ [110].

2.5. Confinement conversion

Unlike the methods mentioned above, which involve MOF crystallization with two dissolved precursors, confinement conversion refers to the formation of MOF membranes via the transformation of the confined solid metal source in the linker solution. Owing to the reaction between a liquid and solid, confinement conversion shows excellent controllability. Peng et al. developed this method to prepare CuBTC membranes [111]. A copper hydroxide nanostrand (CHN) film was prepared by filtration, and subsequently converted to a free-standing CuBTC membrane by immersion in the linker ethanol/water solution at room temperature. After an only 2 h reaction, the CHN film was completely converted to a CuBTC membrane with a thickness of 5 μm . During the conversion, the crystals

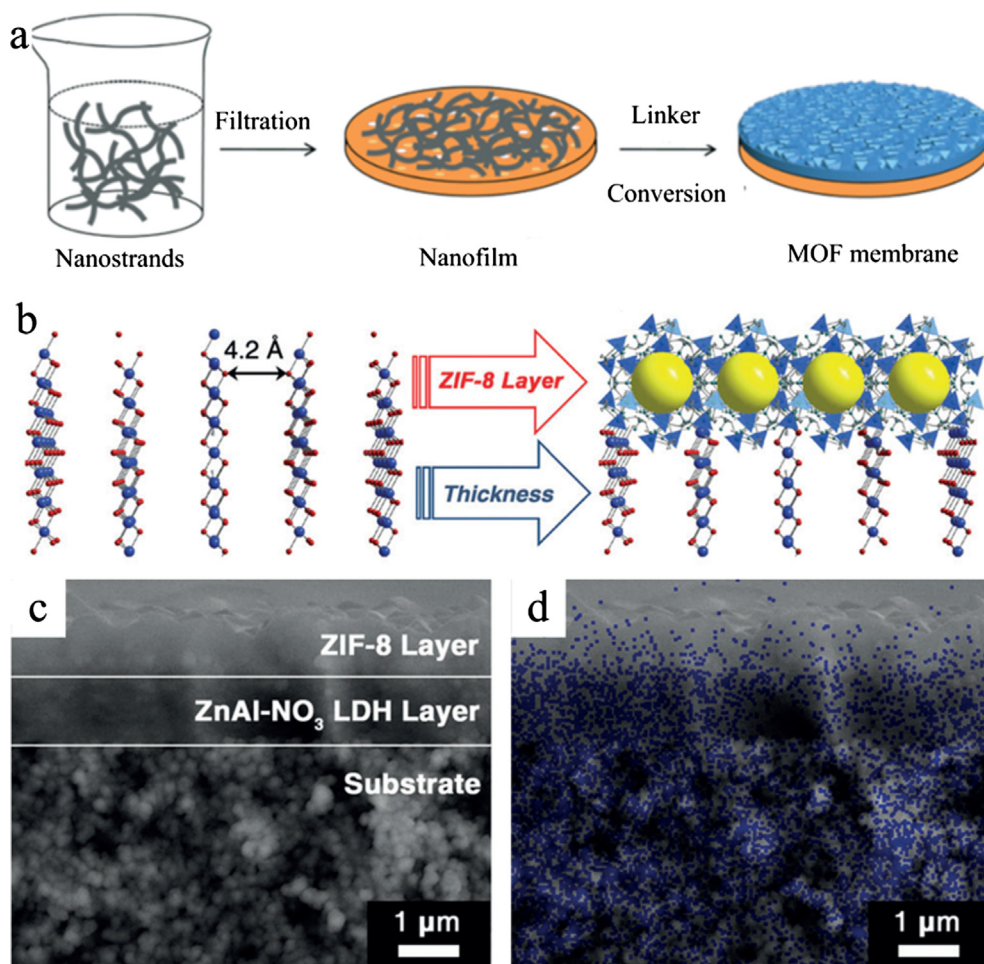


Fig. 10. (a and b) Schematic illustration of ZIF-8 membrane conversion from zinc hydroxide nanostrand and ZnAl-NO₃ LDH layer. (c and d) SEM image and EDX mapping of ZIF-8 membrane for ZnAl-NO₃ LDH layer. Blue dots show O distribution. Adapted from Refs. [112,117] with permission from the Royal Society of Chemistry and Wiley-VCH, respectively.

of the CuBTC membrane changed from cubes to cuboctahedrons with the extension of the reaction time. At room temperature, the membrane showed a high H₂ permeance of $1.58 \times 10^{-6} \text{ mol s}^{-1} \text{ m}^{-2} \text{ Pa}^{-1}$ and selectivities of 6.1 for H₂/CO₂, 5.0 for H₂/N₂, and 4.0 for H₂/CH₄. Employing zinc hydroxide nanostrands (ZHNS) as the metal source, ZIF-8 and MOF-5 membranes were also prepared (Fig. 10a) [112,113]. The ZIF-8 membrane exhibited a high permeance, but a relatively poor molecular sieving property, due to the small thickness of 800 nm. To enhance the selectivity, the converted ZIF-8 layer was used as the seed to synthesize a denser ZIF-8 membrane with a thickness of 2.5 μm, by direct crystallization at 30 °C [112]. After crystallization, higher H₂/N₂ (12.5) and H₂/CH₄ (9.8) ideal selectivities were achieved, while the H₂ permeance was maintained at $47.1 \times 10^{-7} \text{ mol s}^{-1} \text{ m}^{-2} \text{ Pa}^{-1}$. To fabricate a CuBTC membrane on polymeric hollow fiber substrates, the CHN film was deposited on PVDF hollow fibers by vacuum filtration, and converted to a CuBTC membrane by immersion in a linker solution [114]. During the MOF membrane synthesis, a vacuum pump was kept on to prevent the spalling of the CHN film from the hollow fiber. The prepared CuBTC membrane showed a high H₂ permeance of $2.0 \times 10^{-6} \text{ mol s}^{-1} \text{ m}^{-2} \text{ Pa}^{-1}$ and selectivities of 8.1 for H₂/CO₂, 6.5 for H₂/N₂, and 5.4 for H₂/CH₄. The exposed crystal facets of MOF membranes are very important for the separation performance, due to the different pore sizes. The same group fixed Au nanoparticles with immobilized citrate modulators in a CHN film to fabricate a composite CuBTC membrane [115]. After crystallization at room temperature, an oriented cube CuBTC membrane with exposed (0 0 1) facets was formed. For the CuBTC membrane without Au nanoparticles, when a water/ethanol linker solution was applied, a cuboctahedron membrane with both, exposed (0 0 1) and (1 1 1), facets was fabricated; when an ethanol linker solution was employed, an octahedron membrane with exposed (1 1 1) facets was formed. Among these membranes, the cube CuBTC membrane exhibited the highest permeance, but the lowest selectivity of 1.5 in the separation of CO₂ (KD: 3.3 Å) from SF₆ (KD: 5.8 Å), whereas the octahedron CuBTC membrane with exposed (1 1 1) facets showed the lowest CO₂ permeance, but the highest selectivity of 13.1.

Some other metal-based materials can also be employed to fabricate MOF membranes. Liu et al. employed the ZnAl-NO₃ layered double hydroxide (LDH) to fabricate ZIF-8 membranes [116,117]. As shown in Fig. 10b, the LDH layer with a thickness of 2.5 μm was firstly grown on porous Al₂O₃ substrates at 65 °C for 40 h, using the hydrothermal method. The obtained LDH membrane was

immersed in MeIM methanol solution to obtain the composite membrane by solvothermal treatment at 80 °C for 36 h [117]. MeIM reacted with the ZnAl-NO₃ LDH and formed the ZIF-8 membrane. The composite membrane consisted of a bottom LDH layer with a thickness of 1.3 μm and a top ZIF-8 layer with a thickness of 1.1 μm. At 90 °C, the prepared composite membrane exhibited a moderate H₂ permeance of $4.1 \times 10^{-8} \text{ mol s}^{-1} \text{ m}^{-2} \text{ Pa}^{-1}$, with high H₂/CH₄, CO₂/CH₄, and H₂/N₂ selectivities of 54.1, 12.9, and 16.8, respectively. Owing to the high porosity and precise molecular property of ZIF-8, the H₂ permeance and H₂/CH₄ selectivity were enhanced by about 2 and 5 times, respectively, compared with those of the obtained pure LDH membrane. To further improve the selectivity, the LDH membrane was calcined into a ZnO layer and then partially converted to the ZIF-8 membrane. As the residual ZnO layer could effectively suppress the flexibility of the framework, the prepared ZIF-8 composite membrane exhibited higher H₂/N₂ (23.2) and H₂/CH₄ (77.2) selectivities than those of the ZIF-8-ZnAl-NO₃ composite membrane [118]. Drobek et al. converted a ZnO layer, which was prepared by atomic layer deposition, into a ZIF-8 membrane. The membrane showed a H₂ permeance of $1.0 \times 10^{-7} \text{ mol s}^{-1} \text{ m}^{-2} \text{ Pa}^{-1}$, and ideal selectivities of 7.8 for H₂/CO₂ and 12.5 for H₂/CH₄ [119]. In addition to synthesis by conversion in a linker solution, some studies employed metallic oxides such as ZnO to fabricate MOF membranes by simultaneous conversion and direct crystallization in a mixed precursor solution or by partial conversion for seeds and subsequent secondary hydro/solvothermal treatment for continuous membranes [120–123].

2.6. Vapor deposition

For the MOF membranes synthesized using solutions, the reactant transport and fluid dynamic processes are usually complex and should be controlled carefully. Chemical vapor deposition refers to the reaction between solid and gas phases [124]. Stassen et al. demonstrated that a ZIF-8 film with a controlled thickness could be processed by chemical vapor deposition [125]. A zinc oxide film was firstly coated on a dense substrate and subsequently transformed into the ZIF-8 film by MeIM vapor exposure at ~100–150 °C. This method was used to deposit ZIF-8 films on challenging substrates, even on high-aspect-ratio array substrates. However, the atomic layer deposition of a uniform ZnO layer on substrates is complex and hard to scale up. Moreover, synthesis mechanisms for MOF layers with smooth dense substrates and rough porous substrates are very different, and MOF membranes for separation applications have more stringent requirements of continuity than those for MOF films. Li et al. developed gel-vapor deposition (GVD), which combined sol-gel coating of a metal source and vapor deposition of a linker to produce MOF membranes in an environment-

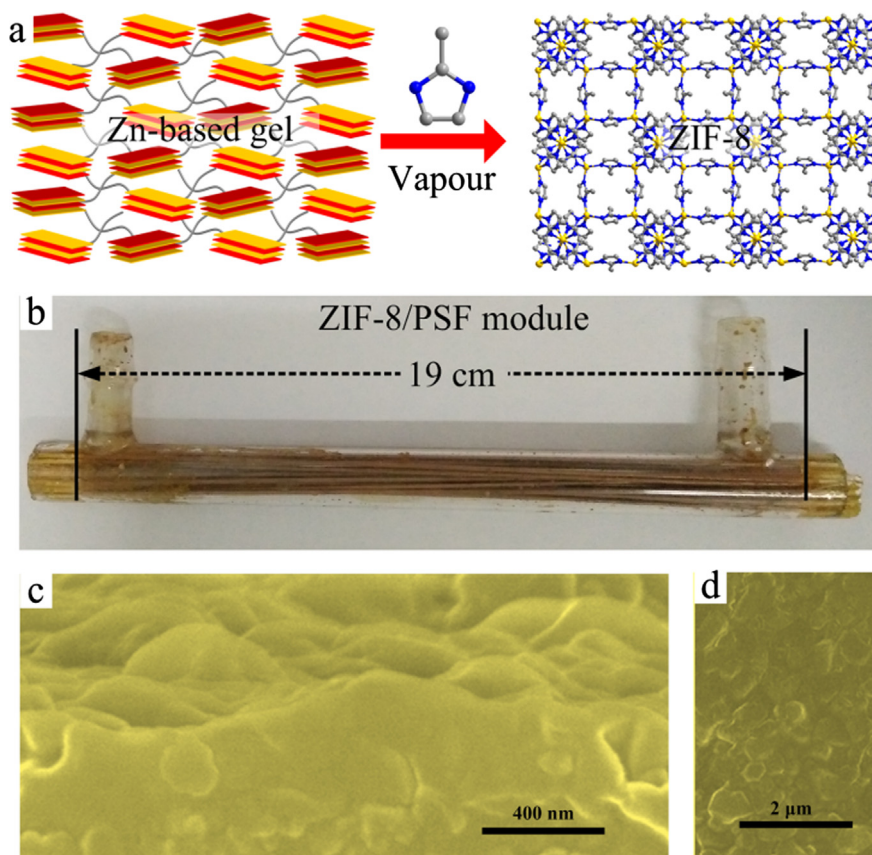


Fig. 11. (a) Schematic illustration of GVD. (b) Digital photograph of ZIF-8 membrane module. (c and d) SEM images of ZIF-8 layer on membrane module. Adapted from Ref. [126] with permission from the Nature Publishing Group.

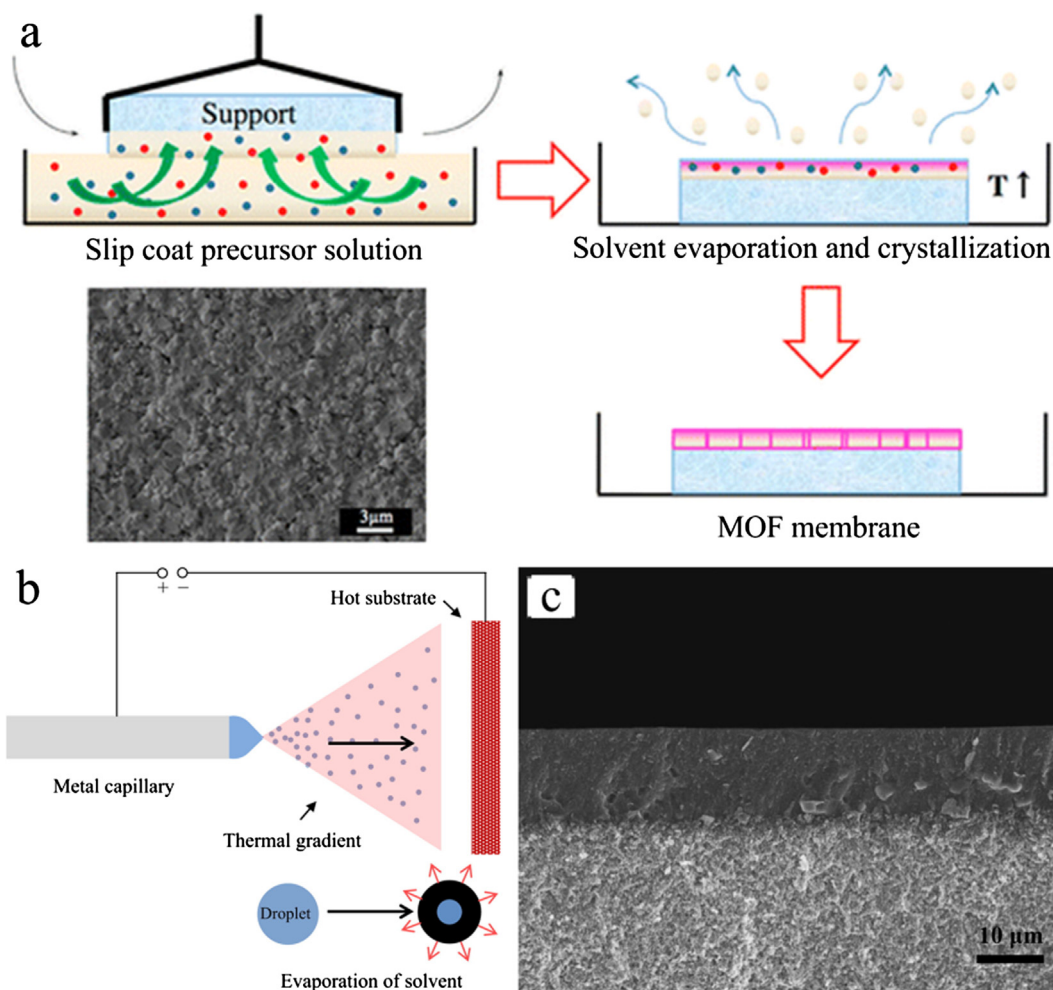


Fig. 12. (a) Schematic illustration of RTD, and SEM image of the prepared CuBTC membrane. (b and c) Schematic illustration of electro spray deposition, and SEM image of the prepared ZIF-7 membrane. Adapted from Refs. [127,128] with permission from the American Chemical Society and Elsevier.

friendly and scalable manner (Fig. 11) [126]. In this method, the metal-based gel, composed of zinc-ethanolamine complexes and layered basic zinc acetate nanocrystals, was firstly coated on PVDF hollow fibers by heat treatment. Then, the organic groups of the gel were substituted using MeIM vapor, to form the ZIF-8 layer. By controlling the procedures of sol-gel coating and vapor deposition, the thickness of the prepared ZIF-8 membrane could be adjusted from tens of nanometers to several micrometers. Unlike the traditional hydro/solvothermal method for MOF membrane synthesis by GVD, pre-treatment of the substrates and solvents during crystallization was not needed, the MOF layers and substrates were compatibly interdigitated, the expensive MOF precursors were reusable, the positions of the MOF layers could be manipulated, and the synthesis process was time-saving. Moreover, GVD was used to process, in situ, a continuous MOF layer on a membrane module with 30 hollow fibers and a 340 cm² membrane area, without deterioration in the permselectivity. The prepared membrane showed a high permeance of $1.2 \times 10^{-5} \text{ mol s}^{-1} \text{ m}^{-2} \text{ Pa}^{-1}$ and a selectivity of 3126 for H₂/C₃H₈ separation, as well as $2.8 \times 10^{-7} \text{ mol s}^{-1} \text{ m}^{-2} \text{ Pa}^{-1}$ and 73.4 for C₃H₆/C₃H₈ separation.

2.7. Others

Some other methods have also been proposed for the scalable production of MOF membranes. Rapid thermal deposition (RTD) was exploited by Shah et al. (Fig. 12a). RTD was used to fabricate continuous MOF membranes via a commercializable route. A porous substrate was coated with a precursor mixture with both the metal salt and linker, and then subjected to heat treatment at high temperatures of ~180–200 °C, for crystallization. This method greatly reduced the synthesis time and consumption of precursors [127]. Employing RTD, ZIF-8 and CuBTC membranes that exhibited good separation performance were fabricated. For the prepared CuBTC membrane, the ideal selectivities for H₂/N₂, H₂/CH₄, and H₂/SF₆ were 13.7, 8.8, and 600, respectively, with a H₂ permeance of $3.0 \times 10^{-7} \text{ mol s}^{-1} \text{ m}^{-2} \text{ Pa}^{-1}$. For the ZIF-8 membrane, the C₃H₆ permeance and C₃H₆/C₃H₈ selectivity were $0.7 \times 10^{-8} \text{ mol s}^{-1} \text{ m}^{-2} \text{ Pa}^{-1}$ and 30, respectively. Owing to the growth of MOF crystals in the porous substrates, the membranes

might possess excellent compatibility. Melgar et al. developed an electrospray deposition method for fabricating uniform and continuous ZIF-7 membranes on alumina substrates [128]. As shown in Fig. 12b and c, this method was simple, reproducible, and time-/precursor-saving. By controlling the sprayed solution volume from 0.05 to 0.5 ml, the membrane thickness could be adjusted from 2 to 22 μm . The prepared ZIF-7 membrane exhibited a H_2/CO_2 selectivity of 18.3, with a H_2 permeance of $3.1 \times 10^{-7} \text{ mol s}^{-1} \text{ m}^{-2} \text{ Pa}^{-1}$, at 150 °C. Considering the unique features of the synthesis procedures and the good performance of the prepared membranes, these two methods show great potential for the large-scale production of MOF membranes for industrial applications. Electrophoretic deposition has been reported for MOF synthesis. However, this method was generally employed to deposit MOF films or seed layers for membrane fabrication [72,129].

3. Modification of MOF membranes

For MOF membrane synthesis, solvents such as methanol, ethanol, and DMF are always required. After crystallization, the solvents and linkers are usually entrapped in the cavities of the frameworks. These guest molecules affect the gas pathways and affinity of the MOF membranes tremendously, and even make the membranes impermeable [50]. Activation, for opening up the pore structures, is critical to the separation performance of MOF membranes. Li et al. found that activation enhanced the H_2 permeance, H_2/N_2 selectivity, and H_2/CO_2 selectivity of the NH_2 -MIL-53 membrane 330, 5.1, and 5.5 times, respectively, compared with those of the as-synthesized membrane [79]. Several methods such as thermal treatment, on-stream activation, and solvent exchange have been proposed to remove the guest molecules in MOF membranes. However, the synthesis and activation processes may lead to crack formation [130]. It is well-known that the mechanical stability of MOFs is relatively weak, especially the low strength against shear force [131,132]. When the applied force on MOFs exceeds the critical point, the frameworks collapse. For polycrystalline MOF membranes, the issue of poor mechanical stability may be aggravated. During membrane synthesis and activation, MOF membranes are immersed into and taken out from organic solvents; the difference in swelling between the substrates and MOF layers produces the shear force, and leads to the formation of defects both at the grain boundaries and in the grains [67]. These defects provide useless molecular transport channels and greatly reduce the selectivity of MOF membranes. The guest molecules entering into and escaping from the frameworks may also lead to the stretching or shrinking of MOF layers, thereby generating cracks.

The molecular separation by MOF membranes is governed by both the sorption property and diffusivity of feed components in the selective layer [133]. In molecular sieving, the sizes of the permeated molecules and blocked molecules, as well as MOF apertures, are vital for separation performance. In theory, the ideal case for separation is that the size of the apertures is larger than that of the permeated molecules, but smaller than that of the blocked molecules. This is the reason for the excellent performance of ultramicroporous MOFs with apertures of 3–6 Å [133–135]. The interaction of MOFs with molecules significantly affects the separation performance as well. Firstly, a superior interaction improves the sorption of penetrated molecules onto MOFs, thus improving the selectivity. UiO-66, a type of MOF with an aperture of 6 Å, and composed of benzene 1,4-dicarboxylic acid (BDC) linkers and Zr-based metal centers, was proposed for the fabrication of membranes to separate CO_2 (KD: 3.3 Å) from CH_4 (KD: 3.8 Å), owing to its good affinity for CO_2 [136]. Secondly, a strong interaction diminishes the diffusion of molecules in MOF membranes. On one hand, the strong affinity of the penetrated molecules toward MOFs suppresses the diffusion of the blocked molecules, and thereby increases the selectivity. Due to the large 1.2 nm aperture size, the MOF-5 membrane showed no selectivity for CO_2/CH_4 at low CO_2 pressure. When a higher CO_2 pressure was applied, the prepared MOF-5 membrane exhibited an outstanding CO_2/CH_4 selectivity of 328 [137,138]. On the other hand, a strong interaction between the blocked molecules and MOFs restrains the diffusion in the membranes, and thereby enhances the selectivity. CuBTC and NH_2 -MIL-53 membranes have aperture sizes of 9.0 and 7.5 Å, respectively [139–142]. The strong interaction between CO_2 molecules and the unsaturated metal sites or $-\text{NH}_2$ functional groups of MOFs leads to a lower CO_2 diffusion rate through CuBTC and NH_2 -MIL-53 membranes. Therefore, the H_2/CO_2 selectivity of these membranes is typically much higher than the Knudsen diffusion selectivity. However, for the membranes with the molecular sieving property, the fabrication of MOF membranes with an aperture size between the sizes of two feed components is uncontrollable, due to the flexibility of the frameworks. The ZIF-7 membrane has a sod-structure with 3.0 Å pore windows, but shows a H_2/CO_2 selectivity usually less than 20, due to the framework flexibility [143–145]. For the membranes governed by the interaction of the MOFs with molecules, the selectivities, for example, for separating CO_2 from N_2 and CH_4 , are usually lower than those of polymeric membranes and MMMs [146–153]. Although MOF membranes have excellent permeance and have been rapidly developed recently, only few membranes satisfy the requirements for industrial application, with respect to separation performance [154,155]. Consequently, further pore size refinement and chemical affinity adjustments are required for preparing better molecular-sieving MOF membranes.

Modification of MOF membranes is advocated to reduce defects, control pore sizes, adjust chemical properties, and integrate introduced nanoparticles, in order to enhance the separation performance and extend the application scope. The types of modified components and their integrated forms dictate the procedures and mechanisms of the modification. In the following section, we discuss modifications ranging from physical coating to epitaxial growth, embedding, occupation, grafting, and substitution. Coating, epitaxial growth, and embedding possibly involve the formation of a chemical interaction between the modified reagents and MOF membranes, but usually do not affect the intrinsic features of the MOFs. Occupation, grafting, and substitution modifications involve both the chemical bond formation between the modified reagents and MOFs, and the changes in the pore structures and affinities, and may even involve the transformation of the metal nodes and linkers. Table 4 shows the modification strategies, membrane properties, and separation performance of modified membranes from the literature.

Table 4
Modification strategies, membrane properties, and separation performance of modified membranes from the literature.

MOF	Substrate	Th (μm)	Method	Component	Per Tem ($^{\circ}\text{C}$)	Gas pair	Before Per ($\times 10^{-8} \text{ mol s}^{-1} \text{ m}^{-2} \text{ Pa}^{-1}$)	After Per ($\times 10^{-8} \text{ mol s}^{-1} \text{ m}^{-2} \text{ Pa}^{-1}$)	Before Sel	After Sel	Ref.
ZIF-8	PE flat	1.5	Coating	PDMS	RT	H ₂ /C ₃ H ₈	–	160.0 ^a	–	22.4 ^a	[156]
ZIF-8	Al ₂ O ₃ disc	2	Coating	PDMS	35	C ₃ H ₆ /C ₃ H ₈	1.8–7.5	1.4–2.4	1–46	23–104	[157]
ZIF-8	Al ₂ O ₃ disc	20	Coating	GO	250	H ₂ /CO ₂	–	12.7	–	14.9	[158]
						H ₂ /N ₂		13.4		90.5	
						H ₂ /CH ₄		12.9		139.1	
ZIF-9	P84 fiber	0.9/1.1	Heteroepitaxial growth	ZIF-8	150	H ₂ /C ₃ H ₈	7.2	11.9	8.0	3816.6	[163]
						H ₂ /CO ₂		8.4		9.6	
ZIF-9	P84 fiber	1.0/1.1	Heteroepitaxial growth	ZIF-67	150	H ₂ /CO ₂	7.2	5.3	8.0	9.0	[163]
ZIF-67	Al ₂ O ₃ disc	0.3/0.7	Heteroepitaxial growth	ZIF-8	RT	C ₃ H ₆ /C ₃ H ₈	4.6	3.7	84.8	209.1	[161]
ZIF-67	Al ₂ O ₃ disc	0.18	Heteroepitaxial growth	ZIF-8	RT	H ₂ /CO ₂	2.1	1.1	6.5	13.2	[162]
						H ₂ /N ₂	3.4	2.1	8.9	9.3	
						H ₂ /CH ₄	2.2	1.7	5.5	11.1	
						H ₂ /C ₂ H ₄	3.5	2.0	8.9	20.6	
						H ₂ /C ₂ H ₆	3.5	1.9	9.6	30.8	
						H ₂ /C ₃ H ₆	3.2	1.7	12.4	49.4	
						H ₂ /C ₃ H ₈	3.0	1.6	10.6	54.7	
UiO-66	SiO ₂	40/60	Heteroepitaxial growth	COF-300	RT	H ₂ /CO ₂	83	38	9.2	17.2	[165]
COF-300	SiO ₂ disc	55/42	Heteroepitaxial growth	[Zn ₂ (bdc) ₂ (dabco)]	RT	H ₂ /CO ₂	81	46	6.0	12.6	[164]
COF-300	SiO ₂ disc	58/42	Heteroepitaxial growth	ZIF-8	RT	H ₂ /CO ₂	81	36	6.0	13.5	[164]
ZIF-7	PVDF fiber	7	Embedding	rGO	RT	H ₂ /CO ₂	–	0.33	–	23.2	[173]
ZIF-8	AAO	0.1	Embedding	GO	25	H ₂ /N ₂	–	5.46 ^a	–	11.1 ^a	[166]
						H ₂ /CH ₄		5.46 ^a		11.2 ^a	
						H ₂ /C ₃ H ₈		5.46 ^a		405.0 ^a	
						CO ₂ /N ₂		3.44 ^a		7.0 ^a	
						CO ₂ /CH ₄		3.44 ^a		7.1 ^a	
						C ₃ H ₆ /C ₃ H ₈		0.16 ^a		12.0 ^a	
ZIF-8	AAO	0.43	Embedding	Porous-GO	25	H ₂ /N ₂	–	117.6 ^a	–	10.0 ^a	[167]
						H ₂ /CH ₄		117.6 ^a		10.4 ^a	
						H ₂ /C ₃ H ₈		117.6 ^a		2409 ^a	
						C ₃ H ₆ /C ₃ H ₈		1.73 ^a		35 ^a	
ZIF-8	AAO	0.24	Embedding	g-C ₃ N ₄	RT	H ₂ /CO ₂	–	3.5	–	26	[168]
ZIF-8	AAO	0.2	Embedding	PDA-CNT	RT	H ₂ /CO ₂	–	2870 ^b	–	14	[169]
						H ₂ /N ₂		2870 ^b		18	
						H ₂ /CH ₄		2870 ^b		35	
						H ₂ /C ₃ H ₈		2870 ^b		950	
ZIF-8	Non	0.55	Embedding	PDA/SWCNT	25	H ₂ /CO ₂	–	57.5	–	34	[170]
						H ₂ /N ₂		63.1 ^a		20 ^a	
						H ₂ /CH ₄		63.1 ^a		38 ^a	
ZIF-8	Non	30	Embedding	CNT	RT	N ₂ /CO ₂	–	2.6 ^b	–	6.9	[171]
ZIF-8	PAN flat	4	Embedding	CA	RT	CO ₂ /N ₂	0.3	0.8	8.1	165.5	[172]

(continued on next page)

Table 4 (continued)

MOF	Substrate	Th (μm)	Method	Component	Per Tem ($^{\circ}\text{C}$)	Gas pair	Before Per ($\times 10^{-8} \text{ mol s}^{-1} \text{ m}^{-2} \text{ Pa}^{-1}$)	After Per ($\times 10^{-8} \text{ mol s}^{-1} \text{ m}^{-2} \text{ Pa}^{-1}$)	After Sel	Ref.
ZIF-8	PVDF fiber	7	Embedding	rGO	RT	H ₂ /CO ₂	-	0.7	18.8	[173]
ZIF-8	PVDF fiber	0.15	Embedding	rGO	RT	H ₂ /CO ₂ H ₂ /N ₂ H ₂ /CH ₄	-	66.7 66.0 63.7	25.3 70.4 90.7	[174]
CuBTC	PVDF fiber	8	Embedding	rGO	RT	H ₂ /CO ₂	-	88	10.0	[173]
MIL-100	PVDF fiber	7.5	Embedding	rGO	RT	H ₂ /CO ₂	-	1.3	12.5	[173]
ZIF-69	Al ₂ O ₃ disc	69	Occupation	[omim][TCM]	30	CO ₂ /N ₂	30–50	0.006–0.004	44–66	[177]
Ni ₂ (L-asp) ₂ (bpe)	Nickel mesh	20–30	Occupation	bpe	25	H ₂ /CO ₂	-	102	24.3	[180]
						H ₂ /N ₂	-	100	12.1	
						H ₂ /CH ₄	-	100	7.77	
ZIF-9	Al ₂ O ₃ disc	30	Occupation/Coating	CNT/[BMIM][TF2N]	25	H ₂ /CO ₂	710.6 ^a	8.42 ^a	40.04 ^a	[178]
						H ₂ /N ₂	710.6 ^a	2.34 ^a	8.48 ^a	
						H ₂ /CH ₄	710.6 ^a	2.86 ^a	10.35 ^a	
ZIF-90	Al ₂ O ₃ disc	20	Grafting	Ethanolamine	200	H ₂ /CO ₂	23.7	7.3	15.3	[58,186]
						H ₂ /N ₂	24.8	11.7	15.8	
						H ₂ /CH ₄	25.1	19.4	18.9	
ZIF-90	Al ₂ O ₃ disc	20	Grafting	APTES	225	H ₂ /CO ₂	29.1	7.2	20.1	[187,188]
						H ₂ /CH ₄	29.0	15.4	70.5	
						H ₂ /C ₃ H ₈	28.5	65.4	458	
ZIF-94	P84 fiber	7.1	Grafting	Nonylamine	35	CO ₂ /CH ₄	3.5	2.2	4.7	[190]
						He/CH ₄	0.5	1.5	79.1	
						H ₂ /CH ₄	0.42	1.6	85.6	
						CO ₂ /CH ₄	0.12	0.53	27.8	
Mg-MOF-74	Al ₂ O ₃ disc	10	Grafting	EDA	25	H ₂ /CO ₂	12	10.5	28	[191]
ZIF-90/ZIF-8	Al ₂ O ₃ disc	1.0	Substitution	Ica	RT	C ₃ H ₆ /C ₃ H ₈	2.1	55	40	[198]
CuBTC/MIL-100	PVDF fiber	20	Substitution	FeCl ₃ ·6H ₂ O	25	H ₂ /CO ₂	201 ^a	6.4 ^a	78	[197]
						H ₂ /N ₂	201 ^a	6.2 ^a	212	
						H ₂ /CH ₄	201 ^a	7.4	312	
ZIF-8-67	Al ₂ O ₃ disc	2.2	Pre-substitution	Zn/Co salts	25	C ₃ H ₆ /C ₃ H ₈	-	0.9	50.5	[199]
ZIF-8-67	Al ₂ O ₃ disc	1.2	Pre-substitution	Zn/Co salts	RT	C ₃ H ₆ /C ₃ H ₈	-	2.0	120.2	[200]
ZIF-9-67	Al ₂ O ₃ disc	30	Pre-substitution	BIM/MeIM	RT	H ₂ /CO ₂	-	1405	8.89	[201]
ZIF-7-8	Al ₂ O ₃ disc	2.0	Pre-substitution	BIM/MeIM	25	H ₂ /CH ₄	16.0	8.4	11.4	[92]
						CO ₂ /CH ₄	5.0	4.5	3.4	
ZIF-8	P84 fiber	1.3	Annealing	Non	35	H ₂ /CH ₄	0.39	0.33	65	[202]
						CO ₂ /CH ₄	0.1	0.067	19.6	
ZIF-93	P84 fiber	2.6	Annealing	Non	100	H ₂ /CH ₄	-	1.0	101.3	[202]
						H ₂ /CH ₄	1.5	1.3	72.4	
						CO ₂ /CH ₄	20.4	0.28	18.4	
ZIF-8	Al ₂ O ₃ disc	0.3	Ripening	MeIM	100	H ₂ /CH ₄	0.47	3.4	103.1	[203]
						C ₃ H ₆ /C ₃ H ₈	-	1.25	120	

^a The data was obtained from the single-component permeation, RT-room temperature.

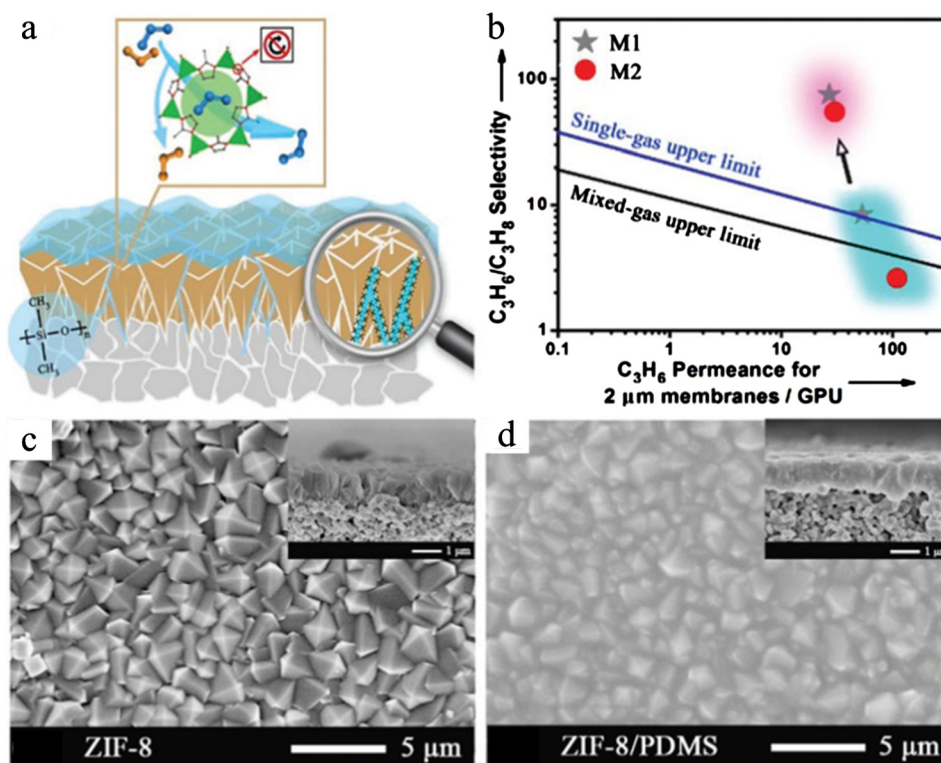


Fig. 13. (a) Scheme of ZIF-8 membrane with PDMS coating layer. (b) C_3H_6/C_3H_8 separation performance of the ZIF-8 membranes with and without PDMS coating. The lines show the upper limits for the C_3H_6/C_3H_8 separation performances of the polymeric membranes. $1 \text{ GPU} = 3.348 \times 10^{-10} \text{ mol s}^{-1} \text{ m}^{-2} \text{ Pa}^{-1}$. (c and d) SEM images of the ZIF-8 membranes with and without PDMS coating. Adapted from Ref. [157] with permission from the Royal Society of Chemistry.

3.1. Coating

To reduce the effect of pinholes on the separation performance, polymers are coated on MOF membranes. The coated polymers generally have a large free volume to maintain the high permeance as much as possible. As a result of pinhole blocking using polymers, the selectivity of the resultant membranes can be enhanced. Barankova et al. fabricated ZIF-8 membranes on polyester (PE) substrates. To better block the potential pinholes and protect the ZIF-8 layer, the prepared ZIF-8 membrane was dipped in methanol solution (50 wt%), pure methanol, methanol/*iso*-octane solution, and pure *iso*-octane sequentially, and then coated with PDMS/*iso*-octane solution (2 wt%) [156]. Although the silicone rubber coating improved the selectivity, the enhancement was limited. The H_2/C_3H_8 ideal selectivity of the PDMS-coated ZIF-8 membrane was only about 22.4. This was attributed to the large hydrocarbon molecules that passed through the silicone rubber faster than hydrogen; for example, the C_3H_8/H_2 selectivity of the silicone membrane was 6.7. The silicone rubbers that exhibit a high permeance and reverse selectivity relative to that of MOF membranes may not effectively enhance the membrane performance. Sheng et al. coated a ZIF-8 membrane with PDMS to improve the C_3H_6/C_3H_8 separation performance. As PDMS blocked the defects and hindered the framework flexibility, the prepared ZIF-8 composite membranes showed a high C_3H_6/C_3H_8 selectivity (Fig. 13). For example, the C_3H_6/C_3H_8 selectivity increased from 3 for the original ZIF-8 membrane to 55 for the coated membrane; however, the C_3H_6 permeance decreased from 2.8 to $1.7 \times 10^{-7} \text{ mol s}^{-1} \text{ m}^{-2} \text{ Pa}^{-1}$. Moreover, due to the excellent hydrophobicity of PDMS, the ZIF-8 composite membrane exhibited improved hydrolytic stability [157].

Graphene oxide (GO) membranes have been verified to exhibit excellent performance in molecular separation. Huang et al. treated the semi-ZIF-8 membranes with a GO solution to obtain bi-continuous GO/ZIF-8 membranes (Fig. 14) [158]. Owing to the capillary forces and covalent bonds, after the deposition of the GO suspension with a concentration of 1 wt% for 5 cycles, the gaps in the semi-ZIF-8 membrane were covered by a GO layer with a thickness of 100 nm; however, the GO covering layer on the ZIF-8 crystals was supposed to be thinner than 2 nm. In gas separation, most of the gas molecules passed through the ZIF-8 crystals and were subjected to molecular sieving. The prepared GO/ZIF-8 membrane showed much higher H_2/CO_2 , H_2/N_2 , H_2/CH_4 , and H_2/C_3H_8 selectivities of 14.9, 90.5, 139.1, and 3816.6, respectively, compared with the continuous ZIF-8 membrane H_2/CO_2 , H_2/N_2 , H_2/CH_4 , and H_2/C_3H_8 selectivities of 8.9, 16.2, 31.5, and 712.6, respectively. However, the composite membrane exhibited a H_2 permeance of $\sim 1.3\text{--}1.4 \times 10^{-7} \text{ mol s}^{-1} \text{ m}^{-2} \text{ Pa}^{-1}$, lower than the pure ZIF-8 membrane H_2 permeance of $\sim 1.8\text{--}2.0 \times 10^{-7} \text{ mol s}^{-1} \text{ m}^{-2} \text{ Pa}^{-1}$ [60].

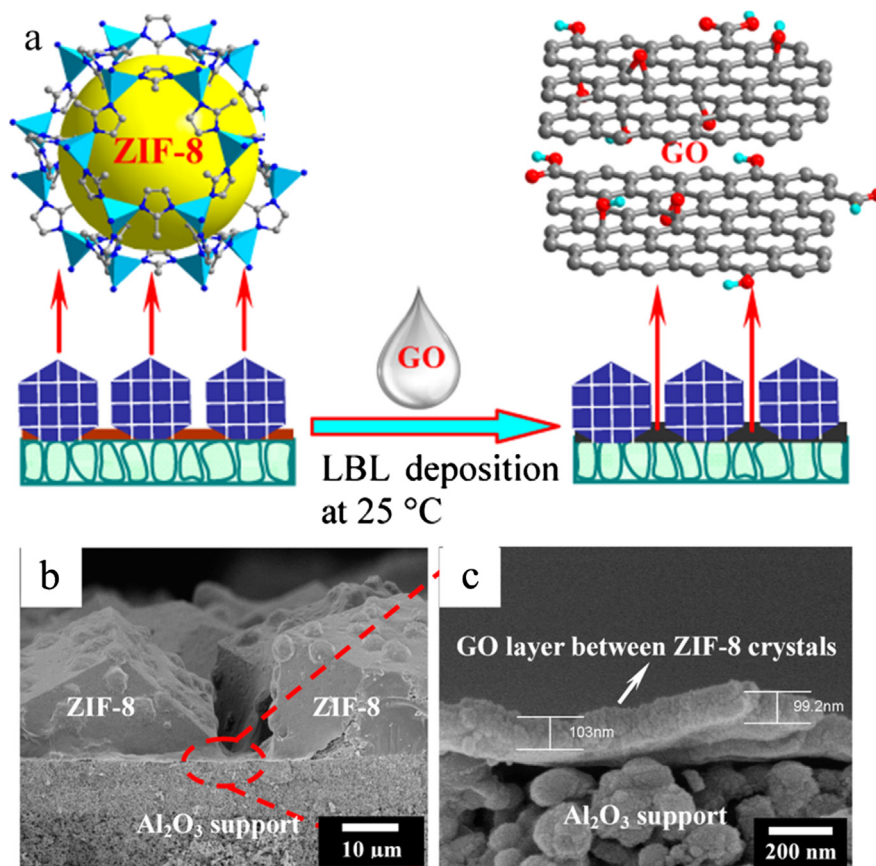


Fig. 14. (a) Scheme of layer-by-layer coating of GO on semi-continuous ZIF-8 layer. (b and c) SEM images of the GO/ZIF-8 composite membrane and GO layer at the gap. Adapted from Ref. [158] with permission from the American Chemical Society.

3.2. Heteroepitaxial growth

Heteroepitaxial growth is an effective strategy to engineer the properties of crystalline materials, and refers to the growth of one crystalline material on another. The different crystals connect with each other by chemical bonds, in heteroepitaxial growth [159,160]. This strategy can not only integrate both the features of the different crystals, but also adjust the microstructure of the interfacial region between the two crystals. As presented in Fig. 15a, Kwon et al. fabricated the heteroepitaxially grown ZIF-8/ZIF-67 membranes by growing ZIF-8 layers on ZIF-67 membranes [161]. A well-intergrown ZIF-67 membrane with a thickness of 700 nm was firstly heteroepitaxially deposited on a ZIF-8 seeded substrate by the secondary solvothermal method. Then, a ZIF-8 layer with a thickness of 300 nm was tertiary heteroepitaxially crystallized on the ZIF-67 membrane after linker treatment. The prepared ZIF-67 membrane displayed a high C₃H₆ permeance of $4.6 \times 10^{-8} \text{ mol s}^{-1} \text{ m}^{-2} \text{ Pa}^{-1}$ and an outstanding C₃H₆/C₃H₈ selectivity of 85. The obtained ZIF-8/ZIF-67 membrane showed a slightly low C₃H₆ permeance of $3.7 \times 10^{-8} \text{ mol s}^{-1} \text{ m}^{-2} \text{ Pa}^{-1}$, with a much higher C₃H₆/C₃H₈ selectivity of 209 (Fig. 15b). The greatly enhanced selectivity was explained by an improvement in the grain boundary structure and an inherently better intercrystalline pathway. Employing the LBL assembly, an ultrathin ZIF-8/ZIF-67 membrane with a thickness of 180 nm was fabricated. This membrane also exhibited good separation performance in H₂/CO₂, H₂/CH₄, H₂/N₂, H₂/C₂H₄, H₂/C₂H₆, H₂/C₃H₆, and H₂/C₃H₈ systems [162].

Heteroepitaxial growth can be used to not only adjust the microstructures of MOF membranes, but also to change the gas adsorption, in order to increase the effect of molecular sieving and reduce that of selectivity-counteractive adsorption. The window diameter (3.0 Å) of ZIF-9 is between the kinetic diameters of H₂ (KD: 2.9 Å) and CO₂ (KD: 3.3 Å), but the preferential adsorption of CO₂ over H₂ affects the selectivity of the ZIF-9 membrane (Fig. 15c). ZIF-8 and ZIF-67 possess larger windows, with a diameter of 3.4 Å, but exhibit a much lower CO₂ affinity due to the MeIm linker. Cacho-Bailo et al. combined the positive molecular sieving of ZIF-9 with the low CO₂ adsorption of ZIF-8 or ZIF-67 to obtain heteroepitaxially grown membranes by microfluidic processing (Fig. 15d) [163]. As the gas-contacted ZIF-67 or ZIF-8 layers reduced the preferential adsorption of CO₂, the ZIF-67/ZIF-9 and ZIF-8/ZIF-9 membranes had higher H₂/CO₂ selectivities of 9.0 and 9.6, respectively, compared with those of the ZIF-8 (7.4) and ZIF-9 (8.0) membranes.

In addition to the heteroepitaxial growth between different MOFs, this method can be further employed to fabricate MOF layers on covalent organic framework (COF) membranes. ZIF-8/COF-300 and Zn₂(bdc)₂(dabco)/COF-300 membranes were synthesized by

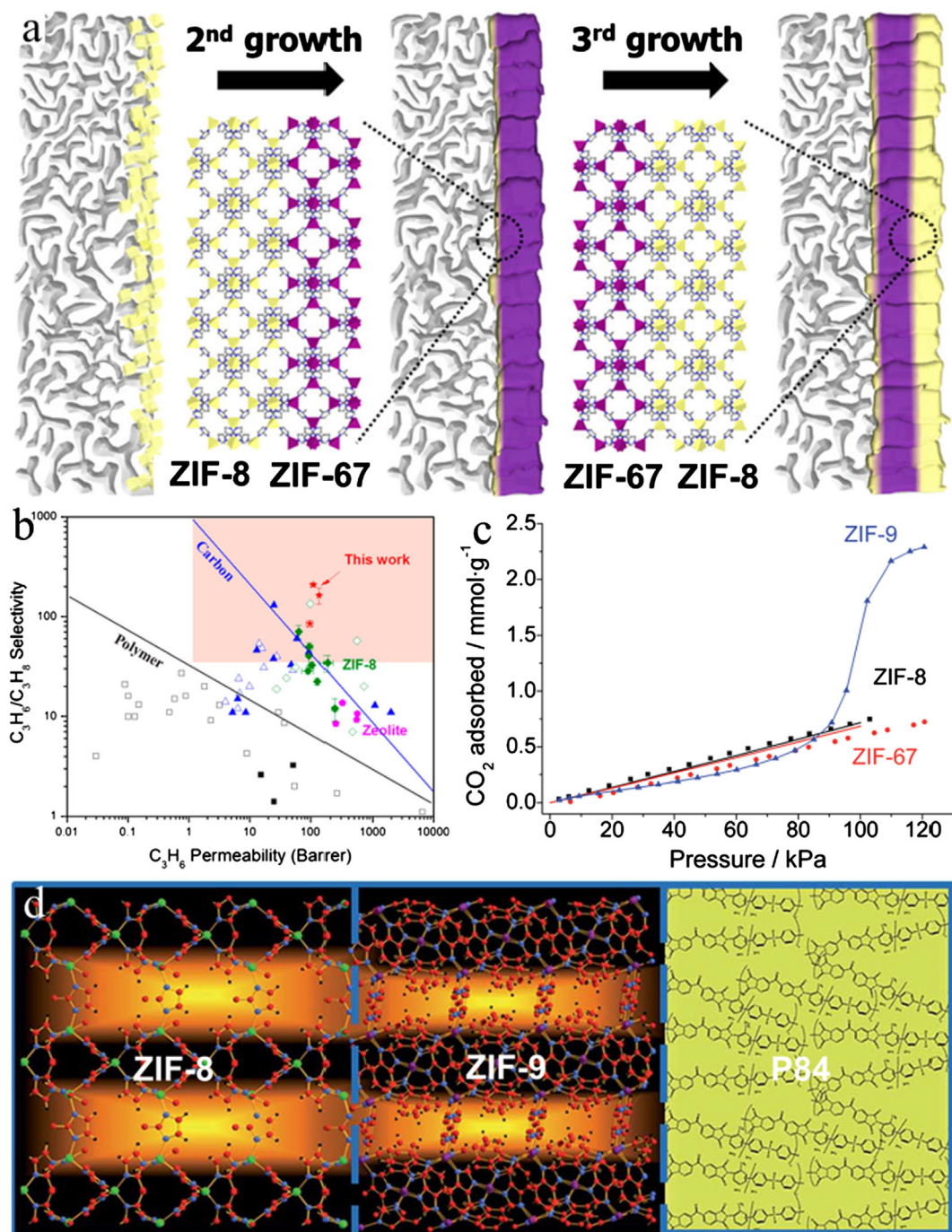


Fig. 15. (a) Schematic illustration of ZIF-8/ZIF-67 membrane synthesis via heteroepitaxial growth. (b) Comparison of C_3H_6/C_3H_8 separation performance between the prepared ZIF-8/ZIF-67 membrane and previously reported membranes. 1 Barrer = $3.348 \times 10^{-16} \text{ m mol s}^{-1} \text{ m}^{-2} \text{ Pa}^{-1}$. (c) CO_2 adsorption of ZIF-8 and ZIF-9. (d) Schematic illustration of ZIF-8/ZIF-9 membrane. Adapted from Refs. [161,163] with permission from the American Chemical Society and Royal Society of Chemistry.

Fu et al. [164]. The membranes had a dense composite layer between the COF and MOF layers (Fig. 16), which consisted of COF crystals and amorphous phase MOFs. The amorphous phase MOFs filled up the gaps between the COFs, and the COF crystals were embedded in the amorphous MOF matrix. The mismatch between the MOF and COF crystal parameters resulted in the formation of amorphous MOFs. Due to the dramatic improvement in the continuity, ZIF-8/COF-300 and $Zn_2(bdc)_2(dabco)/COF-300$ showed higher H_2/CO_2 selectivities of 13.5 and 12.6, respectively, compared with those of the COF-300 (6.0), ZIF-8 (9.1), and $Zn_2(bdc)_2(dabco)$ (7.0) membranes. In contrast, Das et al. heteroepitaxially grew a COF-300 layer on a UiO-66 membrane for a better

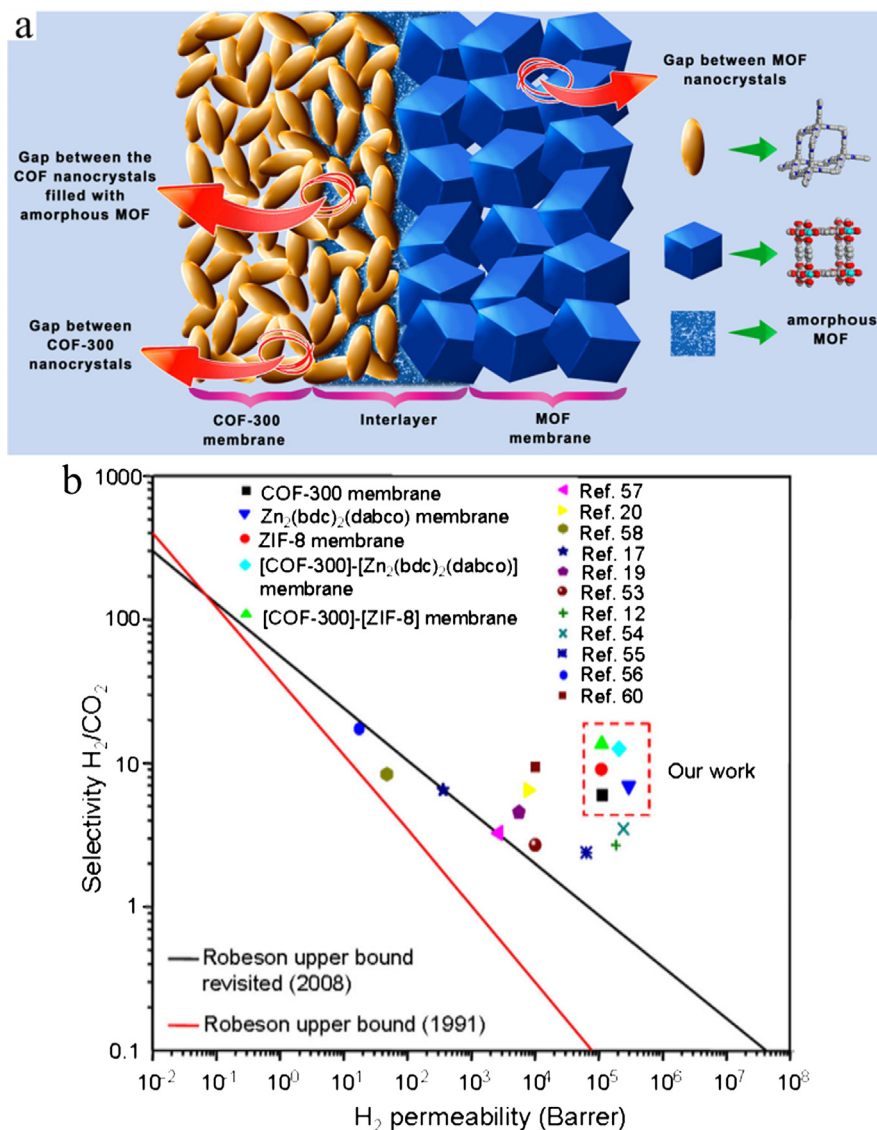


Fig. 16. (a) Schematic illustration of MOF/COF membrane synthesis via heteroepitaxial growth. (b) Comparison of H₂/CO₂ separation performance between the prepared MOF/COF membranes and previously reported membranes. Adapted from Ref. [164] with permission from the American Chemical Society.

separation of a H₂/CO₂ mixture [165].

3.3. Embedding

Unlike the deposition of one dense layer on another, some guests can be embedded into MOFs to control the growth of MOF membranes. Hu et al. employed two-dimensional (2D) hybrid GO@ZIF-8 as the seeding layer to fabricate ultrathin ZIF-8 composite membranes with a thickness of 100 nm, by contra-diffusion synthesis [166]. The hybrid nanosheets, synthesized by in situ crystallization of MOFs on GO, was deposited on anodic aluminum oxide (AAO) substrates to confine the crystallization region and provide heterogeneous nucleation sites for continuous membrane growth. The membrane thus prepared showed H₂/N₂ and CO₂/N₂ ideal selectivities of 11.1 and 7.0, respectively. However, the impermeable GO increased the mass transfer resistance, leading to a low H₂ permeance of $5.5 \times 10^{-8} \text{ mol s}^{-1} \text{ m}^{-2} \text{ Pa}^{-1}$. To improve the permeance of the prepared membranes, as shown in Fig. 17, the GO@MOF composite nanosheets were etched to generate mesopores, before membrane synthesis [167]. Due to the presence of the mesopores in GO, the mass transfer resistance greatly decreased. The prepared membrane with a small thickness of 430 nm showed a much higher H₂ permeance of $1.2 \times 10^{-6} \text{ mol s}^{-1} \text{ m}^{-2} \text{ Pa}^{-1}$ and a high H₂/C₃H₈ ideal selectivity of 2409. Moreover, the embedded nanosheets greatly strengthened the mechanical stability of the composite membranes. Apart from contra-diffusion, Hou et al. employed LBL assembly to obtain ultrathin ZIF-8 membranes with g-C₃N₄ nanosheets [168]. As the strong affinity between g-C₃N₄



Fig. 17. Schematic representation of the growth of MGO@ZIF-8 membrane by contra-diffusion method. Adapted from Ref. [167] with permission from the Royal Society of Chemistry.

and CO₂ reduced the gas diffusion, and g-C₃N₄ possibly changed the transport channels, the 240-nm g-C₃N₄@MOF membrane displayed a high H₂/CO₂ selectivity of 26.

In addition to 2D nanosheets, nanofibers can be embedded into MOF membranes. Shamsaei et al. reported employing one-dimensional materials, as pseudo-seeds, and a nano-scaffold layer for the fabrication of MOF membranes [169]. Polydopamine (PDA) was coated on carbon nanotubes (CNTs) to improve the water dispersibility and heterogeneous nucleation. Then, the modified CNTs were deposited on AAO substrates to fabricate the composite MOF membranes by contra-diffusion method. The prepared ZIF-8 membrane showed excellent mechanical stability due to the presence of CNTs, and could maintain the intact membrane morphology after ultrasonic treatment for 2 h. Compared with that of the ZIF-8 membrane with GO nanosheets, the ZIF-8 membrane embedded with CNTs showed a much higher permeance of $2.87 \times 10^{-5} \text{ mol s}^{-1} \text{ m}^{-2} \text{ Pa}^{-1}$ for H₂, as well as good H₂/CO₂, H₂/N₂, H₂/CH₄, and H₂/C₃H₈ ideal selectivities of 14, 18, 35, and 950, respectively. Zhang et al. also fabricated ZIF-8 membranes using single walled CNTs (SWCNTs) with a PDA coat as the embedded components [170]. After synthesis, a free-standing ZIF-8 membrane with a thickness of 550 nm was formed. The membrane showed an excellent H₂/CO₂ selectivity of 34 and a H₂ permeance of $5.7 \times 10^{-7} \text{ mol s}^{-1} \text{ m}^{-2} \text{ Pa}^{-1}$. The authors found that the separation performance could be adjusted by controlling the SWCNT amount. The CNT film was also employed as a substrate to fabricate ZIF-8 membranes [171]. After the absorption of Zn²⁺ ions, the CNT film was suitable for ZIF-8 membrane fabrication by the solvothermal method. The prepared membrane with a thickness of 30 μm showed a high N₂ permeance and N₂/CO₂ selectivity of 6.9. The higher permeance of N₂ than that of CO₂ was attributed to the residual CO₂ molecules in ZIF-8, due to strongly coordinating interactions. Zero-dimensional (0D) carbonic anhydrase (CA) was introduced into MOF membrane synthesis by Zhang et al. [172]. The CA was firstly embedded in ZIF-8 crystals to form composite particles that were used as seeds for the formation of continuous membranes. Since the CA@ZIF-8 crystals promoted the hydration of CO₂, with the nucleophilic imidazole group reacting with CO₂, and the Zn-based center attracting CO₂, the prepared composite membrane showed a much higher CO₂ permeance and CO₂/N₂ selectivity than those of the pure ZIF-8 membrane under humid conditions. The CO₂/N₂ selectivity of the composite membrane was 165.5.

MOFs can further be crystallized in situ in the interlayer of the nanosheets to form MOF composite membranes. Using the condensation between amino groups and carboxyl groups under high temperatures, Li et al. fabricated a uniform reduced GO (rGO) membrane on ammoniated PVDF hollow fibers by hydrothermal treatment [173]. Utilizing the oxygen polar groups, electro-negativity, and extended interlayer space of the hydrated-state rGO membrane, metal salts were firstly impregnated into the interlayer spaces and subsequently reacted in situ with linkers, to form MOFs (Fig. 18). As the crystalline region is confined in the interlayer spaces, the prepared MOFs showed a nanosheet structure with a thickness of 10–15 nm. The membranes possessed excellent compatibility due to the coordination between the metal centers of the MOFs and the polar groups of rGO. The prepared MOF nanosheets bolstered the rGO layers to form divided layered sheets. The major channels for gas permeation were the pores of the MOFs and the intrinsic defects of rGO. The formed MOF nanosheets controlled the pore size and reduced the swing of rGO, thereby

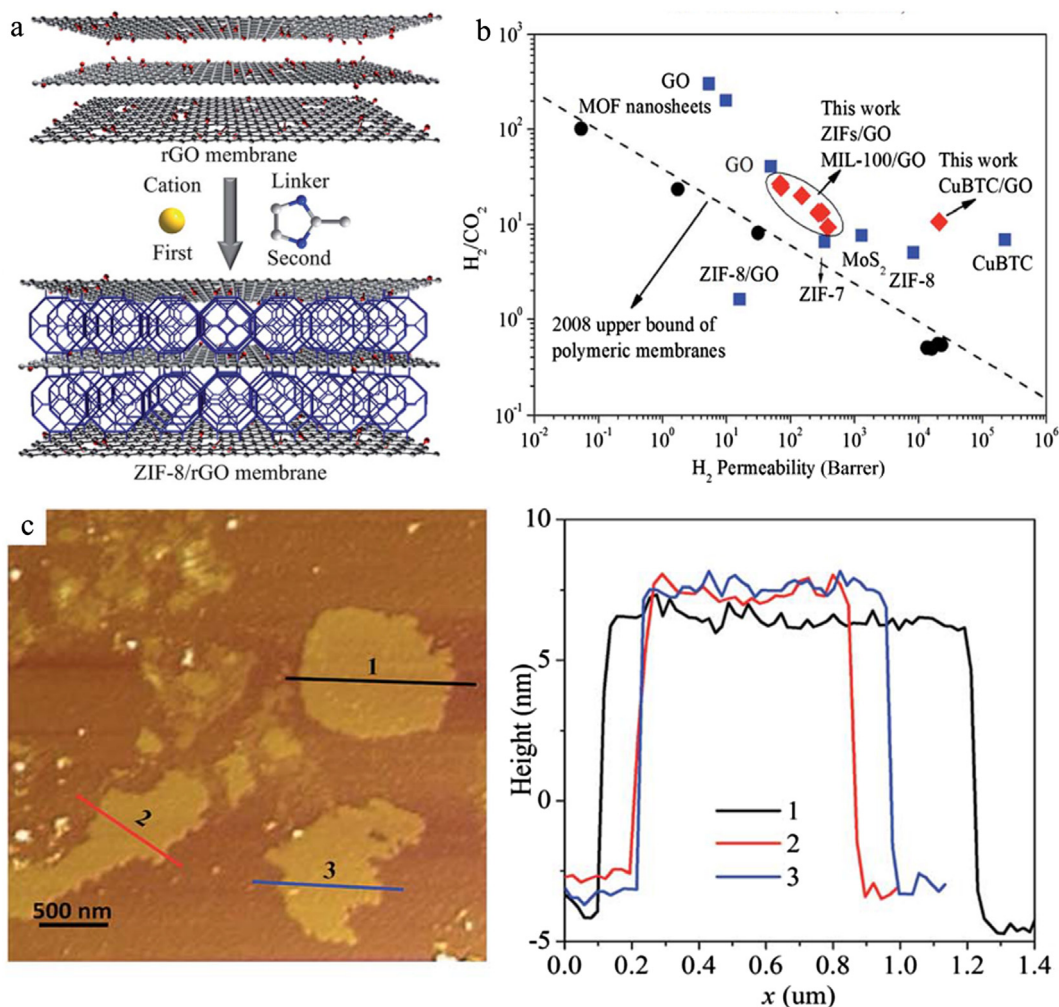


Fig. 18. (a) Schematic illustration of rGO@ZIF-8 membrane synthesized by in situ crystallization in the interlayer of nanosheets. (b) Comparison of H₂/CO₂ separation performance between the prepared rGO@MOF membranes and previously reported membranes. (c) AFM images and height distribution of the ZIF-8 nanosheets. Adapted from Ref. [173] with permission from the Royal Society of Chemistry.

improving the performance further. Various MOF membranes, e.g., rGO@CuBTC, rGO@ZIF-7, rGO@ZIF-8, and rGO@MIL-100 membranes, were synthesized. Relative to the rGO membrane that was impermeable, the prepared ZIF-7, ZIF-8, CuBTC, and MIL-100 composite membranes showed H₂ permeances of 0.33, 0.7, 88, and $1.3 \times 10^{-8} \text{ mol s}^{-1} \text{ m}^{-2} \text{ Pa}^{-1}$, respectively. As the theoretical pore sizes of ZIF-7, ZIF-8, and CuBTC are about 3.0, 3.4, and 9.0 Å, respectively, the ZIF-7 and CuBTC membranes had the lowest and highest permeances, respectively. The moderate performance of the MIL-100 membrane was the result of a relatively poor crystalline structure. In comparison with that of the reported pure MOF membranes, the H₂/CO₂ selectivities of the composite membranes were higher, at 23.2 (ZIF-7), 18.8 (ZIF-8), 10.0 (CuBTC), and 12.5 (MIL-100). To reduce the membrane thickness and improve the permeance, a nanometer-sized rGO layer on ammoniated PVDF hollow fibers was prepared and used as the interface for fabricating ultrathin ZIF-8 composite membranes through interfacial synthesis. The prepared 150-nm rGO@ZIF-8 membrane displayed a higher H₂ permeance of up to $60 \times 10^{-8} \text{ mol s}^{-1} \text{ m}^{-2} \text{ Pa}^{-1}$, with high selectivities of 25.3 (H₂/CO₂), 70.4 (H₂/N₂), and 90.7 (H₂/CH₄) [174].

3.4. Occupation

Occupation is the modification performed by impregnating the intercrystalline gaps and intrinsic pores of MOF membranes with guest reagents. This method can precisely adjust the gas transport channels. The guest reagents are usually ionic liquids (ILs), owing to their chemical tunability, low volatility, thermal stability, high flowability, suitable molecular size, and appropriate molecular affinity [175,176]. 1-octyl-3-methylimidazolium tricyanomethanide ([omim][TCM]) with good CO₂ adsorption ability was first reported to modify the ZIF-69 membrane [177]. The IL/ZIF-69 composite membrane was simply fabricated by immersing the prepared ZIF-69 membrane in the IL. Compared with those of the nonselective pure ZIF-69 membrane, the composite membrane showed much

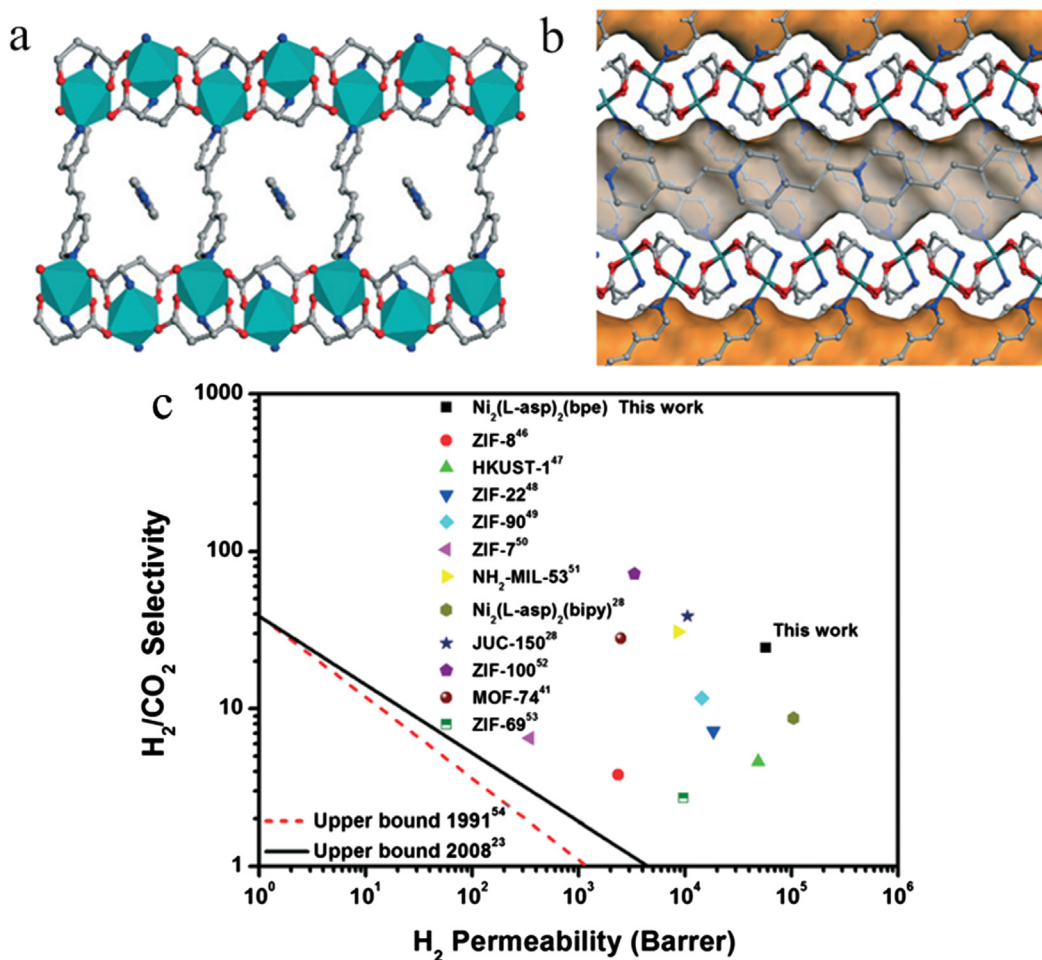


Fig. 19. (a and b) 3D structure of $[\text{Ni}_2(\text{L-asp})_2(\text{bpe})] \cdot (\text{G})$ with linker guest molecules. Ni, C, N, and O are presented in cyan, gray, blue, and red, respectively. (c) Comparison of the H_2/CO_2 separation of the prepared membrane with that of polymeric membranes and other MOF membranes. Adapted from Ref. [180] with permission from the Royal Society of Chemistry.

higher CO_2/N_2 selectivity of 44 and 64 for mixtures with 44 and 75 vol% CO_2 , respectively. The permeance of the composite membrane was higher than that of the pure bulk IL membrane and was about 5.6 (44%) and $3.7 \times 10^{-11} \text{ mol s}^{-1} \text{ m}^{-2} \text{ Pa}^{-1}$ (75%), but it was much lower than that of the pure ZIF-69 membrane. To further enhance the separation performance, occupation and coating were combined to modify MOF membranes [178]. An IL-modified CNT layer was deposited on the ZIF-9 membrane to form a CNT@IL/ZIF-9 membrane through layer-by-layer coating. The CNT@IL filled the defects of the prepared ZIF-9 membrane. Owing to the formation of p-p and cation-p interactions, the coated CNT@IL layer was well-distributed and continuous. The coated CNT@IL layer with good CO_2 selectivity and adsorption capacity could reduce the gas diffusion through the ZIF-9 pores. Therefore, it was more difficult for the CO_2 molecules to pass through the composite membrane, compared to that for other gases. As a result, the composite membrane showed a high H_2/CO_2 ideal selectivity of 40.0. Compared with that of the IL/ZIF-9 membrane, the CNT@IL/ZIF-9 membrane had a higher H_2 permeance of $5.5 \times 10^{-7} \text{ mol s}^{-1} \text{ m}^{-2} \text{ Pa}^{-1}$. To achieve a more precise sieving behavior, Ban et al. impregnated 1-butyl-3-methylimidazolium bis(trifluoromethylsulfonyl)imide ([bmim][Tf2N]) into ZIF-8 to tailor the effective size, through ionothermal synthesis of ZIF-8 in the IL [179]. The modified ZIF-8 particles were blended into the polymer to prepare MMMs with improved separation performance for CO_2/N_2 and CO_2/CH_4 mixtures.

The linkers in the cavities of the frameworks are usually removed by activation, but this also provides the opportunity to adjust the pore structure of the MOF membranes. Kang et al. synthesized $[\text{Ni}_2(\text{L-asp})_2(\text{bpe})] \cdot (\text{G})$ (L-asp: L-aspartic acid, bpe: 1,2-bis(4-pyridyl)ethylene) membranes with encapsulated guest linker molecules in the pores, by the solvothermal method (Fig. 19). The linker molecules reduced the pore size and strengthened the affinity of the MOFs toward CO_2 molecules. The prepared membrane showed high H_2/CO_2 , H_2/N_2 , and H_2/CH_4 selectivities of 24.3, 12.1, and 7.8, respectively, with a commendable H_2 permeance of $1.0 \times 10^{-6} \text{ mol s}^{-1} \text{ m}^{-2} \text{ Pa}^{-1}$. The performance of the membrane in H_2/CO_2 systems surpassed the upper bound of polymeric membranes and was better than that of most reported membranes [180].

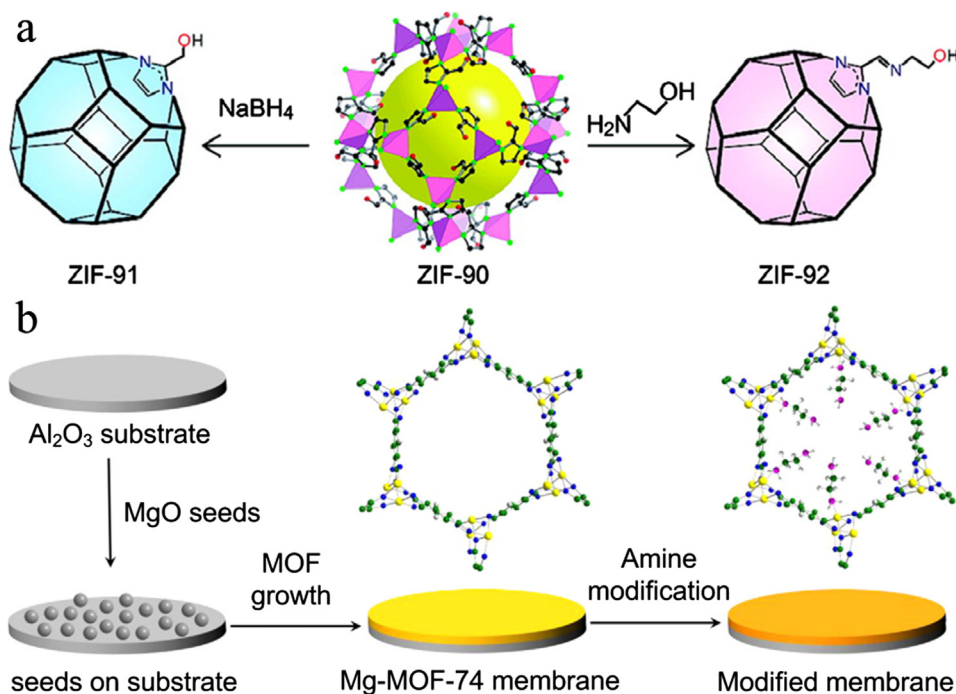


Fig. 20. (a) Transformation of ZIF-90 to ZIF-91 using NaBH_4 , and to ZIF-92 using ethanolamine. (b) Scheme of Mg-MOF-74 membrane synthesis by the solvothermal method, and modification by EDA. Adapted from Refs. [181,191] with permission from the Royal Society of Chemistry.

3.5. Grafting

Although coating, heteroepitaxial growth, embedding, and occupation possibly involve the chemical interaction between the modified components and MOFs, they are mainly based on the regulation of composition, construction, affinity, and pore structure. In grafting, the introduced molecules directly react with the functional groups or metal sites of MOFs [181–184]. The grafted molecules can exceptionally regulate the continuity, adsorption, and pore structure of the frameworks. Yoo et al. introduced surfactants (Span 80 and P123) during the drying process of the IRMOF-3 membrane to prevent crack formation and enhance moisture stability [185]. The surfactants decreased the interfacial tension, thereby suppressing the emergence of pinholes. The surface-adsorbed surfactants enhanced the hydrophobicity and thus the moisture stability. Moreover, the reaction between the anhydrides of the surfactants and the amine groups of the MOFs changed the pore structures of the MOFs.

As shown in Fig. 20a, using the Schiff condensation reaction, ethanolamine with amine groups was grafted onto ZIF-90, with aldehyde groups as linkers [181]. Huang et al. fabricated a ZIF-90 membrane with a thickness of 20 μm by the solvothermal method, and modified it by soaking in an ethanolamine/methanol solution under refluxing at 60 $^\circ\text{C}$. After grafting for 10 h, the selectivities for H_2/CO_2 , H_2/N_2 , and H_2/CH_4 were greatly increased from 7.3, 11.7, and 15.3 of the as-synthesized ZIF-90 membrane to 15.3, 15.8, and 18.9 of the modified ZIF-90 membrane, respectively. With the extension of the grafting time to 24 h, the H_2/CO_2 selectivity further improved to 62.5 [186]. The enhancement of the selectivity was attributed to the constricted aperture and the reduced non-selective defects of the membranes after modification. However, since ethanolamine was small enough to permeate the interior of the ZIF-90 membrane, the permeance of the membrane drastically decreased. After modification for 24 h, the H_2 permeance of the grafted ZIF-90 membrane was only $1.4 \times 10^{-8} \text{ mol s}^{-1} \text{ m}^{-2} \text{ Pa}^{-1}$, which was much smaller than that of the original membrane ($2.4 \times 10^{-7} \text{ mol s}^{-1} \text{ m}^{-2} \text{ Pa}^{-1}$). Moreover, the membrane structure slightly deteriorated due to the long modification time. To maintain the permeation property and shorten the modification time, APTES with amine groups was employed as the grafting reagent [187]. ZIF-90 could react with the large APTES while restraining it on the surface. The modification could be implemented at 110 $^\circ\text{C}$ for only 30 min. The grafted membrane showed excellent H_2/CO_2 , H_2/CH_4 , and $\text{H}_2/\text{C}_3\text{H}_8$ selectivities of 20.1, 71.5, and 458, respectively, with a high H_2 permeance of $2.9 \times 10^{-7} \text{ mol s}^{-1} \text{ m}^{-2} \text{ Pa}^{-1}$. By extending the modification time to 1 h, an outstanding H_2/CH_4 selectivity of 146 was achieved, and the H_2 permeance was maintained at $6.8 \times 10^{-8} \text{ mol s}^{-1} \text{ m}^{-2} \text{ Pa}^{-1}$. Moreover, the membrane also displayed a good CO_2/CH_4 selectivity of 4.7 and CO_2 permeance of $1.2 \times 10^{-8} \text{ mol s}^{-1} \text{ m}^{-2} \text{ Pa}^{-1}$ [188].

Grafting could even integrate ZIF-94 (known as SIM-1) powders with Zn-based centers and 4-methyl-5-imidazolecarboxaldehyde linkers to form a free-standing membrane [189]. The submicron and nanosized ZIF-94 particles were synthesized by the solvothermal method, and then pressed into discs. After modification by vapor EDA, the free-standing membranes were fabricated through cross-linking by the Schiff base condensation reaction. The obtained membranes showed a high water flux of 205 (submicron crystals) and 460 $\text{g m}^{-2} \text{ h}^{-1}$ (nanosized crystals), but impermeability for ethanol. The topological structure of ZIF-94 can be changed by grafting modification. Cacho-Bailo et al. fabricated a ZIF-94 membrane on the inner surface of hollow fibers by microfluidic processing, and

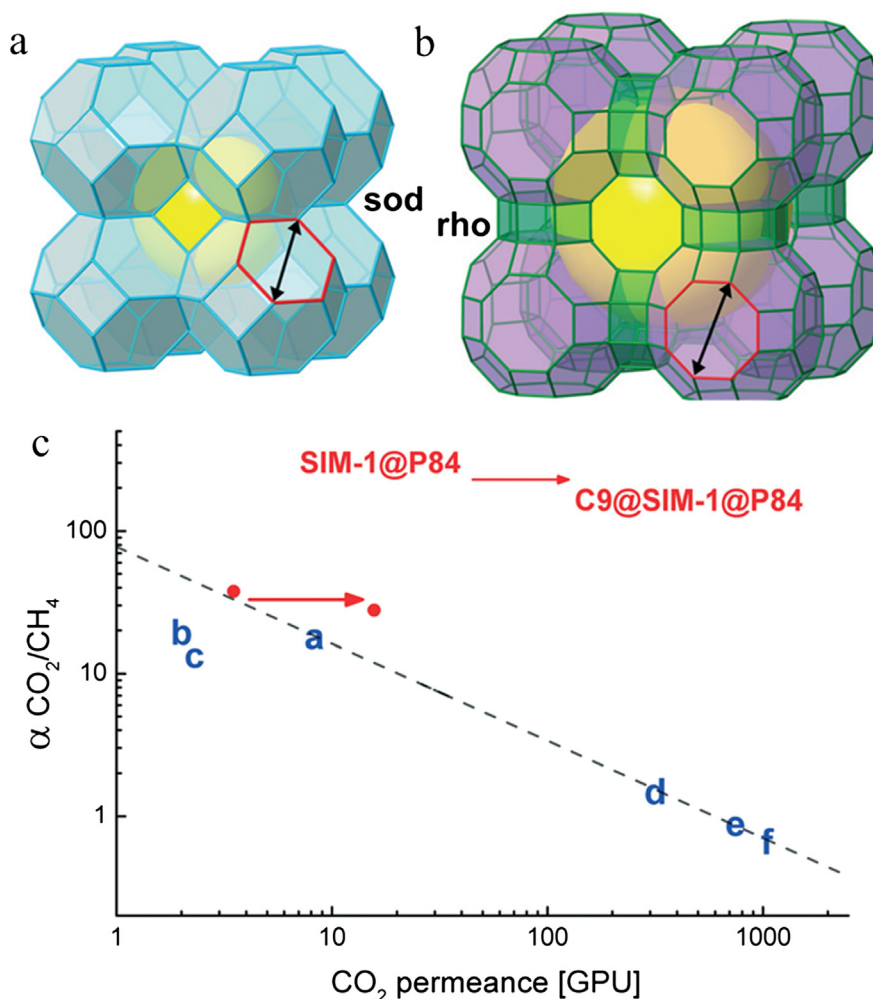


Fig. 21. (a and b) Crystalline structures of ZIF-94 with sod structure and ZIF-93 with rho structure. (c) CO_2/CH_4 separation performance of the prepared ZIF-94 membrane and the modified ZIF-94 membrane. The lowercase letters in c are the separation performances of previously reported membranes. Adapted from Ref. [190] with permission from the Royal Society of Chemistry.

then grafted it with hexylamine and nonylamine [190]. The ZIF-94 membrane exhibited He, H_2 , and CO_2 permeances of 0.5, 0.42, and $0.12 \times 10^{-8} \text{ mol s}^{-1} \text{ m}^{-2} \text{ Pa}^{-1}$, and outstanding He/ CH_4 , H_2/CH_4 , and CO_2/CH_4 selectivities of 160, 136, and 37.7, respectively. After modification by imine condensation, the prepared ZIF-94 with a sod structure was transformed to ZIF-93 with an rho structure (Fig. 21). As ZIF-93 had a larger window diameter and poorer CO_2 affinity than that of ZIF-94, the modified membrane showed higher permeances of 1.5 (He), 1.6 (H_2), and $0.53 (\text{CO}_2) \times 10^{-8} \text{ mol s}^{-1} \text{ m}^{-2} \text{ Pa}^{-1}$, but lower selectivities of 79.1 (He/ CH_4), 85.6 (H_2/CH_4), and 27.8 (CO_2/CH_4) than those of the prepared ZIF-94 membrane.

In addition to the utilization of the reaction between the linkers and grafted reagents, the unsaturated metal centers are employed as active sites for grafting. For modification, Wang et al. immersed the prepared Mg-MOF-74 membrane in EDA toluene solution at 110°C for 2 h [191]. The amine groups of EDA could bind to the open metal sites (Fig. 20b). After modification, the apparent activation energy of the membrane for H_2 permeation remained unchanged, from 7.65 to 7.71 kJ mol^{-1} , while the activation energy for CO_2 permeation almost doubled, from 11.4 to 20.9 kJ mol^{-1} . This demonstrated that the modification greatly changed the chemical properties of the framework. The EDA molecules strengthened the affinity for CO_2 and subsequently reduced the diffusion of CO_2 through the modified membrane. The H_2/CO_2 selectivity greatly increased from 10.5 for the original membrane to 28 for the modified membrane. Accordingly, the H_2 permeance decreased from 12 to $8.2 \times 10^{-8} \text{ mol s}^{-1} \text{ m}^{-2} \text{ Pa}^{-1}$.

3.6. Substitution

Till date, tens of thousands of MOFs have been synthesized and investigated. Comparatively, the types of MOFs that have been employed to prepare separation membranes are few, due to the strict requirements of continuity, and the special synthesis conditions. Substitution to replace the metal centers or linkers is used to obtain new types of MOFs or adjust the pore structures and properties of

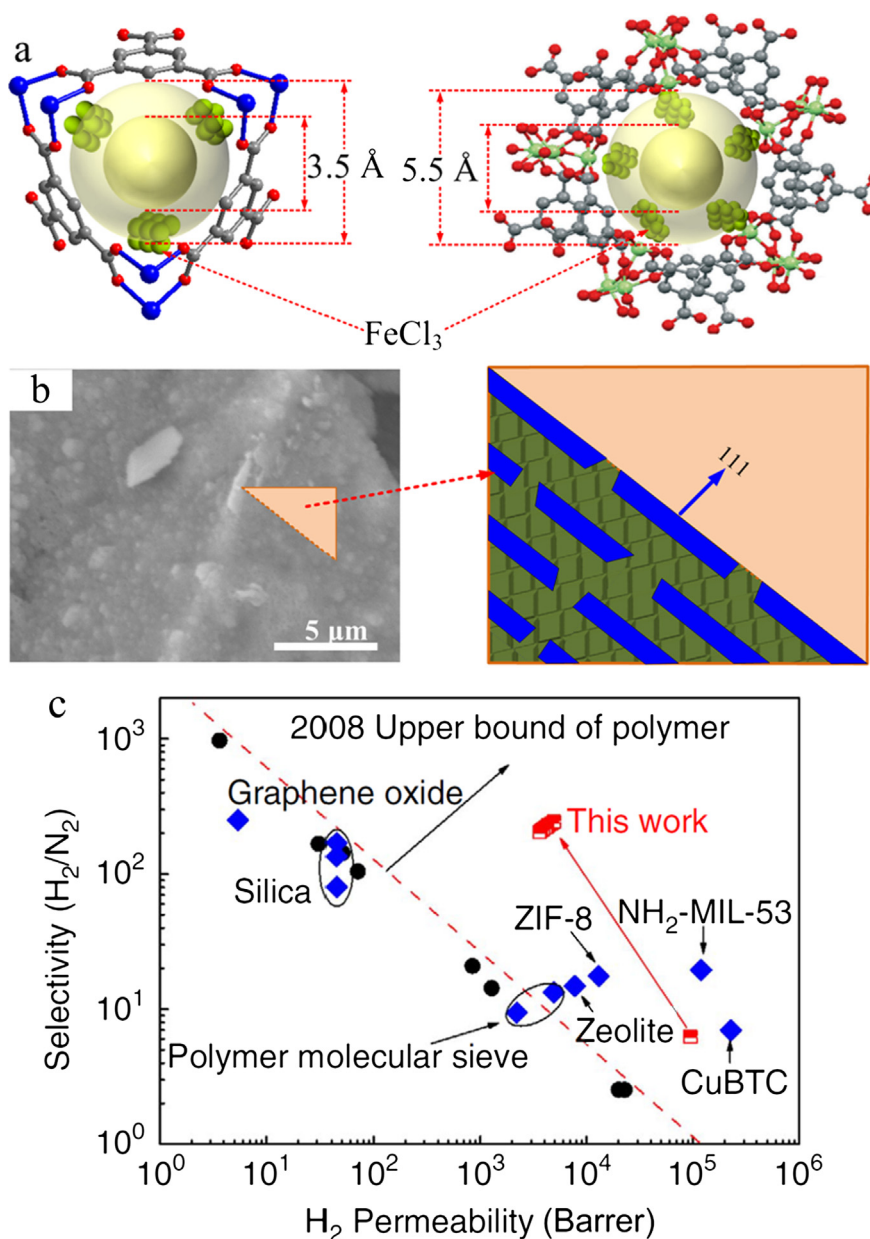


Fig. 22. (a) Pore structure of CuBTC and MIL-100 in composite membranes. C, O, Cu, and Fe are presented as gray, red, blue, and green balls, respectively. (b) Scheme of the prepared MIL-100@CuBTC membrane. The green and blue parts show the formed MIL-100 and the CuBTC with exposed (1 1 1) facets. (c) Comparison of the prepared membrane with previously reported membranes for H₂/CO₂ separation. Adapted from Ref. [197] with permission from the Nature Publishing Group.

MOFs [192–196]. To increase the types and improve the separation performance of MOF membranes, Li et al. developed the transformation method, which was based on cation substitution, to realize the connection of different MOF membranes [197]. This method could transform, in situ, one synthesized MOF membrane into another that had a different topological structure and had been difficult to synthesize. Additionally, this method can change the pore structure of MOFs by metal salt immobilization and selective crystal facet exposure. A CuBTC hollow fiber membrane was synthesized by the solvothermal method and partially transformed to MIL-100 by Fe³⁺ substitution. The as-synthesized CuBTC membrane showed a high H₂ permeance of $2.3 \times 10^{-6} \text{ mol s}^{-1} \text{ m}^{-2} \text{ Pa}^{-1}$, but moderate H₂/CO₂ (6.4), H₂/O₂ (5.6), H₂/N₂ (6.2), and H₂/CH₄ (6.2) ideal selectivities. After transformation, the modified CuBTC/MIL-100 composite membrane showed lower a H₂ permeance of $8.8 \times 10^{-8} \text{ mol s}^{-1} \text{ m}^{-2} \text{ Pa}^{-1}$, but much higher H₂/CO₂ (77.6), H₂/O₂ (170.6), H₂/N₂ (217.0), and H₂/CH₄ (335.7) ideal selectivities. In binary mixture separation, the selectivities for H₂/CO₂, H₂/N₂, and H₂/CH₄ were still 78.2, 212.5, and 321.3, respectively. The performance of the prepared composite membrane was better than those of the polymeric and MOF membranes in earlier studies (Fig. 22). The excellent separation performance was

attributed to the selectively exposed (1 1 1) facets with 3.5 Å pores of the residual CuBTC, and the shrunken gaps and pores of the MOFs due to metal salt filling. In addition to cation substitution, linker exchange was developed to improve the permeance. The ZIF-8 membrane with MeIM linkers was exchanged by 2-imidazolecarboxaldehyde (Ica). Due to the larger 5.0 Å pore size of the Ica-exchanged ZIF-8 (ZIF-90) than that of ZIF-8 (4.0 Å), and the greatly reduced ZIF-8 thickness, the modified membrane showed a much higher C₃H₆ permeance of $7.8 \times 10^{-8} \text{ mol s}^{-1} \text{ m}^{-2} \text{ Pa}^{-1}$, which was four times that of the pure ZIF-8 membrane. On the other hand, since the grain boundary of the MOF membrane remained intact, the C₃H₆/C₃H₈ selectivity was relatively stable. Moreover, using the imine condensation reaction, the externally modified ZIF-8 (ZIF-90) membranes could be decorated with hydrocarbon chains to improve water resistance [198].

Substitution can be carried out during the process of membrane synthesis. By simultaneously adding zinc and cobalt salts into MeIM-containing precursors, Wang et al. synthesized ZIF-8-67 composite membranes, and found that the metal-substitution strategy could be used to adjust the grain boundary and regulate the effective aperture of MOF membranes [199]. With an increase in the Zn/Co ratio, the C₃H₆/C₃H₈ selectivity increased from 1.4 for the ZIF-67 membrane without zinc to 50.5 for the ZIF-8-67 with 90% zinc and 83.6 for the ZIF-8 membrane without cobalt. Hillman et al. also reported the fabrication of composite ZIF-8-67 membranes with both Co-based and Zn-based centers [200]. The authors observed a blue-shift of metal to nitrogen bands in the IR spectrum, which indicated the enhanced stiffness of the bonds. The degree of blue shift increased with the Co/Zn ratio. The stiff bond suppressed the flexibility of the frameworks and subsequently reduced the window size. Due to the smaller aperture, the ZIF-8-67 membrane with a Zn/Co ratio of 1 showed much a higher C₃H₆/C₃H₈ selectivity of 120.2 than that of the ZIF-8 membrane (62.9). The ZIF-8-67 membrane with a thickness of 1.2 μm exhibited a high C₃H₆ permeance of $2.0 \times 10^{-8} \text{ mol s}^{-1} \text{ m}^{-2} \text{ Pa}^{-1}$. Apart from metal substitution, Zhang et al. proposed the use of mixed linkers of MeIM and benzimidazole (BIM) to synthesize composite ZIF-9-67 membranes [201]. Compared with single linker solutions, the mixed linker solution was better for obtaining a continuous membrane. After solvothermal treatment, a ZIF-9-67 membrane with a thickness of 30 μm was formed. The prepared membrane displayed good CO₂ capture performance with a high H₂ permeance of $1.4 \times 10^{-5} \text{ mol s}^{-1} \text{ m}^{-2} \text{ Pa}^{-1}$ and ideal selectivities of 8.9 (H₂/CO₂), 2.3 (CO/CO₂), 3.3 (N₂/CO₂), and 2.4 (CH₄/CO₂). Based on contra-diffusion and microwave synthesis, Hillman et al. prepared ZIF-7-8 membranes with mixed linkers of BIM and MeIM. By tuning the linker ratio, the permeance and selectivity of the prepared ZIF-7-8 membranes for H₂/CH₄ and CO₂/CH₄ separations could be changed to some extent [92].

3.7. Others

Thermal annealing is usually employed to improve the selectivity of polymeric membranes. MOF membranes supported by polymeric substrates can also be annealed to enhance the MOF–polymer adhesion. Cacho-Bailo et al. fabricated ZIF-8 membranes with a thickness of 1.3 μm on the inner surface of P84 hollow fibers, by microfluidic processing, and then modified the membranes by thermal annealing at 175 °C for 24 h. After annealing, the compatibility of the membrane was greatly enhanced. Compared with those of the original membrane, the permeances of the annealed membrane deteriorated from 0.39 and $0.1 \times 10^{-5} \text{ mol s}^{-1} \text{ m}^{-2} \text{ Pa}^{-1}$ to 0.33 and $0.067 \times 10^{-5} \text{ mol s}^{-1} \text{ m}^{-2} \text{ Pa}^{-1}$ for H₂ and CO₂, respectively, but the selectivities greatly improved from 32.4 and 10.5 to 65 and 19.6 for H₂/CH₄ and CO₂/CH₄, respectively, at 35 °C. The ZIF-93 membrane was also annealed, and exhibited a similar phenomenon [202].

A ripening growth refers to the crystallization of bigger crystals from smaller ones. Kwon et al. fabricated a ZIF-8 seeding layer and treated it with linker vapor to prepare continuous ZIF-8 membranes. As water promotes linker deprotonation and improves molecule mobility, the presence of water in the linker vapor enhanced the ripening process. After ripening, the seeding layer showed substantial changes in morphology and was transformed into a continuous ZIF-8 membrane. The prepared ZIF-8 membrane with a thickness of approximately 300 nm exhibited a C₃H₆ permeance of $1.25 \times 10^{-8} \text{ mol s}^{-1} \text{ m}^{-2} \text{ Pa}^{-1}$ and C₃H₆/C₃H₈ selectivity of 120. However, this method had poor reproducibility. The performance of the different membranes displayed a high variation [203].

4. Application of MOF membranes

Due to the intrinsic microporous structures, MOF membranes show excellent performance in the separation of small molecules. As mentioned above and in previous reviews, MOF membranes are usually applied in gas separation for H₂ purification, CO₂ capture, and hydrocarbon separation, as well as in pervaporation for the separation of organic/water and organic mixtures [34–37]. The modification for eliminating cracks, refining channels, and tuning sorption properties is normally devoted to the improvement of the selectivity. In some special situations, separation membranes are required to possess stimuli responsiveness, i.e., the membranes should be able to alter their separation features under different external environmental conditions, including temperature, light, pH, and magnetic fields [204,205]. In addition, to integrate the catalysis and separation features in order to simplify the operation process, catalysts are embedded in or deposited on the membranes to obtain catalysis functions [206]. In addition to improving the molecular sieving property, modification can be employed to endow the MOF membranes with new functions and extend their application scope.

Recently, MOF membranes with excellent water stability have been employed for nanofiltration. Moreover, because MOFs have a great potential to load functional components, some modified MOF membranes with new functions have been reported. In this section, we discuss the applications of MOF membranes, including nanofiltration, ionic sieving, stimuli responsiveness, and catalysis.

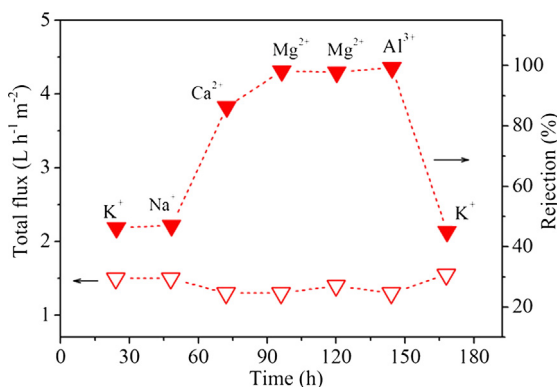


Fig. 23. Nanofiltration performance of the prepared UiO-66 membrane. Adapted from Ref. [220] with permission from the American Chemical Society.

4.1. Nanofiltration

Nanofiltration membranes can block multivalent ions and small organic molecules. Owing to its efficiency and environment-friendly properties, the nanofiltration process is widely employed for water treatment and organic separation [207,208]. Polymers such as cellulose acetates and polyamides are the dominant materials for the production of nanofiltration membranes. Various materials, including diamond-like carbon, graphene and its derivatives, and porous polymers, are also employed for nanofiltration membrane fabrication [209–214]. Owing to the sub-nanometer-sized pore structures, MOF membranes are employed for nanofiltration as well. Initially, MOF particles are usually dispersed in polymeric membranes as fillers to improve permeability [215–219]. Recently, Li et al. demonstrated the feasibility of nanofiltration using continuous MOF membranes directly [220]. Due to the high valence of its Zr center, UiO-66 showed excellent water stability and could maintain the topological structure after water exposure for several months, at the least. Employing the solvothermal method, a continuous UiO-66 membrane with a thickness of about 2.0 μm was synthesized on ceramic hollow fibers. As a result of the small aperture size of $\sim 6.0 \text{ \AA}$, the membrane displayed high Ca^{2+} (hydrated diameter, HD: 8.2 \AA), Mg^{2+} (HD: 8.6 \AA), and Al^{3+} (HD: 9.5 \AA) rejections of 86.3%, 98.0%, and 99.3%, respectively. However, due to the linker dynamics, K^+ (HD: 6.6 \AA) and Na^+ (HD: 7.2 \AA) rejections were 45.7% and 47.0%, respectively (Fig. 23). Furthermore, the permeance of the membrane was only $0.14 \text{ L h}^{-1} \text{ m}^{-2} \text{ bar}^{-1}$ due to the relatively thicker selective layer compared with that of polyamide membranes, and the permeability achieved was $0.28 \text{ L h}^{-1} \text{ m}^{-2} \text{ bar}^{-1}$. The UiO-66 membrane was also used for pervaporation [221,222], and showed a high flux of $4.1\text{--}6.0 \text{ kg h}^{-1} \text{ m}^{-2}$ and an excellent separation factor of over 45,000 in the separation of water from *i*-butanol, furfural, and tetrahydrofuran [221].

Nanofiltration has also been proposed for the removal of dyes from water. The ZIF-8 membrane synthesized by interfacial synthesis was employed for dye removal. The interfacial synthesis was performed with zinc nitrate aqueous solution, MeIM octanol solution, and a PES substrate. The prepared membrane showed a high water permeance of $27.7 \text{ kg h}^{-1} \text{ m}^{-2} \text{ bar}^{-1}$ and Rose bengal rejection of 98.9%. Since the methyl groups of the linker obstruct the contact between the metal centers and guest molecules and lead to a hydrophobic pore structure, the ZIF-8 membrane also showed high ethanol and isopropanol permeances of 21.4 and $10.4 \text{ kg h}^{-1} \text{ m}^{-2} \text{ bar}^{-1}$, respectively, along with corresponding Rose bengal rejections of 83.9% and 93.5% [84]. By controlling the substrate structure, MeIM/ Zn^{2+} ratio, and reaction time, the performance of the prepared ZIF-8 membrane could be enhanced greatly. For example, the water permeance showed a high variation from 5.6 to $37.5 \text{ L h}^{-1} \text{ m}^{-2} \text{ bar}^{-1}$ with a change in the molar MeIM/ Zn^{2+} ratio from 1.9 to 15.9 [223]. Yang et al. reported chelation-assisted interfacial synthesis for preparing MOF membranes. This method was carried out by electrostatic deposition of polyethyleneimine with chelated Zn^{2+} ions on hydrolyzed PAN substrates and subsequent interfacial reaction with MeIM in hexane solution. The formed ZIF-8 crystals showed 3D-ordered architectures. The water permeance of the prepared membrane was $\sim 75\text{--}97 \text{ L h}^{-1} \text{ m}^{-2} \text{ bar}^{-1}$, whereas the Methyl blue, Congo red, and Acid fuchsin rejections were 98.9%, 99.2%, and 87.2%, respectively. However, the membrane showed a poor salt rejection of $< 10\%$ [224]. The CuBTC membrane was also employed for organic solvent nanofiltration, but it showed relatively poor rejection due to the possible existence of pinholes in the membrane [225].

4.2. Ionic sieving

Lithium is widely applied in batteries, ceramics, and metal composite materials. The purification of lithium ions is very important. Various techniques, including solvent extraction, ion-exchange, adsorption, and membrane separation, have been successfully applied for lithium purification [226–228]. MOF membranes are employed to separate the molecules with different sizes or affinities [229]. Recently, MOF composite membranes were utilized to sieve ionic mixtures. Based on the size-selectivity of MOFs and the affinity between sulfonate groups and alkaline metal ions, Guo et al. fabricated a CuBTC composite membrane with embedded polymer polystyrene sulfonate (PSS) to realize lithium-ion purification. Compared with those of the pristine CuBTC membrane, the PSS@CuBTC-6.7 membrane with PSS proportion of 6.7 wt% showed about five orders higher Li^+ ion conductivity of 1.89×10^{-3}

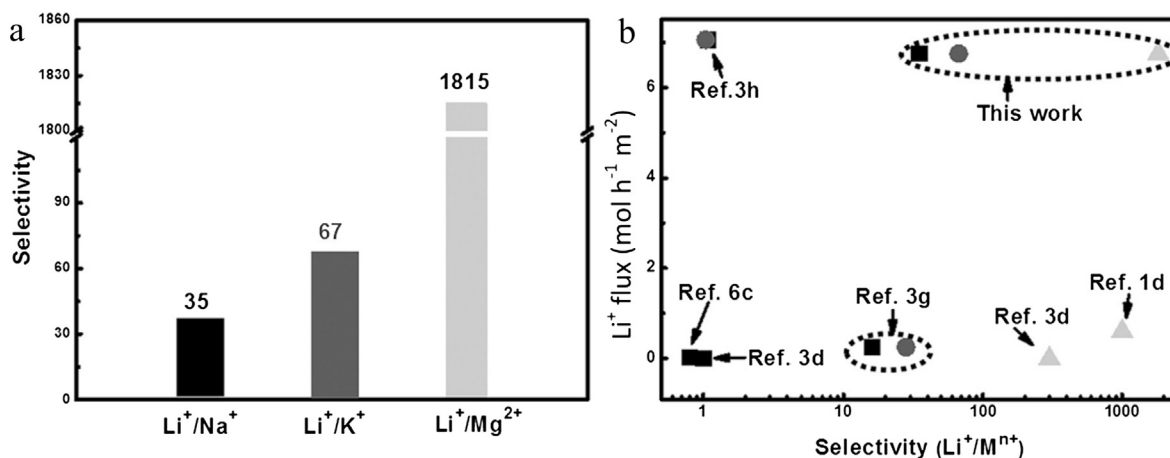


Fig. 24. (a) Ion selectivities of PSS@CuBTC-6.7. (b) Comparison of the performance of PSS@HKUST-1-6.7 membrane for Li⁺/Na⁺, Li⁺/K⁺, and Li⁺/Mg²⁺. Li⁺/Na⁺: square; Li⁺/K⁺: circle; and Li⁺/Mg²⁺: triangle. Adapted from Ref. [229] with permission from Wiley-VCH.

and $5.53 \times 10^{-4} \text{ S cm}^{-1}$ at 70 and 25 °C, respectively. In the binary separation of Li⁺ ions from K⁺, Na⁺, and Mg²⁺ ions, the membrane displayed an Li⁺ ion flux of $6.75 \text{ mol h}^{-1} \text{ m}^{-2}$ and outstanding Li⁺/K⁺, Li⁺/Na⁺, and Li⁺/Mg²⁺ selectivities of 67, 35, and 1815, respectively (Fig. 24). The authors explained that size-sieving and binding affinity simultaneously governed the ion permselectivity. In comparison with the pore size of CuBTC, K⁺, Na⁺, and Li⁺ ions have smaller HDs of 7.6, 6.6, and 7.2 Å, respectively. Hence, the Li⁺/K⁺ and Li⁺/Na⁺ selectivities were mainly attributed to the difference in affinities between the sulfonate groups and ions. For the much higher Li⁺/Mg²⁺ selectivity, in addition to the disparity in the binding affinity, the size-sieving played an important role as that of the large Mg²⁺ HD of 8.6 Å. Zhang et al. employed the GO@ZIF-8 membrane fabricated by contra-diffusion to separate LiCl from other chlorine salts. The membrane showed Li⁺/Na⁺, Li⁺/K⁺, and Li⁺/Rb⁺ selectivity ratios of 1.4, 2.2, and 4.6, respectively [230].

Lithium–sulfur batteries show a great potential for energy storage [231]. However, the decomposition of discharge/charge polysulfide intermediates in organic electrolytes decreases the capacity and cycle life [232]. To solve this issue, Bai et al. designed MOF-based ionic sieve membranes as battery separators, which suppressed polysulfide migration but allowed Li⁺ ion permeation [233]. The composite MOF membrane synergistically contained MOF nanoparticles and GO laminates. As the window size of CuBTC is between the hydrated diameters of Li⁺ ions and polysulfides, CuBTC was employed to fabricate the MOF@GO composite membranes. As expected, the membranes showed an excellent efficiency for polysulfide blocking and outstanding stability (Fig. 25). Peng et al. also fabricated interpenetrated MOF/CNT composite membranes by confinement conversion for application in lithium–sulfur batteries [234,235]. The CNTs interpenetrated the MOF crystals and provided both structural integrity and conductivity, whereas the MOFs with strong sulfur confinement greatly improved the cyclability.

4.3. Stimuli responsiveness

Stimuli-responsive membranes can switch their separation behaviors based on environmental stimuli. Traditional membranes can be modified to obtain stimuli responsiveness [236,237]. MOFs can also be functionalized with stimuli-responsive reagents to achieve the responsiveness [238,239]. Based on the switching of azobenzene moieties between the cis- and trans-configuration under visible and ultraviolet lights (Fig. 26a), Wang et al. synthesized Cu₂(AzoBPDC)₂(AzoBiPyB) membranes with 2-phenyldiazonyl-4,40-biphenyldicarboxylic acid (AzoBPDC) linkers [240]. The permeance and selectivity of the obtained membrane could be smartly regulated. The trans-to-cis and cis-to-trans isomerizations of the linkers were adjusted by irradiation with lights of 365 and 455 nm wavelength. In H₂/CO₂ separation, after switching the azobenzene in the membrane from trans to cis or vice versa, the H₂ permeance varied slightly but the CO₂ permeance increased or decreased significantly between 4 and $10 \times 10^{-8} \text{ mol s}^{-1} \text{ m}^{-2} \text{ Pa}^{-1}$. Consequently, the H₂/CO₂ selectivity also varied between 8.0 and 3.0 at the cis and trans states (Fig. 26b). The membrane showed similar properties in N₂/CO₂ separation, with the selectivity between 8.5 and 5.5. Moreover, the responsive function had excellent long-term stability, and could maintain the performance after operation for five cycles, at the least. Knebel et al. synthesized an ultrathin UiO-67 membrane with a thickness of 200 nm and loaded it with intelligent light-responsive azobenzene guest molecules [241]. The membrane also showed excellent stimuli responsiveness, with the H₂/CO₂ selectivity between 10 and 14 under irradiation with light of 365 and 455 nm wavelength. Furthermore, the Cu₂(F₂AzoBDC)₂(dabco) membrane with fluorinated azobenzene linkers was synthesized and investigated [242]. The linker of the framework could reversibly switch between the trans and cis states under visible light with wavelengths of 400 and 530 nm. Based on this switching, the H₂/C₂H₄ and H₂/C₃H₈ selectivities could be changed from 8.2 and 13.0 to 6.7 and 8.7, respectively. More recently, Knebel et al. found that electric fields could be employed to control the gas transport across MOF membranes [243]. The ZIF-8 membrane prepared by contra-diffusion synthesis was employed for gas separation, by applying an external electric field. The results revealed that the E-field polarization could cause the transformation of the ZIF-8 structure to polymorphs. As this state possessed more rigid lattices, the gas permeance decreased. Therefore, the separation

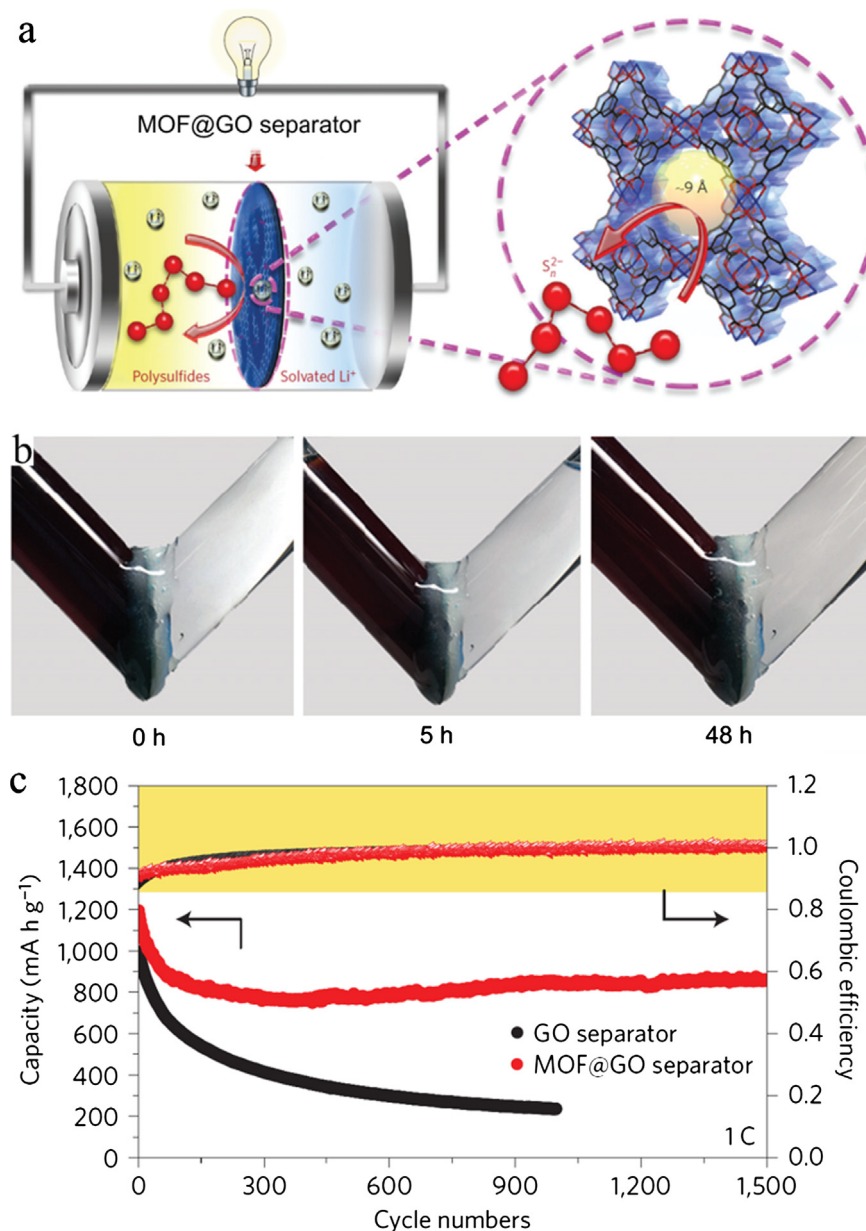


Fig. 25. (a) Schematic presentation of GO@CuBTC membrane in lithium–sulfur battery. (b) Li^+ ion and polysulfide permeation properties through the GO@CuBTC membrane. The GO@CuBTC membrane retained the polysulfides over 48 h. (c) Cycling performance of lithium–sulfur batteries with GO@CuBTC membrane and with GO membrane. Adapted from Ref. [233] with permission from the Nature Publishing Group.

performance could be switched smartly.

Apart from the light-responsive features, MOF membranes showed thermo-responsive features as well. Wang et al. fabricated MOF membranes using nanosheets with a thickness of 1.9 nm as building blocks, which were exfoliated from layered MAMS-1 ($\text{Ni}_8(5\text{-bbdc})_6(\text{m-OH})_4$) particles [244]. Due to the layered structure, the prepared membranes with a thickness of 40 nm had two transport channels, a pore structure with a size of 2.9 Å in the monolayer and an interlayered pathway with a size of 5 Å between the sheets. Owing to the thermal vibration of the tert-butyl groups (Fig. 27a and b), the membranes showed thermo-responsive separation properties. When the temperature increased from 20 to 120 °C, the H_2 permeance significantly varied between 0.5 and $14.4 \times 10^{-8} \text{ mol s}^{-1} \text{ m}^{-2} \text{ Pa}^{-1}$, but the CO_2 permeance hardly changed, thus leading to the variation of the H_2/CO_2 selectivity between 5 and 245 (Fig. 27c). The variation tendency was not linear with the increase in temperature. The H_2 permeance initially increased from 13.1 to $14.4 \times 10^{-8} \text{ mol s}^{-1} \text{ m}^{-2} \text{ Pa}^{-1}$ with an increase in the temperature from 20 to 40 °C and then decreased to $0.5 \times 10^{-8} \text{ mol s}^{-1} \text{ m}^{-2} \text{ Pa}^{-1}$ at a temperature of 120 °C. However, because H_2/CO_2 separation in industrial applications is usually performed at a high temperature, it is better to obtain membranes with excellent thermal stability [245,246].

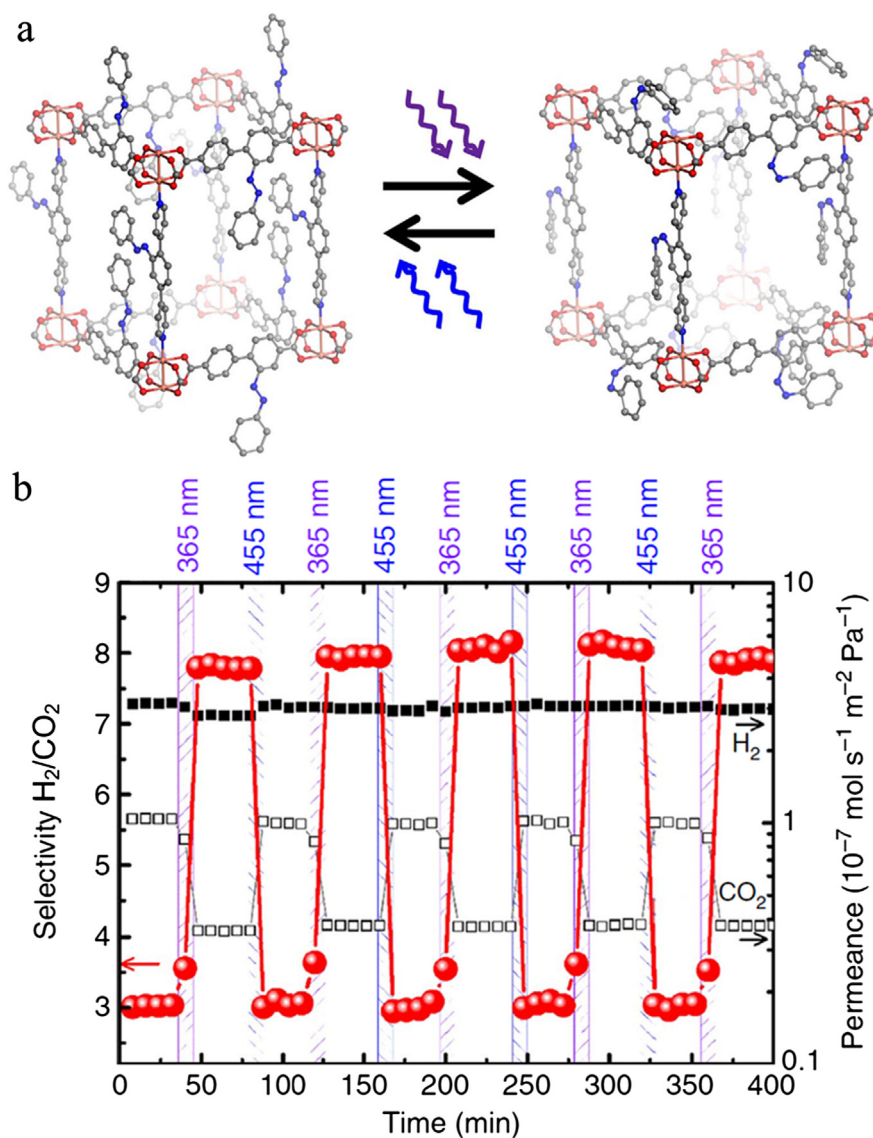


Fig. 26. (a) Chemical structure of $\text{Cu}_2(\text{AzoBPDC})_2(\text{AzoBiPyB})$ with azobenzene groups in trans and cis states. (b) Gas permeances and H_2/CO_2 selectivity of the prepared membrane under irradiation with light of 365 and 455 nm wavelength for 5 min each. Adapted from Ref. [240] with permission from the Nature Publishing Group.

4.4. Catalysis

Catalysis membranes realize the conversion and separation of mixed molecules simultaneously. Unlike the MOF particles with impregnated catalysts, which can be synthesized by solution impregnation, gas-phase deposition, and in situ MOF growth [247–251], MOF catalysis membranes are usually synthesized by growing the MOF layer with intrinsic catalysis properties or with catalysts. Mao et al. used confinement conversion to uniformly encapsulate various heterogeneous functional components into CuBTC membranes [252]. The functional components, including ions, CNTs, proteins, polymeric spheres, and nanoparticles were firstly embedded into the deposited CHN film, and then the film was transformed into the CuBTC membrane through linker solution immersion. By embedding the different components, the synthesized CuBTC composite membranes exhibited some unique properties, including electric conductivity, bioactive electrochemical sensing, and catalysis. By encapsulating Au nanoparticles (NPs) with a diameter of 5 nm, the obtained Au NP/CuBTC membrane could be applied for size-selective hydrogenation of olefins. When pure Au NPs were used as catalysts, both n-hexene and cis-stilbene were converted completely. However, when the composite membrane was employed, only n-hexene passed through the membrane and was catalyzed (Fig. 28).

As a result of the composition, including metal centers and organic linkers, the MOFs had catalytic activity inherently. Yu et al. employed an AAO substrate as the template and metal source for preparing $\text{NH}_2\text{-MIL-53/AAO}$ composite membranes [253]. After in situ growth, the MOF plates with a diameter of 198 nm were formed both on the surface and in the channels of the AAO substrate.

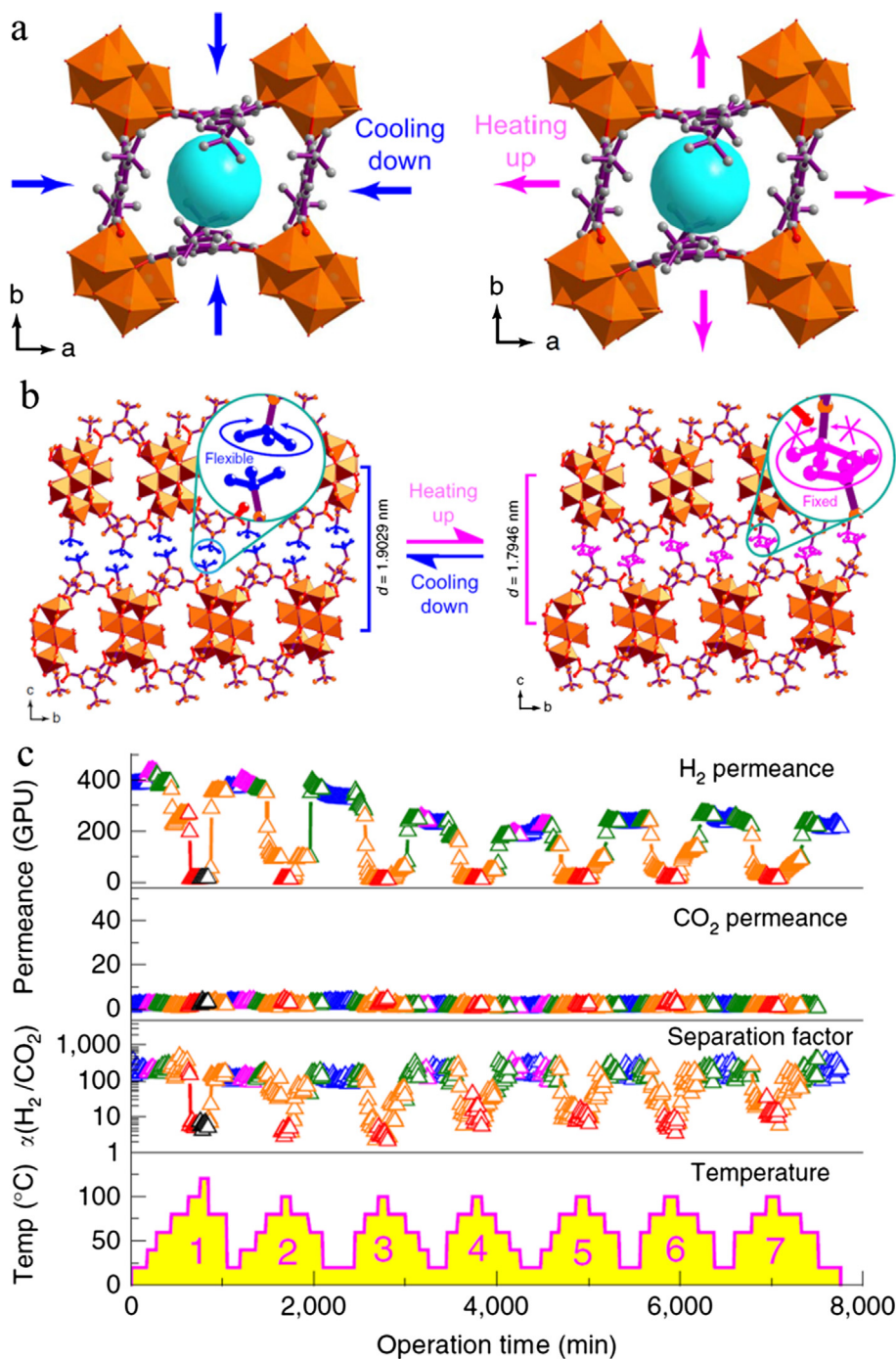


Fig. 27. (a) Illustration of the expansion and shrinkage of MAMS-1. (b) Illustration of the shrinkage and expansion of the interlayer distance of MAMS-1 membrane. (c) Gas permeance and H_2/CO_2 selectivity of the prepared membrane under seven heating/cooling cycles. Different colors represent various temperatures; blue: 20 $^\circ\text{C}$; magenta: 40 $^\circ\text{C}$; olive: 60 $^\circ\text{C}$; orange: 80 $^\circ\text{C}$; red: 100 $^\circ\text{C}$; and black: 120 $^\circ\text{C}$. 1 GPU = $3.348 \times 10^{-10} \text{ mol s}^{-1} \text{ m}^{-2} \text{ Pa}^{-1}$. Adapted from Ref. [244] with permission from the Nature Publishing Group.

Moreover, by adjusting the reaction time, the MOF loading could be controlled easily. The prepared MIL-53-NH₂/AAO membrane was employed for the application of Knoevenagel condensation, and displayed excellent performance and stability for the condensation of benzaldehyde and malononitrile. Zhang fabricated ZIF-8/NaA composite membranes on a stainless-steel plate to fabricate a microreactor [254]. The membrane showed outstanding performance with about 100% product yield in the condensation of ethyl cyanoacetate and benzaldehyde.

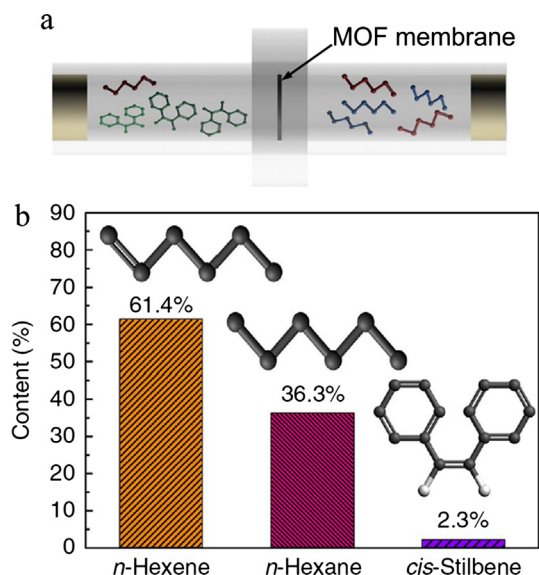


Fig. 28. (a) Membrane reactor with MOF catalysis membrane for size-selective hydrogenation. (b) Hydrocarbon composition of the permeate solution. Adapted from Ref. [252] with permission from the Nature Publishing Group.

5. Conclusions and outlook

This review summarizes the production, modification, and application of MOF membranes. The production methodologies are classified as direct crystallization, interfacial/contra-diffusion synthesis, layer-by-layer assembly, confinement conversion, microfluidic processing, and vapor deposition. The synthesis mechanisms and merits of these methods are discussed. The modification improves the performance distinctly, by changing the construction, microstructure, affinity, and pore size of the MOF membranes. The mechanisms and strategies for the modification of MOF membranes are analyzed and categorized into coating, heteroepitaxial growth, embedding, occupation, grafting, and substitution, with respect to the combination form. The application of MOF membranes, including gas separation, nanofiltration, ionic sieving, stimuli responsiveness, and catalysis, are reviewed, and the separation mechanisms are analyzed. Although tremendous advances in the production, modification, and application of MOF membranes have been achieved recently, some opportunities and challenges still exist for further development.

The production of MOF membranes with a large membrane area is very important for industrial application. However, the membrane area of reported MOF membranes is typically only several square centimeters. Li et al. fabricated an MOF membrane module with a membrane area of 340 square centimeters by gel-vapor deposition [126], but the large-scale production of MOF membranes is still a significant challenge. Various methods are proposed for membrane production. Direct crystallization is the most investigated method and can prepare MOF membranes under mild conditions. However, the modification of substrates through seeding and grafting increases the complexity of the synthesis procedures. Mixed precursor solutions for the direct crystallization and related microfluidic processing lead to the formation of crystals in bulk, which results in the wastage of the expensive linker reagents. Interfacial synthesis and related microfluidic processing greatly reduce the consumption of MOF precursors due to the use of non-interfering metal salt and linker solutions; however, the requirement of two immiscible solutions limits the types of MOFs for membrane synthesis. Contra-diffusion synthesis does not require synthesis solutions, but the crystallization region should be controlled carefully to prepare continuous membranes, due to the uncertain interface. Confinement conversion simplifies the crystallization process, but the complicated synthesis procedures of the metal sources hinder the large-scale production of MOF membranes; furthermore, the incomplete conversion of the metal source may decrease the permeance. Layer-by-layer assembly requires only mild synthesis conditions and exhibit great controllability; however, the poor microstructures of the prepared membranes lead to a deterioration in the separation performance. Vapor deposition has been demonstrated for the production of MOF membranes; however, a high synthesis temperature is required to generate the linker vapors. To solve the above issues and use the opportunities, further investigation should focus on how to produce MOF membranes with both a large membrane area and good continuity. Synthesis under mild conditions should be developed, and the procedures should be simplified further. In addition to the commonly used MOFs, including ZIFs, MOF-5, CuBTC, NH_2 -MIL-53, and UiO-66, other types of MOFs should be employed for membrane fabrication to improve the application scope and performance. Moreover, to reduce the costs of MOF membrane production, the utilization of the expensive MOF precursors, especially the linkers, should be significantly improved.

Modification of the MOF membranes is proposed for improving their performance. The microstructures of the MOF membranes should be controlled more precisely. For MOF membranes, only the sub-nanometer-sized defects are unexpected. As modification usually changes the construction of the whole membrane, selectivity is strengthened, but permeance is suppressed. Further study is needed to selectively modify the cracks other than both the invalid defects and effective pores of MOF membranes, in order to achieve a higher permeance. Moreover, the types of materials and molecules involved in modification are relatively few. Due to the properties

of the separation system, it is better to introduce more modification reagents for synthesizing composite membranes with targeted adsorption affinities and pore structures. Furthermore, the modification processes of MOF membranes are complicated, and are regarded as a hindrance for practical application. Along with effective performance improvement, the processes of modification should be simplified as far as possible. In addition, the modification should be designed with precise targets. For example, in H_2/CO_2 separation, the pore size of the MOFs should be controlled or the difference in affinities of the MOFs for two feed gas components should be increased, by modification. This should be the design with respect to the molecular dynamics.

The application of MOF membranes with high efficiency is the main goal of studies. The first reported MOF-5 membrane showed permeation properties in accordance with the Knudsen diffusion [36]. After development, many MOF membranes, including ZIF-8, ZIF-95, ZIF-100, and NH_2 -MIL-53, show a great potential for practical application. More MOF membranes with different topological structures should be synthesized and investigated. ZIF-8 membranes have been proposed to separate H_2 from N_2 , CH_4 , and hydrocarbons, initially. Thereafter, ZIF-8 membranes have been demonstrated with a sharp cut-off between C_3H_6 and C_3H_8 . Therefore, in addition to the synthesis of new MOF membranes, we should develop new applications based on the pore structure and adsorption properties of the MOFs. Similar to the reports of stimuli responsiveness, new functions should be explored in addition to separation, through the synthesis of MOF membranes using MOFs with special properties or the hybridization of MOF membranes using substances with expected functions, in order to apply MOF membranes in a new field. The performance of MOF membranes under harsh conditions should be enhanced. For example, the C_3H_6/C_3H_8 selectivity of ZIF-8 membranes decreases greatly with an increase in the feed pressure. However, the pressure of practical C_3H_6/C_3H_8 mixtures is typically high. The separation of H_2/CO_2 under high temperatures is a great challenge, due to the increased diffusion of both the molecules. Unpleasantly, H_2/CO_2 mixtures are often produced with huge amounts of heat. More studies should also focus on the long-term stability of MOF membranes.

We hope that understanding the mechanism of production, modification, and application of MOF membranes will be helpful in developing MOF application and membrane separation.

Acknowledgements

This work was supported by the National Natural Science Foundation of China [Grant Number 51708252], Fundamental Research Funds for the Central Universities [Grant Number 21617322], and Jinan University [Grant Number 88016674].

References

- [1] Shannon MA, Bohn PW, Elimelech M, Georgiadis JG, Marinas BJ, Mayes AM. Science and technology for water purification in the coming decades. *Nature* 2008;452:301–10.
- [2] Elimelech M, Phillip WA. The future of seawater desalination: energy, technology, and the environment. *Science* 2011;333:712–7.
- [3] Park HB, Kamcev J, Robeson LM, Elimelech M, Freeman BD. Maximizing the right stuff: The trade-off between membrane permeability and selectivity. *Science* 2017. 356:eaab0530.
- [4] Lively RP, Sholl DS. From water to organics in membrane separations. *Nat Mater* 2017;16:276–9.
- [5] Werber JR, Osuji CO, Elimelech M. Materials for next-generation desalination and water purification membranes. *Nat Rev Mater* 2016;1:16018.
- [6] Denny MS, Moreton JC, Benz L, Cohen SM. Metal-organic frameworks for membrane-based separations. *Nat Rev Mater* 2016;1:16078.
- [7] Robeson LM. The upper bound revisited. *J Membr Sci* 2008;320:390–400.
- [8] Seoane B, Coronas J, Gascon I, Benavides ME, Karvan O, Caro J, et al. Metal-organic framework based mixed matrix membranes: a solution for highly efficient CO_2 capture? *Chem Soc Rev* 2015;44:2421–54.
- [9] Dechnik J, Gascon J, Doonan CJ, Janiak C, Sumbly CJ. Mixed-matrix membranes. *Angew Chem Int Ed* 2017;56:9292–310.
- [10] Xiang L, Sheng L, Wang C, Zhang L, Pan Y, Li Y. Amino-functionalized ZIF-7 nanocrystals: improved intrinsic separation ability and interfacial compatibility in mixed-matrix membranes for CO_2/CH_4 separation. *Adv Mater* 2017;29:1606999.
- [11] Matsumoto M, Kitaoka T. Ultraselective gas separation by nanoporous metal-organic frameworks embedded in gas-barrier nanocellulose films. *Adv Mater* 2016;28:1765–9.
- [12] Wang Z, Wang D, Zhang S, Hu L, Jin J. Interfacial design of mixed matrix membranes for improved gas separation performance. *Adv Mater* 2016;28:3399–405.
- [13] Deng YH, Chen JT, Chang CH, Liao KS, Tung KL, Price WE, et al. A drying-free, water-based process for fabricating mixed-matrix membranes with outstanding pervaporation performance. *Angew Chem Int Ed* 2016;55:12793–6.
- [14] Jeon MY, Kim D, Kumar P, Lee PS, Rangnekar N, Bai P, et al. Ultra-selective high-flux membranes from directly synthesized zeolite nanosheets. *Nature* 2017;543:690–4.
- [15] Huang Y, Wang L, Song Z, Li S, Yu M. Growth of high-quality, thickness-reduced zeolite membranes towards N_2/CH_4 separation using high-aspect-ratio seeds. *Angew Chem Int Ed* 2015;54:10843–7.
- [16] Feng X, Zong Z, Elsaïdi SK, Jasinski JB, Krishna R, Thallapally PK, et al. Kr/Xe separation over a chabazite zeolite membrane. *J Am Chem Soc* 2016;138:9791–4.
- [17] Jiang J, Wang L, Peng L, Cai C, Zhang C, Wang X, et al. Preparation and characterization of high performance CHA zeolite membranes from clear solution. *J Membr Sci* 2017;527:51–9.
- [18] Zhou C, Wang N, Qian Y, Liu X, Caro J, Huang A. Efficient synthesis of dimethyl ether from methanol in a bifunctional zeolite membrane reactor. *Angew Chem Int Ed* 2016;55:12678–82.
- [19] Chng ML, Xiao Y, Chung TS, Toriida M, Tamai S. Enhanced propylene/propane separation by carbonaceous membrane derived from poly (aryl ether ketone)/2,6-bis(4-azidobenzylidene)-4-methyl-cyclohexanone interpenetrating network. *Carbon* 2009;47:1857–66.
- [20] Ma X, Lin YS, Wei X, Knief J. Ultrathin carbon molecular sieve membrane for propylene/propane separation. *AIChE J* 2016;62:491–9.
- [21] Koh DY, McCool BA, Deckman HW, Lively RP. Reverse osmosis molecular differentiation of organic liquids using carbon molecular sieve membranes. *Science* 2016;353:804–7.
- [22] Liu G, Jin W, Xu N. Graphene-based membranes. *Chem Soc Rev* 2015;44:5016–30.
- [23] Joshi RK, Carbone P, Wang FC, Kravets VG, Su Y, Grigorieva IV, et al. Precise and ultrafast molecular sieving through graphene oxide membranes. *Science* 2014;343:752–4.
- [24] Kim HW, Yoon HW, Yoon SM, Yoo BM, Ahn BK, Cho YH, et al. Selective gas transport through few-layered graphene and graphene oxide membranes. *Science* 2013;342:91–5.
- [25] Li H, Song Z, Zhang X, Huang Y, Li S, Mao Y, et al. Ultrathin, molecular-sieving graphene oxide membranes for selective hydrogen separation. *Science* 2013;342:95–8.
- [26] Huang H, Song Z, Wei N, Shi L, Mao Y, Ying Y, et al. Ultrafast viscous water flow through nanostrand-channelled graphene oxide membranes. *Nat Commun*

- 2013;4:2979.
- [27] Furukawa H, Cordova KE, O’Keeffe M, Yaghi OM. The chemistry and applications of metal-organic frameworks. *Science* 2013;341:1230444–51.
- [28] Wang C, Liu X, Demir NK, Chen JP, Li K. Applications of water stable metal-organic frameworks. *Chem Soc Rev* 2016;45:5107–34.
- [29] Zhang G, Zhang J, Su P, Xu Z, Li W, Shen C, et al. Non-activation MOF arrays as a coating layer to fabricate a stable superhydrophobic micro/nano flower-like architecture. *Chem Commun* 2017;53:8340–3.
- [30] Zhang C, Wang B, Li W, Huang S, Kong L, Li Z, et al. Conversion of invisible metal-organic frameworks to luminescent perovskite nanocrystals for confidential information encryption and decryption. *Nat Commun* 2017;8:1138.
- [31] Hermes S, Schröder F, Chelmoski R, Wöll C, Fischer RA. Selective nucleation and growth of metal-organic open framework thin films on patterned COOH/CF₃-terminated self-assembled monolayers on Au(111). *J Am Chem Soc* 2005;127:13744–5.
- [32] Hermes S, Zacher D, Baunemann A, Wöll C, Fischer RA. Selective growth and MOCVD loading of small single crystals of MOF-5 at alumina and silica surfaces modified with organic self-assembled monolayers. *Chem Mater* 2007;19:2168–73.
- [33] Liu J, Wöll C. Surface-supported metal-organic framework thin films: fabrication methods, applications, and challenges. *Chem Soc Rev* 2017;46:5730–70.
- [34] Qiu S, Xue M, Zhu G. Metal-organic framework membranes: from synthesis to separation application. *Chem Soc Rev* 2014;43:6116–40.
- [35] Yao J, Wang H. Zeolitic imidazolate framework composite membranes and thin films: synthesis and applications. *Chem Soc Rev* 2014;43:4470–93.
- [36] Li W, Zhang Y, Li Q, Zhang G. Metal-organic framework composite membranes: synthesis and separation applications. *Chem Eng Sci* 2015;135:232–57.
- [37] Kang Z, Fan L, Sun D. Recent advances and challenges of metal-organic framework membranes for gas separation. *J Mater Chem A* 2017;5:10073–91.
- [38] Liu Y, Ng Z, Khan EA, Jeong HK, Ching C, Lai Z. Synthesis of continuous MOF-5 membranes on porous alpha-alumina substrates. *Microporous Mesoporous Mater* 2009;118:296–301.
- [39] Guo H, Zhu G, Hewitt IJ, Qiu S. “Twin copper source” growth of metal-organic framework membrane: Cu₃(BTC)₂ with high permeability and selectivity for recycling H₂. *J Am Chem Soc* 2009;131:1646–7.
- [40] Ranjan R, Tsapatsis M. Microporous metal-organic framework membrane on porous support using the seeded growth method. *Chem Mater* 2009;21:4920–4.
- [41] Yoo Y, Lai Z, Jeong HK. Fabrication of MOF-5 membranes using microwave-induced rapid seeding and solvothermal secondary growth. *Microporous Mesoporous Mater* 2009;123:100–6.
- [42] Bux H, Liang F, Li Y, Cravillon J, Wiebcke M, Caro J. Zeolitic imidazolate framework membrane with molecular sieving properties by microwave-assisted solvothermal synthesis. *J Am Chem Soc* 2009;131:16000–1.
- [43] Kang Z, Ding J, Fan L, Xue M, Zhang D, Gao L, et al. Preparation of a MOF membrane with 3-aminopropyltriethoxysilane as covalent linker for xylene isomers separation. *Inorg Chem Commun* 2013;30:74–8.
- [44] Sun YX, Yang F, Wei Q, Wang NX, Qin X, Zhang SK, et al. Oriented nano-microstructure-assisted controllable fabrication of metal-organic framework membranes on nickel foam. *Adv Mater* 2016;28:2374–81.
- [45] Lu HY, Zhu SP. Interfacial synthesis of free-standing metal-organic framework membranes. *Eur J Inorg Chem* 2013;8:1294–300.
- [46] Liu Y, Ban Y, Yang W. Microstructural engineering and architectural design of metal-organic framework membranes. *Adv Mater* 2017;29:1606949.
- [47] Li P, Wang Z, Qiao Z, Liu Y, Cao X, Li W, et al. Recent developments in membranes for efficient hydrogen purification. *J Membr Sci* 2015;495:130–68.
- [48] Yang Q, Li L, Tan W, Sun Y, Wang H, Ma J, et al. Exceptional high selectivity of hydrogen/methane separation on a phosphonate-based MOF membrane with exclusion of methane molecules. *Chem Commun* 2017;53:9797–800.
- [49] Kong C, Du H, Chen L, Chen B. Nanoscale MOF/organosilica membranes on tubular ceramic substrates for highly selective gas separation. *Energy Environ Sci* 2017;10:1812–9.
- [50] Li YS, Liang FY, Bux H, Feldhoff A, Yang WS, Caro J. Molecular sieve membrane: supported metal-organic framework with high hydrogen selectivity. *Angew Chem Int Ed* 2010;49:548–51.
- [51] Venna SR, Carreon MA. Highly permeable zeolite imidazolate framework-8 membranes for CO₂/CH₄ separation. *J Am Chem Soc* 2010;132:76–8.
- [52] Bux H, Feldhoff A, Cravillon J, Wiebcke M, Li YS, Caro J. Oriented zeolitic imidazolate framework-8 membrane with sharp H₂/C₃H₈ molecular sieve separation. *Chem Mater* 2011;23:2262–9.
- [53] Kang Z, Xue M, Fan L, Huang L, Guo L, Wei G, et al. Highly selective sieving of small gas molecules by using an ultra-microporous metal-organic framework membrane. *Energy Environ Sci* 2014;7:4053–60.
- [54] Mao YY, Cao W, Li JW, Sun LW, Peng XS. HKUST-1 membranes anchored on porous substrate by hetero MIL-110 nanorod array seeds. *Chem Eur J* 2013;19:11883–6.
- [55] Huang A, Chen Y, Liu Q, Wang N, Jiang J, Caro J. Synthesis of highly hydrophobic and permselective metal-organic framework Zn(BDC)(TED)(0.5) membranes for H₂/CO₂ separation. *J Membr Sci* 2014;454:126–32.
- [56] Kong L, Zhang X, Liu H, Qiu J. Synthesis of a highly stable ZIF-8 membrane on a macroporous ceramic tube by manual-rubbing ZnO deposition as a multi-functional layer. *J Membr Sci* 2015;490:354–63.
- [57] Friebe S, Geppert B, Steinbach F, Caro J. Metal-organic framework UiO-66 layer: a highly oriented membrane with good selectivity and hydrogen permeance. *ACS Appl Mater Interfaces* 2017;9:12878–85.
- [58] Huang A, Dou W, Caro J. Steam-stable zeolitic imidazolate framework ZIF-90 membrane with hydrogen selectivity through covalent functionalization. *J Am Chem Soc* 2010;132:15562–4.
- [59] Huang A, Bux H, Steinbach F, Caro J. Molecular-sieve membrane with hydrogen permselectivity: ZIF-22 in LTA topology prepared with 3-aminopropyltriethoxysilane as covalent linker. *Angew Chem Int Ed* 2010;49:4958–61.
- [60] Liu Q, Wang N, Caro J, Huang A. Bio-inspired polydopamine: a versatile and powerful platform for covalent synthesis of molecular sieve membranes. *J Am Chem Soc* 2013;135:17679–82.
- [61] Huang A, Chen Y, Wang N, Hu Z, Jiang J, Caro J. A highly permeable and selective zeolitic imidazolate framework ZIF-95 membrane for H₂/CO₂ separation. *Chem Commun* 2012;48:10981–3.
- [62] Huang A, Liu Q, Wang N, Caro J. Highly hydrogen permselective ZIF-8 membranes supported on polydopamine functionalized macroporous stainless-steel-nets. *J Mater Chem A* 2014;22:8246–51.
- [63] Wang N, Liu Y, Qiao Z, Diestel L, Zhou J, Huang A, et al. Polydopamine-based synthesis of a zeolite imidazolate framework ZIF-100 membrane with high H₂/CO₂ selectivity. *J Mater Chem A* 2015;3:4722–8.
- [64] Ben T, Lu C, Pei C, Xu S, Qiu S. Polymer-supported and free-standing metal-organic framework membrane. *Chem Eur J* 2012;18:10250–3.
- [65] McCarthy MC, Guerrero VV, Barnett G, Jeong HK. Synthesis of zeolitic imidazolate framework films and membranes with controlled microstructure. *Langmuir* 2010;26:14636–41.
- [66] Hu YX, Dong XL, Nan JP, Jin WQ, Ren XM, Xu NP, et al. Metal-organic framework membranes fabricated via reactive seeding. *Chem Commun* 2011;47:737–9.
- [67] Dong XL, Huang K, Liu SN, Ren RF, Jin WQ, Lin YS. Synthesis of zeolitic imidazolate framework-78 molecular-sieve membrane: defect formation and elimination. *J Mater Chem* 2012;22:19222–7.
- [68] Kang Z, Xue M, Fan L, Ding J, Guo L, Gao L, et al. “Single nickel source” in situ fabrication of a stable homochiral MOF membrane with chiral resolution properties. *Chem Commun* 2013;49:10569–71.
- [69] Dong XL, Lin YS. Synthesis of an organophilic ZIF-71 membrane for pervaporation solvent separation. *Chem Commun* 2013;49:1196–8.
- [70] Pan Y, Li T, Lestari G, Lai Z. Effective separation of propylene/propane binary mixtures by ZIF-8 membranes. *J Membr Sci* 2012;390–391:93–8.
- [71] Pan Y, Wang B, Lai Z. Synthesis of ceramic hollow fiber supported zeolitic imidazolate framework-8 (ZIF-8) membranes with high hydrogen permeability. *J Membr Sci* 2012;421–422:292–8.
- [72] He G, Dakhchoune M, Zhao J, Huang S, Agrawal KV. Electrophoretic nuclei assembly for crystallization of high-performance membranes on unmodified supports. *Adv Funct Mater* 2018;28:1707427.
- [73] Brown AJ, Johnson JR, Lydon ME, Koros WJ, Jones CW, Nair S. Continuous polycrystalline zeolitic imidazolate framework-90 membranes on polymeric hollow fibers. *Angew Chem Int Ed* 2012;51:10615–8.

- [74] Hou J, Sutrisna PD, Zhang Y, Chen V. Formation of ultrathin, continuous metal-organic framework membranes on flexible polymer substrates. *Angew Chem Int Ed* 2016;55:3947–51.
- [75] Li W, Yang Z, Zhang G, Fan Z, Meng Q, Shen C, et al. Stiff metal-organic framework-polyacrylonitrile hollow fiber composite membranes with high gas permeability. *J Mater Chem A* 2014;2:2110–8.
- [76] Li W, Meng Q, Li X, Zhang C, Fan Z, Zhang G. Non-activation ZnO array as a buffering layer to fabricate strongly adhesive metal-organic framework/PVDF hollow fiber membranes. *Chem Commun* 2014;50:9711–3.
- [77] Su P, Li W, Zhang C, Meng Q, Shen C, Zhang G. Metal based gels as versatile precursors to synthesize stiff and integrated MOF/polymer composite membranes. *J Mater Chem A* 2015;3:20345–51.
- [78] Li W, Meng Q, Zhang C, Zhang G. Metal-organic framework/PVDF composite membranes with high H₂ permselectivity synthesized by ammoniation. *Chem Eur J* 2015;21:7224–30.
- [79] Li W, Su P, Zhang G, Shen C, Meng Q. Preparation of continuous NH₂-MIL-53 membrane on ammoniated polyvinylidene fluoride hollow fiber for efficient H₂ purification. *J Membr Sci* 2015;495:384–91.
- [80] Ameloot R, Vermoortele F, Vanhove W, Roeffaers MJB, Sels BF, Vos DED. Interfacial synthesis of hollow metal-organic framework capsules demonstrating selective permeability. *Nat Chem* 2011;3:382–7.
- [81] Li W, Zhang Y, Xu Z, Meng Q, Fan Z, Ye S, et al. Assembly of MOF microcapsules with size-selective permeability on cell walls. *Angew Chem Int Ed* 2016;55:955–9.
- [82] Yao JF, Dong DH, Li D, He L, Xu GS, Wang HT. Contra-diffusion synthesis of ZIF-8 films on a polymer substrate. *Chem Commun* 2011;47:2559–61.
- [83] He M, Yao JF, Li LX, Zhong ZX, Chen FY, Wang HT. Aqueous solution synthesis of ZIF-8 films on a porous nylon substrate by contra-diffusion method. *Microporous Mesoporous Mater* 2013;179:10–6.
- [84] Li Y, Wee LH, Volodin A, Martensa JA, Vankelecom IFJ. Polymer supported ZIF-8 membranes prepared via an interfacial synthesis method. *Chem Commun* 2015;51:918–20.
- [85] Shamsaei E, Lin X, Low ZX, Abbasi Z, Hu Y, Liu JZ, et al. Aqueous phase synthesis of ZIF-8 membrane with controllable location on an asymmetrically porous polymer substrate. *ACS Appl Mater Interfaces* 2016;8:6236–44.
- [86] Barankova E, Tan X, Villalobos LF, Litwiller E, Peinemann KV. A metal chelating porous polymeric support: the missing link for a defect-free metal-organic framework composite membrane. *Angew Chem Int Ed* 2017;56:2965–8.
- [87] Xie Z, Yang JH, Wang JQ, Bai J, Yin HM, Yuan B, et al. Deposition of chemically modified Al₂O₃ particles for high performance ZIF-8 membrane on a macroporous tube. *Chem Commun* 2012;48:5977–9.
- [88] Huang K, Li Q, Liu G, Shen J, Guan K, Jin W. A ZIF-71 hollow fiber membrane fabricated by contra-diffusion. *ACS Appl Mater Interfaces* 2015;7:16157–60.
- [89] Kwon HT, Jeong HK. In situ synthesis of thin zeolitic-imidazolate framework ZIF-8 membranes exhibiting exceptionally high propylene/propane separation. *J Am Chem Soc* 2013;135:10763–8.
- [90] Kwon HT, Jeong HK. Highly propylene-selective supported zeolite-imidazolate framework (ZIF-8) membranes synthesized by rapid microwave-assisted seeding and secondary growth. *Chem Commun* 2013;49:3854–6.
- [91] Kwon HT, Jeong HK. Improving propylene/propane separation performance of Zeolitic-Imidazolate framework ZIF-8 membranes. *Chem Eng Sci* 2015;124:20–6.
- [92] Hillman F, Brito J, Jeong HK. Rapid one-pot microwave synthesis of mixed-linker hybrid zeolitic-imidazolate framework membranes for tunable gas separations. *ACS Appl Mater Interfaces* 2018;10:5586–93.
- [93] Shekhah O, Wang H, Kowarik S, Schreiber F, Paulus M, Tolan M, et al. Step-by-step route for the synthesis of metal-organic frameworks. *J Am Chem Soc* 2007;129:15118–9.
- [94] Shekhah O, Wang H, Paradinas M, Ocal C, Schüpbach B, Terfort A, et al. Controlling interpenetration in metal-organic frameworks by liquid-phase epitaxy. *Nat Mater* 2009;8:481–4.
- [95] Sakaida S, Otsubo K, Sakata O, Song C, Fujiwara A, Takata M, et al. Crystalline coordination framework endowed with dynamic gate-opening behaviour by being downsized to a thin film. *Nat Chem* 2016;8:377–83.
- [96] Zhuang JL, Terfort A, Wöll C. Formation of oriented and patterned films of metal-organic frameworks by liquid phase epitaxy: a review. *Coord Chem Rev* 2016;307:391–424.
- [97] Shekhah O, Swaidan R, Belmabkhout Y, Plessis MD, Jacobs T, Barbour L, et al. The liquid phase epitaxy approach for the successful construction of ultra-thin and defect-free ZIF-8 membranes: pure and mixed gas transport study. *Chem Commun* 2014;50:2089–92.
- [98] Nagaraju D, Bhagat DG, Banerjee R, Kharul UK. In situ growth of metal-organic frameworks on a porous ultrafiltration membrane for gas separation. *J Mater Chem A* 2013;1:8828–35.
- [99] Chernikova V, Shekhah O, Eddaoudi M. Advanced fabrication method for the preparation of MOF thin films: liquid-phase epitaxy approach meets spin coating method. *ACS Appl Mater Interfaces* 2016;8:20459–64.
- [100] Hurtle S, Friebe S, Wohlgemuth J, Wöll C, Caro J, Heinke L. Sprayable, large-area metal-organic framework films and membranes of varying thickness. *Chem Eur J* 2017;23:2294–8.
- [101] Huang K, Dong ZY, Li QQ, Jin WQ. Growth of a ZIF-8 membrane on the inner-surface of a ceramic hollow fiber via cycling precursors. *Chem Commun* 2013;49:10326–8.
- [102] Cacho-Bailo F, Catalán-Aguirre S, Etxeberria-Benavides M, Karvan O, Sebastian V, Téllez C, et al. Metal-organic framework membranes on the inner-side of a polymeric hollow fiber by microfluidic synthesis. *J Membr Sci* 2015;476:277–85.
- [103] Cacho-Bailo F, Caro G, Etxeberria-Benavides M, Karvan O, Téllez C, Coronas J. High selectivity ZIF-93 hollow fiber membranes for gas separation. *Chem Commun* 2015;51:11283–5.
- [104] Lee MJ, Hamid MRA, Lee J, Kim JS, Lee YM, Jeong HK. Ultrathin zeolitic-imidazolate framework ZIF-8 membranes on polymeric hollow fibers for propylene/propane separation. *J Membr Sci* 2018;559:28–34.
- [105] Brown AJ, Brunelli NA, Eum K, Rashidi F, Johnson JR, Koros WJ, et al. Interfacial microfluidic processing of metal-organic framework hollow fiber membranes. *Science* 2014;345:72–5.
- [106] Eum K, Rowanaghi A, Choi D, Bhave RR, Jones CW, Nair S. Fluidic processing of high-performance ZIF-8 membranes on polymeric hollow fibers: mechanistic insights and microstructure control. *Adv Funct Mater* 2016;26:5011–8.
- [107] Eum K, Ma C, Rowanaghi A, Jones CW, Nair S. ZIF-8 membranes via interfacial microfluidic processing in polymeric hollow fibers: efficient propylene separation at elevated pressures. *ACS Appl Mater Interfaces* 2016;8:25337–42.
- [108] Eum K, Ma C, Koh DY, Rashidi F, Li Z, Jones CW, et al. Zeolitic imidazolate framework membranes supported on macroporous carbon hollow fibers by fluidic processing techniques. *Adv Mater Interfaces* 2017;4:1700080.
- [109] Biswal BP, Bhaskar A, Banerjee R, Kharul UK. Selective interfacial synthesis of metal-organic frameworks on a polybenzimidazole hollow fiber membrane for gas separation. *Nanoscale* 2015;7:7291–8.
- [110] Marti AM, Wickramanayake W, Dahe G, Sekizkardes A, Bank TL, Hopkinson DP, et al. Continuous flow processing of ZIF-8 membranes on polymeric porous hollow fiber supports for CO₂ capture. *ACS Appl Mater Interfaces* 2017;7:5678–82.
- [111] Mao Y, Shi L, Huang H, Cao W, Li J, Sun L, et al. Room temperature synthesis of free-standing HKUST-1 membranes from copper hydroxide nanostrands for gas separation. *Chem Commun* 2013;49:5666–8.
- [112] Li J, Cao W, Mao Y, Ying Y, Sun L, Peng X. Zinc hydroxide nanostrands: unique precursors for synthesis of ZIF-8 thin membranes exhibiting high size-sieving ability for gas separation. *CrystEngComm* 2014;16:9788–91.
- [113] Hu P, Yang Y, Mao Y, Li J, Cao W, Ying Y, et al. Room temperature synthesis of ZIF-8 membranes from seeds anchored in gelatin films for gas separation. *CrystEngComm* 2015;17:1576–82.
- [114] Mao Y, Li J, Cao W, Ying Y, Sun L, Peng X. Pressure-assisted synthesis of HKUST-1 thin film on polymer hollow fiber at room temperature toward gas

- separation. *ACS Appl Mater Interfaces* 2014;6:4473–9.
- [115] Mao Y, Su B, Cao W, Li J, Ying Y, Ying W, et al. Specific oriented metal-organic framework membranes and their facet-tuned separation performance. *ACS Appl Mater Interfaces* 2014;6:15676–85.
- [116] Liu Y, Wang N, Pan JH, Steinbach F, Caro J. In-situ synthesis of MOF membranes on ZnAl-CO₃ LDH buffer layer-modified substrates. *J Am Chem Soc* 2014;136:14353–6.
- [117] Liu Y, Pan JH, Wang N, Steinbach F, Liu X, Caro J. Remarkably enhanced gas separation by partial self-conversion of a laminated membrane to metal-organic frameworks. *Angew Chem Int Ed* 2015;54:3028–32.
- [118] Liu Y, Peng Y, Wang N, Li Y, Pan JH, Yang W, et al. Significantly enhanced separation using ZIF-8 membranes by partial conversion of calcined layered double hydroxide precursors. *ChemSusChem* 2015;8:3582–6.
- [119] Drobek M, Bechelany M, Vallicari C, Chaaya AA, Charmette C, Salvador-Levehang C, et al. An innovative approach for the preparation of confined ZIF-8 membranes by conversion of ZnO ALD layers. *J Membr Sci* 2015;475:39–46.
- [120] Zhang XF, Liu YG, Kong LY, Liu HO, Qiu JS, Han W, et al. A simple and scalable method for preparing low-defect ZIF-8 tubular membranes. *J Mater Chem A* 2013;1:10635–8.
- [121] Zhang XF, Liu YG, Li SH, Kong LY, Liu HO, Li YS, et al. New membrane architecture with high performance: ZIF-8 membrane supported on vertically aligned ZnO nanorods for gas permeation and separation. *Chem Mater* 2014;26:1975–81.
- [122] Neelakanda P, Barankova E, Peinemann KV. Polymer supported ZIF-8 membranes by conversion of sputtered zinc oxide layers. *Microporous Mesoporous Mater* 2016;220:215–9.
- [123] Wang X, Sun M, Meng B, Tan X, Liu J, Wang S, et al. Formation of continuous and highly permeable ZIF-8 membranes on porous alumina and zinc oxide hollow fibers. *Chem Commun* 2016;52:13448–51.
- [124] Stassen I, De Vos D, Ameloot R. Vapor-phase deposition and modification of metal-organic frameworks: state-of-the-art and future directions. *Chem Eur J* 2016;22:14452–60.
- [125] Stassen I, Styles M, Grecni G, Gorp HV, Vanderlinden W, De Feyter S, et al. Chemical vapour deposition of zeolitic imidazolate framework thin films. *Nat Mater* 2016;15:304–10.
- [126] Li W, Su P, Li Z, Xu Z, Wang F, Ou H, et al. Ultrathin metal-organic framework membrane production by gel-vapour deposition. *Nat Commun* 2017;8:406.
- [127] Shah MN, Gonzalez MA, McCarthy MC, Jeong HK. An unconventional rapid synthesis of high performance metal-organic framework membranes. *Langmuir* 2013;29:7896–902.
- [128] Melgar VMA, Kwon HT, Kim J. Direct spraying approach for synthesis of ZIF-7 membranes by electrospray deposition. *J Membr Sci* 2014;459:190–6.
- [129] Hod I, Bury W, Karlin DM, Deria P, Kung CW, Katz MJ, et al. Directed growth of electroactive metal-organic framework thin films using electrophoretic deposition. *Adv Mater* 2014;26:6295–300.
- [130] Shah MN, McCarthy MC, Sachdeva S, Lee AK, Jeong HK. Current status of metal-organic framework membranes for gas separations: promises and challenges. *Ind Eng Chem Res* 2012;51:2179–99.
- [131] Tan JC, Cheetham AK. Mechanical properties of hybrid inorganic-organic framework materials: establishing fundamental structure-property relationships. *Chem Soc Rev* 2011;40:1059–80.
- [132] Wu H, Yildirim T, Zhou W. Exceptional mechanical stability of highly porous zirconium metal-organic framework UiO-66 and its important implications. *J Phys Chem Lett* 2013;4:925–30.
- [133] Koros WJ, Zhang C. Materials for next-generation molecularly selective synthetic membranes. *Nat Mater* 2017;16:289–97.
- [134] Yin H, Wang J, Xie Z, Yang J, Bai J, Lu J, et al. A highly permeable and selective amino-functionalized MOF CAU-1 membrane for CO₂-N₂ separation. *Chem Commun* 2014;50:3699–701.
- [135] Jian Y, Yin H, Chang F, Cheng L, Yang J, Mu W, et al. Facile synthesis of highly permeable CAU-1 tubular membranes for separation of CO₂/N₂ mixtures. *J Membr Sci* 2017;522:140–50.
- [136] Wu D, Maurin G, Yang Q, Serre C, Jobic H, Zhong C. Computational exploration of a Zr-carboxylate based metal-organic framework as a membrane material for CO₂ capture. *J Mater Chem A* 2014;2:1657–61.
- [137] Rui Z, James JB, Kasik A, Lin YS. Metal-organic framework membrane process for high purity CO₂ production. *AIChE J* 2016;62:3836–41.
- [138] Rui Z, James JB, Lin YS. Highly CO₂ perm-selective metal-organic framework membranes through CO₂ annealing post-treatment. *J Membr Sci* 2018;555:97–104.
- [139] Guerrero VV, Yoo Y, McCarthy MC, Jeong HK. HKUST-1 membranes on porous supports using secondary growth. *J Mater Chem* 2010;20:3938–43.
- [140] Zhang F, Zo X, Gao X, Fan S, Sun F, Ren H, et al. Hydrogen selective NH₂-MIL-53(Al) MOF membranes with high permeability. *Adv Funct Mater* 2012;22:3583–90.
- [141] Zhou SY, Zou XQ, Sun FX, Zhang F, Fan SJ, Zhao HJ, et al. Challenging fabrication of hollow ceramic fiber supported Cu₃(BTC)₂ membrane for hydrogen separation. *J Mater Chem* 2012;22:10322–8.
- [142] Li W, Zhang G, Zhang C, Meng Q, Fan Z, Gao C. Synthesis of trinity metal-organic framework membranes for CO₂ capture. *Chem Commun* 2014;50:3214–6.
- [143] Li YS, Bux H, Feldhoff A, Li GL, Yang WS, Caro J. Controllable synthesis of metalorganic frameworks: from MOF nanorods to oriented MOF membranes. *Adv Mater* 2010;22:3322–6.
- [144] Noh SJ, Yoon SP, Han J, Park S, Kim J. Synthesis and characterization of ZIF-7 membranes by in situ method. *J Nanosci Nanotechnol* 2015;15:575–8.
- [145] Go Y, Lee JH, Shamsudin IK, Kim J, Othman MR. Microporous ZIF-7 membranes prepared by in-situ growth method for hydrogen separation. *Int J Hydrogen Energ* 2016;41:10366–73.
- [146] Liao J, Wang Z, Gao C, Li S, Qiao Z, Wang M, et al. Fabrication of high-performance facilitated transport membranes for CO₂ separation. *Chem Sci* 2014;5:2843–9.
- [147] Shen J, Liu G, Huang K, Jin W, Lee KR, Xu N. Membranes with fast and selective gas-transport channels of laminar graphene oxide for efficient CO₂ capture. *Angew Chem Int Ed* 2015;54:578–82.
- [148] Wang S, Li X, Wu H, Tian Z, Xin Q, He G, et al. Advances in high permeability polymer-based membrane materials for CO₂ separations. *Energy Environ Sci* 2016;9:1863–90.
- [149] Qiao Z, Zhao S, Wang J, Wang S, Wang Z, Guiver MD. A highly permeable aligned montmorillonite mixed-matrix membrane for CO₂ separation. *Angew Chem Int Ed* 2016;55:9321–5.
- [150] Jiang X, Li S, Shao L. Pushing CO₂-philic membrane performance to the limit by designing semi-interpenetrating networks (SIPN) for sustainable CO₂ separations. *Energy Environ Sci* 2017;10:1339–44.
- [151] Shamsabadi AA, Seidi F, Salehi E, Nozari M, Rahimpour A, Soroush M. Efficient CO₂-removal using novel mixed-matrix membranes with modified TiO₂ nanoparticles. *J Mater Chem A* 2017;5:4011–25.
- [152] Zhang J, Schott JA, Li Y, Zhan W, Mahurin SM, Nelson K, et al. Membrane-based gas separation accelerated by hollow nanosphere architectures. *Adv Mater* 2017;29:1603797.
- [153] Ghalei B, Sakurai K, Kinoshita Y, Wakimoto K, Isfahani AP, Song Q, et al. Enhanced selectivity in mixed matrix membranes for CO₂ capture through efficient dispersion of amine-functionalized MOF nanoparticles. *Nat Energy* 2017;2:17086.
- [154] Peng Y, Li YS, Ban YJ, Jin H, Jiao WM, Liu XL, et al. Metal-organic framework nanosheets as building blocks for molecular sieving membranes. *Science* 2014;346:1356–9.
- [155] Peng Y, Li Y, Ban Y, Yang W. Two-dimensional metal-organic framework nanosheets for membrane-based gas separation. *Angew Chem Int Ed* 2017;56:9757–61.
- [156] Barankova E, Pradeep N, Peinemann KV. Zeolite-imidazolate framework (ZIF-8) membrane synthesis on a mixed-matrix substrate. *Chem Commun* 2013;49:9419–21.
- [157] Sheng L, Wang C, Yang F, Xiang L, Huang X, Yu J, et al. Enhanced C₃H₆/C₃H₈ separation performance on MOF membranes through blocking defects and

- hindering framework flexibility by silicone rubber coating. *Chem Commun* 2017;53:7760–3.
- [158] Huang A, Liu Q, Wang N, Zhu Y, Caro J. Bicontinuous zeolitic imidazolate framework ZIF-8@GO membrane with enhanced hydrogen selectivity. *J Am Chem Soc* 2014;136:14686–9.
- [159] Yoo Y, Jeong HK. Heteroepitaxial growth of isoreticular metal-organic frameworks and their hybrid films. *Cryst Growth Des* 2010;10:1283–8.
- [160] Shekhah O, Hirai K, Wang H, Uehara H, Kondo M, Diring S, et al. MOF-on-MOF heteroepitaxy: perfectly oriented $[Zn_2(nc)_2(dabco)]_n$ grown on $[Cu_2(nc)_2(dabco)]_n$ thin films. *Dalton Trans* 2011;40:4954–8.
- [161] Kwon HT, Jeong HK, Lee AS, An HS, Lee JS. Heteroepitaxially grown zeolitic imidazolate framework membranes with unprecedented propylene/propane separation performances. *J Am Chem Soc* 2015;137:12304–11.
- [162] Knebel A, Wulfert-Holzmann P, Friebe S, Pavel J, Strauß I, Mundstock A, et al. Hierarchical nanostructures of metal-organic frameworks applied in gas separating ZIF-8-on-ZIF-67 membranes. *Chem Eur J* 2018;24:5728–33.
- [163] Cacho-Bailo F, Matito-Martos I, Perez-Carbajo J, Etxeberria-Benavides M, Karvan O, Sebastián V, et al. On the molecular mechanisms for the H_2/CO_2 separation performance of zeolite imidazolate framework two-layered membranes. *Chem Sci* 2017;8:325–33.
- [164] Fu J, Das S, Xing G, Ben T, Valtchev V, Qiu S. Fabrication of COF-MOF composite membranes and their highly selective separation of H_2/CO_2 . *J Am Chem Soc* 2016;138:7673–80.
- [165] Das S, Ben T. A [COF-300]-[UiO-66] composite membrane with remarkably high permeability and H_2/CO_2 separation selectivity. *Dalton Trans* 2018;47:7206–12.
- [166] Hu Y, Wei J, Liang Y, Zhang H, Zhang X, Shen W, et al. Zeolitic imidazolate framework/graphene oxide hybrid nanosheets as seeds for the growth of ultrathin molecular sieving membranes. *Angew Chem Int Ed* 2016;55:2048–52.
- [167] Hu Y, Wu Y, Devendran C, Wei J, Liang Y, Matsukata M, et al. Preparation of nanoporous graphene oxide by nanocrystal-masked etching: toward a nacre-mimetic metal-organic framework molecular sieving membrane. *J Mater Chem A* 2017;5:16255–62.
- [168] Hou J, Wei Y, Zhou S, Wang Y, Wang H. Highly efficient H_2/CO_2 separation via an ultrathin metal-organic framework membrane. *Chem Eng Sci* 2018;182:180–8.
- [169] Shamsaei E, Lin X, Wan L, Tong Y, Wang H. A one-dimensional material as a nano-scaffold and a pseudo-seed for facilitated growth of ultrathin, mechanically reinforced molecular sieving membranes. *Chem Commun* 2016;52:13764–7.
- [170] Zhang S, Wang Z, Ren H, Zhang F, Jin J. Nanoporous film-mediated growth of ultrathin and continuous metal-organic framework membranes for high-performance hydrogen separation. *J Mater Chem A* 2017;5:1962–6.
- [171] Dumele L, He L, Hill M, Zhu B, Duke M, Schütz J, et al. Seeded growth of ZIF-8 on the surface of carbon nanotubes towards self-supporting gas separation membranes. *J Mater Chem A* 2013;1:9208–14.
- [172] Zhang Y, Wang H, Liu J, Hou J, Zhang Y. Enzyme-embedded metal-organic framework membranes on polymeric substrates for efficient CO_2 capture. *J Mater Chem A* 2017;5:19954–62.
- [173] Li W, Zhang Y, Su P, Xu Z, Zhang G, Shen C, et al. Metal-organic framework channelled graphene composite membranes for H_2/CO_2 separation. *J Mater Chem A* 2016;4:18747–52.
- [174] Li W, Shi J, Li Z, Wu W, Xia Y, Yu Y, et al. Hydrothermally reduced graphene oxide interfaces for synthesizing high-performance metal-organic framework hollow fiber membranes. *Adv Mater Interfaces* 2018. <https://doi.org/10.1002/admi.201800032>.
- [175] Fujie K, Yamada T, Ikeda R, Kitagawa H. Introduction of an ionic liquid into the micropores of a metal-organic framework and its anomalous phase behavior. *Angew Chem Int Ed* 2014;53:11302–5.
- [176] Fujie K, Otsubo K, Ikeda R, Yamada T, Kitagawa H. Low temperature ionic conductor: ionic liquid incorporated within a metal-organic framework. *Chem Sci* 2015;6:4306–10.
- [177] Tziaila O, Veziri C, Papatryfon X, Beltsios KG, Labropoulos A, Iliev B, et al. Zeolite imidazolate framework-ionic liquid hybrid membranes for highly selective CO_2 separation. *J Phys Chem C* 2013;117:18434–40.
- [178] Huang Y, Xiao Y, Huang H, Liu Z, Liu D, Yang Q, et al. Ionic liquid functionalized multi-walled carbon nanotubes/zeolitic imidazolate framework hybrid membranes for efficient H_2/CO_2 separation. *Chem Commun* 2015;51:17281–4.
- [179] Ban Y, Li Z, Li Y, Peng Y, Jin H, Jiao W, et al. Confinement of ionic liquids in nanocages: tailoring molecular sieving property of ZIF-8 for membrane-based CO_2 capture. *Angew Chem Int Ed* 2015;54:15483–7.
- [180] Kang Z, Fan L, Wang S, Sun D, Xue M, Qiu S. In situ confinement of free linkers within a stable MOF membrane for highly improved gas separation properties. *CrystEngComm* 2017;19:1601–6.
- [181] Morris W, Doonan CJ, Furukawa H, Banerjee R, Yaghi OM. Crystals as molecules: postsynthesis covalent functionalization of zeolitic imidazolate frameworks. *J Am Chem Soc* 2008;130:12626–7.
- [182] Cohen SM. Postsynthetic methods for the functionalization of metal-organic frameworks. *Chem Rev* 2012;112:970–1000.
- [183] Song YF, Cronin L. Postsynthetic covalent modification of metal-organic framework (MOF) materials. *Angew Chem Int Ed* 2008;47:4635–7.
- [184] Garzón-Tovar L, Rodríguez-Hermida S, Imaz I, Maspocho D. Spray drying for making covalent chemistry: postsynthetic modification of metal-organic frameworks. *J Am Chem Soc* 2017;139:897–903.
- [185] Yoo Y, Varela-Guerrero V, Jeong HK. Isoreticular metal-organic frameworks and their membranes with enhanced crack resistance and moisture stability by surfactant-assisted drying. *Langmuir* 2011;27:2652–7.
- [186] Huang A, Caro J. Covalent post-functionalization of zeolitic imidazolate framework ZIF-90 membrane for enhanced hydrogen selectivity. *Angew Chem Int Ed* 2011;50:4979–82.
- [187] Huang A, Wang N, Kong C, Caro J. Organosilica-functionalized zeolitic imidazolate framework ZIF-90 membrane with high gas-separation performance. *Angew Chem Int Ed* 2012;51:10551–5.
- [188] Huang A, Liu Q, Wang N, Caro J. Organosilica functionalized zeolitic imidazolate framework ZIF-90 membrane for CO_2/CH_4 separation. *Microporous Mesoporous Mater* 2014;192:18–22.
- [189] Marti AM, Tran D, Balkus Jr. KJ. Fabrication of a substituted imidazolate material 1 (SIM-1) membrane using post synthetic modification (PSM) for pervaporation of water/ethanol mixtures. *J Porous Mater* 2015;22:1275–84.
- [190] Cacho-Bailo F, Etxeberria-Benavides M, Karvan O, Téllez C, Coronas J. Sequential amine functionalization inducing structural transition in an aldehyde-containing zeolitic imidazolate framework: application to gas separation membranes. *CrystEngComm* 2017;19:1545–54.
- [191] Wang N, Mundstock A, Liu Y, Huang A, Caro J. Amine-modified Mg-MOF-74/CPO-27-Mg membrane with enhanced H_2/CO_2 separation. *Chem Eng Sci* 2015;124:27–36.
- [192] Deria P, Mondloch JE, Karagiari O, Bury W, Hupp JT, Farha OK. Beyond post-synthesis modification: evolution of metal-organic frameworks via building block replacement. *Chem Soc Rev* 2014;43:5896–912.
- [193] Han Y, Li JR, Xie Y, Guo G. Substitution reactions in metal-organic frameworks and metal-organic polyhedra. *Chem Soc Rev* 2014;43:5952–81.
- [194] Grancha T, Ferrando-Soria J, Zhou HC, Gascon J, Seoane B, Pasán J, et al. Postsynthetic improvement of the physical properties in a metal-organic framework through a single crystal to single crystal transmetalation. *Angew Chem Int Ed* 2015;54:6521–5.
- [195] Li T, Kozłowski MT, Doud EA, Blakely MN, Rosi NL. Stepwise ligand exchange for the preparation of a family of mesoporous MOFs. *J Am Chem Soc* 2013;135:11688–91.
- [196] Takaishi S, DeMarco EJ, Pellin MJ, Farha OK, Hupp JT. Solvent-assisted linker exchange (SALE) and post-assembly metallation in porphyrinic metal-organic framework materials. *Chem Sci* 2013;4:1509–13.
- [197] Li W, Zhang Y, Zhang C, Meng Q, Xu Z, Su P, et al. Transformation of metal-organic frameworks for molecular sieving membranes. *Nat Commun* 2016;7:11315.
- [198] Lee MJ, Kwon HT, Jeong HK. High-flux zeolitic imidazolate framework membranes for propylene/propane separation by postsynthetic linker exchange. *Angew Chem Int Ed* 2018;57:156–61.
- [199] Wang C, Yang F, Sheng L, Yu J, Yao K, Zhang L, et al. Zinc-substituted ZIF-67 nanocrystals and polycrystalline membranes for propylene/propane separation.

- Chem Commun 2016;52:12578–81.
- [200] Hillman F, Zimmerman JM, Paek SM, Hamid MRA, Lim WT, Jeong HK. Rapid microwave-assisted synthesis of hybrid zeolitic-imidazolate frameworks with mixed metals and mixed linkers. *J Mater Chem A* 2017;5:6090–9.
- [201] Zhang C, Xiao Y, Liu D, Yang Q, Zhong C. A hybrid zeolitic imidazolate framework membrane by mixed-linker synthesis for efficient CO₂ capture. *Chem Commun* 2013;9:600–2.
- [202] Cacho-Bailo F, Caro G, Exteberría-Benavides M, Karvan O, Téllez C, Coronas J. MOF-polymer enhanced compatibility: post-annealed zeolite imidazolate framework membranes inside polyimide hollow fibers. *RSC Adv* 2016;6:5881–9.
- [203] Kwon HT, Jeong HK, Lee AS, An HS, Lee T, Jang E, et al. Defect-induced ripening of zeolitic-imidazolate framework ZIF-8 and its implication to vapor-phase membrane synthesis. *Chem Commun* 2016;52:11669–72.
- [204] Fujiwara M, Imura T. Photo induced membrane separation for water purification and desalination using azobenzene modified anodized alumina membranes. *ACS Nano* 2015;9:5705–12.
- [205] Wen L, Xiao K, Sainath AVS, Komura M, Kong XY, Xie G, et al. Engineered asymmetric composite membranes with rectifying properties. *Adv Mater* 2016;28:757–63.
- [206] Wang C, Wu Y, Lu J, Zhao J, Cui J, Wu X, et al. Bioinspired synthesis of photocatalytic nanocomposite membranes based on synergy of Au-TiO₂ and polydopamine for degradation of tetracycline under visible light. *ACS Appl Mater Interfaces* 2017;9:23687–97.
- [207] Shi B, Marchetti P, Peshev D, Zhang S, Livingston AG. Will ultra-high permeance membranes lead to ultra-efficient processes? Challenges for molecular separations in liquid systems. *J Membr Sci* 2017;525:35–47.
- [208] Karan S, Jiang Z, Livingston AG. Sub-10 nm polyamide nanofilms with ultrafast solvent transport for molecular separation. *Science* 2015;348:1347–51.
- [209] Karan S, Samitsu S, Peng X, Kurashima K, Ichinose I. Ultrafast viscous permeation of organic solvents through diamond-like carbon nanosheets. *Science* 2012;335:444–7.
- [210] Wang L, Boutilier MSH, Kidambi PR, Jang D, Hadjiconstantinou NG, Karnik R. Fundamental transport mechanisms, fabrication and potential applications of nanoporous atomically thin membranes. *Nat Nanotechnol* 2017;12:509–22.
- [211] Surwade SP, Smirnov SN, Vlassiok IV, Unocic RR, Veith GM, Dai S, et al. Water desalination using nanoporous single-layer graphene. *Nat Nanotechnol* 2015;10:459–64.
- [212] Mi B. Graphene oxide membranes for ionic and molecular sieving. *Science* 2014;343:740–2.
- [213] Akbari A, Sheath P, Martin ST, Shinde DB, Shaibani M, Banerjee PC, et al. Large-area graphene-based nanofiltration membranes by shear alignment of discotic nematic liquid crystals of graphene oxide. *Nat Commun* 2016;7:10891.
- [214] Gorgojo P, Karan S, Wong HC, Jimenez-Solomon MF, Cabral JT, Livingston AG. Ultrathin polymer films with intrinsic microporosity: anomalous solvent permeation and high flux membranes. *Adv Funct Mater* 2014;24:4729–37.
- [215] Basu S, Maes M, Cano-Odena A, Alaerts L, De Vos DE, Vankelecom IFJ. Solvent resistant nanofiltration (SRNF) membranes based on metal-organic frameworks. *J Membr Sci* 2009;344:190–8.
- [216] Sorribas S, Gorgojo P, Téllez C, Coronas J, Livingston AG. High flux thin film nanocomposite membranes based on metal-organic frameworks for organic solvent nanofiltration. *J Am Chem Soc* 2013;135:15201–8.
- [217] Zhang R, Ji S, Wang N, Wang L, Zhang G, Li JR. Coordination-driven in situ self-assembly strategy for the preparation of metal-organic framework hybrid membranes. *Angew Chem Int Ed* 2014;53:9775–9.
- [218] Denny MS, Cohen SM. In situ modification of metal-organic frameworks in mixed-matrix membranes. *Angew Chem Int Ed* 2015;54:9029–32.
- [219] Wang N, Li X, Wang L, Zhang L, Zhang G, Ji S. Nanoconfined zeolitic imidazolate framework membranes with composite layers of nearly zero thickness. *ACS Appl Mater Interfaces* 2016;8:21979–83.
- [220] Liu X, Demir NK, Wu Z, Li K. Highly water-stable zirconium metal-Organic framework UiO-66 membranes supported on alumina hollow fibers for desalination. *J Am Chem Soc* 2015;137:6999–7002.
- [221] Liu X, Wang C, Wang B, Li K. Novel organic-dehydration membranes prepared from zirconium metal-organic frameworks. *Adv Funct Mater* 2017;27:1604311.
- [222] Miyamoto M, Hori K, Goshima T, Takaya N, Oumi Y, Uemiy S. An organoselective zirconium-based metal-organic-framework UiO-66 membrane for pervaporation. *Eur J Inorg Chem* 2017;14:2094–9.
- [223] Li Y, Wee LH, Martens JA, Vankelecom IFJ. Interfacial synthesis of ZIF-8 membranes with improved nanofiltration performance. *J Membr Sci* 2017;523:561–6.
- [224] Yang L, Wang Z, Zhang J. Highly permeable zeolite imidazolate framework composite membranes fabricated via a chelation assisted interfacial reaction. *J Mater Chem A* 2017;5:15342–55.
- [225] Campbell J, Davies RP, Braddock DC, Livingston AG. Improving the permeance of hybrid polymer/metal-organic framework (MOF) membranes for organic solvent nanofiltration (OSN)-development of MOF thin films via interfacial synthesis. *J Mater Chem A* 2015;3:9668–74.
- [226] Swain B. Separation and purification of lithium by solvent extraction and supported liquid membrane, analysis of their mechanism: a review. *J Chem Technol Biotechnol* 2016;91:2549–62.
- [227] Park HA, Kim YJ, Kwon IS, Klosterman L, Bettinger CJ. Lithium purification from aqueous solutions using bioinspired redox-active melanin membranes. *Polym Int* 2016;65:1331–8.
- [228] Swain B. Recovery and recycling of lithium: a review. *Sep Purif Technol* 2017;172:388–403.
- [229] Guo Y, Ying Y, Mao Y, Peng X, Chen B. Polystyrene sulfonate threaded through a metal-organic framework membrane for fast and selective lithium-ion separation. *Angew Chem Int Ed* 2016;55:15120–4.
- [230] Zhang H, Hou J, Hu Y, Wang P, Ou R, Jiang L, et al. Ultrafast selective transport of alkali metal ions in metal organic frameworks with subnanometer pores. *Sci Adv* 2018. 4:eaq0066.
- [231] Bruce PG, Freunberger SA, Hardwick LJ, Tarascon JM. Li-O₂ and Li-S batteries with high energy storage. *Nat Mater* 2012;11:19–29.
- [232] Zhou GM, Paek E, Hwang GS, Manthiram A. Long-life Li/poly sulphide batteries with high sulphur loading enabled by lightweight three-dimensional nitrogen/sulphur-codoped graphene sponge. *Nat Commun* 2015;6:7760.
- [233] Bai S, Liu X, Zhu K, Wu S, Zhou H. Metal-organic framework-based separator for lithium-sulfur batteries. *Nat Energy* 2016;1:16094.
- [234] Mao Y, Li G, Guo Y, Li Z, Liang C, Peng X, et al. Foldable interpenetrated metal-organic frameworks/carbon nanotubes thin film for lithium-sulfur batteries. *Nat Commun* 2017;8:14628.
- [235] Liu Y, Li G, Guo Y, Ying Y, Peng X. Flexible and binder-free hierarchical porous carbon film for supercapacitor electrodes derived from MOFs/CNT. *ACS Appl Mater Interfaces* 2017;9:14043–50.
- [236] Zhang X, Zhou J, Wei R, Zhao W, Sun S, Zhao C. Design of anion species/strength responsive membranes via in-situ crosslinked copolymerization of ionic liquids. *J Membr Sci* 2017;535:158–67.
- [237] Ma B, Ju XJ, Luo F, Liu YQ, Wang Y, Liu Z, et al. Facile fabrication of composite membranes with dual thermo- and pH-responsive characteristics. *ACS Appl Mater Interfaces* 2017;9:14409–21.
- [238] Park J, Yuan D, Pham KT, Li JR, Yakovenko A, Zhou HC. Reversible alteration of CO₂ adsorption upon photochemical or thermal treatment in a metal-organic framework. *J Am Chem Soc* 2012;134:99–102.
- [239] Krause S, Bon V, Stoeckl U, Senkowska I, Töbrens DM, Wallacher D, et al. A stimuli-responsive zirconium metal-organic framework based on supermolecular design. *Angew Chem Int Ed* 2017;56:10676–80.
- [240] Wang Z, Knebel A, Grosjean S, Wagner D, Bräse S, Wöll C, et al. Tunable molecular separation by nanoporous membranes. *Nat Commun* 2016;7:13872.
- [241] Knebel A, Sundermann L, Mohmeyer A, Strauß I, Friebe S, Behrens P, et al. Azobenzene guest molecules as light-switchable CO₂ valves in an ultrathin UiO-67 membrane. *Chem Mater* 2017;29:3111–7.
- [242] Meller K, Knebel A, Zhao F, Bleger D, Caro J, Heinke L. Switching thin films of azobenzene-containing metal-organic frameworks with visible light. *Chem Eur J* 2017;23:5434–8.
- [243] Knebel A, Geppert B, Volkmann K, Kolokolov DI, Stepanov AG, Twiefel J, et al. Defibrillation of soft porous metal-organic frameworks with electric fields.

- Science 2017;358:347–51.
- [244] Wang X, Chi C, Zhang K, Qian Y, Gupta KM, Kang Z, et al. Reversed thermo-switchable molecular sieving membranes composed of two-dimensional metal-organic nanosheets for gas separation. *Nat Commun* 2017;8:14460.
- [245] Yang T, Shi GM, Chung TS. Symmetric and asymmetric zeolitic imidazolate frameworks (ZIFs)/polybenzimidazole (PBI) nanocomposite membranes for hydrogen purification at high temperatures. *Adv Energy Mater* 2012;2:1358–67.
- [246] Japip S, Liao KS, Chung TS. Molecularly tuned free volume of vapor cross-linked 6FDA-Durene/ZIF-71 MMMs for H₂/CO₂ separation at 150 °C. *Adv Mater* 2017;29:1603833.
- [247] Yang D, Odoh SO, Wang TC, Farha OK, Hupp JT, Cramer CJ, et al. Metal-organic framework nodes as nearly ideal supports for molecular catalysts: NU-1000 and UiO-66-supported iridium complexes. *J Am Chem Soc* 2015;137:7391–6.
- [248] Zhang W, Lu G, Cui C, Liu Y, Li S, Yan W, et al. A family of metal-organic frameworks exhibiting size-selective catalysis with encapsulated noble-metal nanoparticles. *Adv Mater* 2014;26:4056–60.
- [249] Yang Q, Xu Q, Yu SH, Jiang HL. Pd Nanocubes@ZIF-8: integration of plasmon-driven photothermal conversion with a metal-organic framework for efficient and selective catalysis. *Angew Chem Int Ed* 2016;55:3685–9.
- [250] Yang Q, Xu Q, Jiang HL. Metal-organic frameworks meet metal nanoparticles: synergistic effect for enhanced catalysis. *Chem Soc Rev* 2017;46:4774–808.
- [251] Chen L, Luque R, Li Y. Controllable design of tunable nanostructures inside metal-organic frameworks. *Chem Soc Rev* 2017;46:4614–30.
- [252] Mao Y, Li J, Cao W, Ying Y, Hu P, Liu Y, et al. General incorporation of diverse components inside metal-organic framework thin films at room temperature. *Nat Commun* 2014;5:5532.
- [253] Yu Y, Wu XJ, Zhao M, Ma Q, Chen J, Chen B, et al. Anodized aluminum oxide templated synthesis of metal-organic frameworks used as membrane reactors. *Angew Chem Int Ed* 2017;56:578–81.
- [254] Zhang G, Zhang T, Zhang X, Yeung KL. Continuous flow ZIF-8/NaA composite membrane microreactor for efficient Knoevenagel condensation. *Catal Commun* 2015;68:93–6.